AD-A065 584 MCDONNELL AIRCRAFT CO ST LOUIS MO F/G 11/6

DEFINITION AND NON-DESTRUCTIVE DETECTION OF CRITICAL ADHESIVE B--ETC(U)

JUL 78 H T CLARK F33615-75-C-5209

UNCLASSIFIED AFML-TR-78-108 NL

1 OF 1

AD A065584

END

DATE FILMED

5-79

DDC

AFML-TR-78-108

LEVEL II

12

AD A065584

DEFINITION AND NON-DESTRUCTIVE DETECTION OF CRITICAL ADHESIVE BOND-LINE FLAWS

MCDONNELL AIRCRAFT COMPANY
MCDONNELL DOUGLAS CORPORATION
P.O. BOX 516
ST. LOUIS, MISSOURI 63166

DDC
RECEIVED
MAR 13 1979
C

DDC FILE COPY

JULY 1978

TECHNICAL REPORT AFML-TR-78-108
FINAL REPORT FOR PERIOD
27 JUNE 1975 - 31 JULY 1978

Approved for Public Release; Distribution Unlimited

AIR FORCE MATERIALS LABORATORY
AIR FORCE WRIGHT AERONAUTICAL LABORATORIES
AIR FORCE SYSTEMS COMMAND
WRIGHT-PATTERSON AIR FORCE BASE, OHIO 45433

79 03 12 054

NOTICE

When Government drawings, specifications, or other data are used for any purpose other than in connection with a definitely related Government procurement operation, the United States Government thereby incurs no responsibility nor any obligation whatsoever; and the fact that the government may have formulated, furnished, or in any way supplied the said drawings, specifications, or other data, is not to be regarded by implication or otherwise as in any manner licensing the holder or any other person or corporation, or conveying any rights or permission to manufacture, use, or sell any patented invention that may in any way be related thereto.

This report has been reviewed by the Information Office (OI) and is releasable to the National Technical Information Service (NTIS). At NTIS, it will be available to the general public, including foreign nations.

This technical report has been reviewed and is approved for publication.

HERBERT S. SCHWARTZ
Project Monitor

T. J. REINHART, JR., Chief
Composites, Adhesives and Fibrous Materials Branch

FOR THE COMMANDER

J. M. KELBLE, Chief
Nonmetallic Materials Division

"If your address has changed, if you wish to be removed from our mailing list, or if the addressee is no longer employed by your organization please notify AFML/MBC, W-PAFB, OH 45433 to help us maintain a current mailing list".

Copies of this report should not be returned unless return is required by security considerations, contractual obligations, or notice on a specific document.

AIR FORCE/56780/16 January 1979 — 340

UNCLASSIFIED

SECURITY CLASSIFICATION OF THIS PAGE (When Data Entered)

REPORT DOCUMENTATION PAGE

READ INSTRUCTIONS BEFORE COMPLETING FORM

1. REPORT NUMBER
AFML-TR-78-108

2. GOVT ACCESSION NO.

3. RECIPIENT'S CATALOG NUMBER

4. TITLE (and Subtitle).
DEFINITION AND NON-DESTRUCTIVE DETECTION OF CRITICAL ADHESIVE BOND-LINE FLAWS.

5. TYPE OF REPORT & PERIOD COVERED
Final Report.
27 Jun 75 - 31 Jul 78

6. PERFORMING ORG. REPORT NUMBER

7. AUTHOR(s)
H. T. Clark

8. CONTRACT OR GRANT NUMBER(s)
F33615-75-C-5209

9. PERFORMING ORGANIZATION NAME AND ADDRESS
McDonnell Aircraft Company
McDonnell Douglas Corporation
P.O. Box 516
St. Louis, Missouri 63166

10. PROGRAM ELEMENT, PROJECT, TASK AREA & WORK UNIT NUMBERS
486U-01-08 01

11. CONTROLLING OFFICE NAME AND ADDRESS
Air Force Materials Laboratory (MBC)
Wright-Patterson AFB, Ohio 45433

12. REPORT DATE
Jul[redacted]78

13. NUMBER OF PAGES
84

14. MONITORING AGENCY NAME & ADDRESS (if different from Controlling Office)
AFPRO
McDonnell Douglas Corporation
P. O. Box 516
St. Louis, Missouri 63166

15. SECURITY CLASS. (of this report)
Unclassified

15a. DECLASSIFICATION/DOWNGRADING SCHEDULE

16. DISTRIBUTION STATEMENT (of this Report)
Approved for public release; distribution unlimited.

AFML TR-78-108

17. DISTRIBUTION STATEMENT (of the abstract entered in Block 20, if different from Report)

18. SUPPLEMENTARY NOTES

19. KEY WORDS (Continue on reverse side if necessary and identify by block number)
Adhesive Bonds, Fatigue of Flawed Bondlines, Non-destructive Inspection, NDE of Flaw Growth, Flaw Growth Rate, Bonded Joints, Environment, Cycle Rate

20. ABSTRACT (Continue on reverse side if necessary and identify by block number)
Fatigue tests were conducted on adhesive bonded aluminum specimens with intentionally induced adhesive bondline flaws. Specimen design details, materials, type of surface preparation, and test loadings were selected to be representative of those on the bonded wide-body fuselage test article designed and built in the PABST program.

over

DD FORM 1 JAN 73 1473 EDITION OF 1 NOV 65 IS OBSOLETE

UNCLASSIFIED

SECURITY CLASSIFICATION OF THIS PAGE (When Data Entered)

403111

Tests conducted in this report show that bondline flaws loaded primarily in shear did not grow whereas those loaded by peel or tension forces did exhibit flaw growth. Flaw growth rate was higher at the slow rate of two cycles per hour than for a fast-cycle rate of 30 Hz. Bondline flaws grew incrementally with load cycles and could be tracked by state-of-the-art NDE.

FOREWORD

This report was prepared by McDonnell Aircraft Company (MCAIR), St. Louis, Missouri, for the Composite and Fibrous Materials Branch, Non-Metallic Materials Division, Air Force Materials Laboratory, Wright-Patterson Air Force Base, Ohio under Contract F33615-75-C-5209, "Definition and Non-Destructive Detection of Critical Adhesive Bond-Line Flaws". The contract was administered by Herbert S. Schwartz, Project Engineer, AFML/MBC.

The Structural Research Department of McDonnell Aircraft Company had primary responsibility for the performance of this program. The program manager for MCAIR was J. F. Schier. The principal investigator was H. T. Clark. Dr. L. J. Hart-Smith supported the analysis efforts and served as an interface with the Primary Adhesive Bonded Structure Technology (PABST) Program conducted at the Douglas Aircraft Company (DAC). R. J. Roehrs and T. S. Jones of the Materials and Processes Department (MCAIR) coordinated all NDE activities. J. H. Gruss, J. F. Harrell, J. W. Parks, and J. E. Skorat, MCAIR Structural Laboratories, performed the test program. J. L. Merkel, MCAIR Advanced Materials Fabrication Facility, was responsible for fabricating the Complex Specimens.

This report covers work accomplished during the period June 1975 through July 1978.

This report was released by the author in July 1978 for publication.

ACCESSION for
NTIS White Section
DDC Buff Section
UNANNOUNCED
JUSTIFICATION
DISTRIBUTION/AVAILABILITY CODES
SPECIAL
A

TABLE OF CONTENTS

Section		Page
1.	INTRODUCTION AND SUMMARY	1
2.	PHASE I - REVIEW OF EXPERIENCE WITH FLAWS	3
2.1	Preliminary Preparation	3
2.1.1	Specimen Design Details	3
2.1.2	Materials Selection	6
2.2	Review of Experience with Flaws and Methods of Detection	8
2.3	Methods of Flaw Introduction	11
2.3.1	Adhesive Cut-Out	12
2.3.2	Wire Insertion	12
2.3.3	Mechanical Damage	12
2.4	Methods of Flaw Detection	13
3.	PHASE II - SIMPLE SPECIMEN EVALUATION	16
3.1	Phase II Test Plan	16
3.2	Specimen Analysis	19
3.3	Test Procedure	29
3.4	Fast-Cycle Fatigue Tests	33
3.4.1	Results of Preliminary Testing on Effect of Cycle Rate	34
3.4.2	Results of Fast-Cycle (30 Hz) Fatigue Testing	35
3.5	Slow Cycle Fatigue Tests	52
3.6	Summary of Residual Strength Tests	67
4.	PHASE III - NDE Assessment (Complex Specimens)	76
4.1	Design and Fabrication of Complex Specimens	76
4.2	Assessment of NDE Methods	78
4.2.1	Radiography	79
4.2.2	Through-Transmission Ultrasonics	79
4.2.3	Ultrasonic Resonance	80
4.2.4	Eddy-Sonics	80
4.2.5	Tetrobromo-Ethane	80
4.3	Documentation of NDE Procedures	81
5.	CONCLUSIONS	83
6.	REFERENCES	84

79 09 12 054

LIST OF ILLUSTRATIONS

Figure		Page
1	Typical Adhesive Bonded Joints on Wide Body Fuselage	4
2	Double-Doubler and Double-Strap Test Specimens.	5
3	Single-Doubler Test Specimen	5
4	Single-Strap Test Specimen	6
5	Skin-to-Substructure Tee Specimen	7
6	Flaws From Lack of Pressure Are Visible In Radiograph	11
7	Flaw Producing Mechanism - 3/4 In. Adhesive Gap	12
8	Flaw Producing Mechanism - 0.015 Wire Insertion	13
9	Multi-tone C-Scan of Flawed Specimen	14
10	Idealization of Shear Stress-Strain Curve	20
11	Double-Doubler and Double-Strap Specimen	21
12	Equivalence of Double-Doubler and Double-Strap Joints	22
13	Shear Stress Distributions Are Similar Over a Wide Range of Loads	24
14	Single-Doubler Specimen	25
15	Single-Strap Joint Specimen	26
16	Skin-to-Substructure Specimen	28
17	Test Loads For Skin-to-Substructure Specimens	28
18	Fast-Cycle Fatigue Test Set-up For Tee Specimens	30
19	Fast-Cycle Fatigue Test Set-up For Metal-Lap Specimens	31
20	Test Set-Up For Preliminary Investigations On the Effect of Cycle Rate	32

LIST OF ILLUSTRATIONS (Continued)

Figure		Page
21	Slow-Cycle Test Fixtures	33
22	Full-Scale Radiograph of Double-Doubler Specimen No. 1	36
23	Full-Scale C-Scans of Specimen No. 1 Before and After Cycling	37
24	C-Scans of Single-Strap Specimen No. 5	49
25	Single-Strap Specimen No. 32 After Residual Strength Test (Fast Cycle)	50
26	Flaw Growth Characteristics of Single-Strap Specimens	51
27	C-Scans of Double-Strap Specimen No. 7 Before and After Cycling	58
28	C-Scans of Double-Strap Specimen No. 2 Before and After Cycling	59
29	Residual Strength Tests of Single-Strap Specimens	74
30	Complex Specimen - Internal Longeron	77
31	Complex Specimen - External Longeron	78
32	Complex Specimen - Shear Panel	79

LIST OF TABLES

Table		Page
1	Generic Flaw Types and Producing Mechanisms	9
2	Frequency of Rejectable Flaws in Adhesively Bonded Assemblies	10
3	Fast-Cycle (30 Hz) Test Matrix	17
4	DAC-Cycle Test Matrix	18
5	Adhesive Properties Used in Bonded Joint Analyses	20
6	Comparison of Applied Loads to PABST Loads For Single-Doubler Specimens	25
7	Single-Strap Specimen Analysis Summary	27
8	Results of Preliminary Tests on Effect of Cycle Rate	34
9	Results of Double-Doubler and Double-Strap Specimen Tests (Fast Cycle)	39
10	Results of Single-Doubler Specimen Tests (Fast Cycle)	41
11	Results of Single-Strap Specimen Tests (Fast Cycle)	45
12	Results of Skin-to-Substructure (Tee) Specimens (Fast Cycle)	53
13	Results of Double-Strap Specimen Tests (DAC Cycle)	57
14	Results of Single-Doubler Specimen Tests (DAC Cycle)	60
15	Results of Single-Strap Specimen Tests (DAC Cycle)	63
16	Results of Skin-to-Substructure (Tee) Specimen Tests (DAC Cycle)	68

1. INTRODUCTION AND SUMMARY

Adhesive bonding has been used in secondary structural applications for many years on both fighter and transport type aircraft. In order to exploit the potential of adhesive bonding to achieve light-weight economical structure and improved performance, the Primary Adhesive Bonded Structure Technology Program (PABST) (References 1 and 2) was initiated by the Air Force to demonstrate adhesive bonding in highly loaded, primary aircraft structures. A number of related technologies were explored independent of the main fuselage structure development program. This is one such investigation and is concerned with (a) the detection of bondline flaws by NDE and (b) the distinction between bond flaws which grow under cyclic loading and those which do not. This work was coordinated with another technology program (Reference 3) to evaluate the use of fracture mechanics methodology to predict flaw growth and fracture of adhesive bonded structures with pre-existing flaws.

The specific objectives of this program were to:

- o determine the most commonly occurring flaws and their most likely locations
- o determine behavior of most commonly occurring flaws under cyclic loading
- o assess ability of NDE techniques to detect flaws and flaw growth due to cyclic loading
- o determine effect of temperature and moisture on flaw growth rate
- o assess effect of cycle rate on flaw growth

The program was conducted in three phases:

Phase I - Review of Experience with Flaws

Phase II - Simple Specimen Evaluation

Phase III - NDE Assessment (Complex Specimens)

---

(1) AFFDL-TR-76-141, "Primary Adhesively Bonded Structure Technology (PABST); Phase Ib: Preliminary Design", dated December 1976.

(2) AFFDL-TR-77-135, "Primary Adhesively Bonded Structure Technology (PABST); Phase II: Detail Design", dated August 1977.

(3) AFML-TR-77-163, "Fracture Mechanics for Structural Adhesive Bonds", dated August 1977.

Phase I consisted of a development of specimen design details, selection of materials, review of experience with bonded structures to determine types of manufacturing defects likely to occur and where they are likely to occur, and a study to determine how to reproduce manufacturing defects of different sizes, shapes, and location without artificial means.

Phase II consisted of fabricating flawed panels from which test specimens were machined and fatigue tested to determine critical flaw type and sensitivity of growth rate to specimen configuration, flaw type, and environmental exposure. Both fast cycle testing (30 Hz) and slow cycle testing (2 cycles per hour) were employed.

Phase III consisted of fabricating complex specimens that closely represented actual design detail configurations. These specimens were fabricated with intentionally induced bondline defects and were carefully inspected using state-of-the-art NDE techniques. A set of these specimens were fabricated as standards for the Air Force to be used in evaluating the capability of new NDE equipment to detect bondline flaws.

2. PHASE I - REVIEW OF EXPERIENCE WITH FLAWS

In Phase I, three basic tasks were accomplished in preparation for conducting the Phase II test program. They are: - Preliminary Preparation; - Review of Experience With Flaws and Methods of Detection; - Evaluation of Methods of Flaw Introduction.

2.1 Preliminary Preparation

In this task, specimen design details, materials, and type of surface preparation were selected which are representative of bonded joints in the wide body fuselage design of the PABST Program.

2.1.1 Specimen Design Details - Although the types of bonded joints found in conceptual designs of large fuselage structure appear to be of unlimited variety, there exists a commonality of design loadings, internal stress distributions, and failure modes, such that tests of a few types of idealized test specimens could provide information on effects of defects required for this program.

Representative geometric configurations, typical of joints utilized in the PABST fuselage structure, are illustrated in Figure 1. The types of joints are categorized as circumferential skin splices, longitudinal skin splices, bonded doublers, and skin-to-substructure joints.

Longitudinal skin splices as shown in Figure 1(a), are subjected to hoop tension loadings induced by internal pressurization and, depending on location, to in-plane shear from fuselage bending or torsion. Such splices are of the double-strap variety, with the inner strap a simple strip of sheet material or the base leg of the stringer to which the joint has been anchored for stability. This kind of joint is accurately represented by the double-doubler or double-strap specimen shown in Figure 2. It is also representative of symmetric doublers, stiffener runouts, and single bond joints which are supported on moment-resistant foundations to limit structural deflections.

Bonded doublers, as shown in Figure 1(b), (c), and (e), are used as local reinforcements within a panel to add thickness for a mechanical joint, and for reinforcements at stiffener runouts. Bonded doublers can be employed in either a single or double bond configuration and, depending on the thickness of the doubler, can be stabilized by a local stiffener to minimize out-of-plane deflections.

The single-doubler specimen configuration shown in Figure 3 was designed to produce representative shear and peel stresses found in an unsupported bonded doubler. In this configuration, without the parallel load path of double-bond joints, it experiences slightly higher peel stresses than the double-doubler specimen.

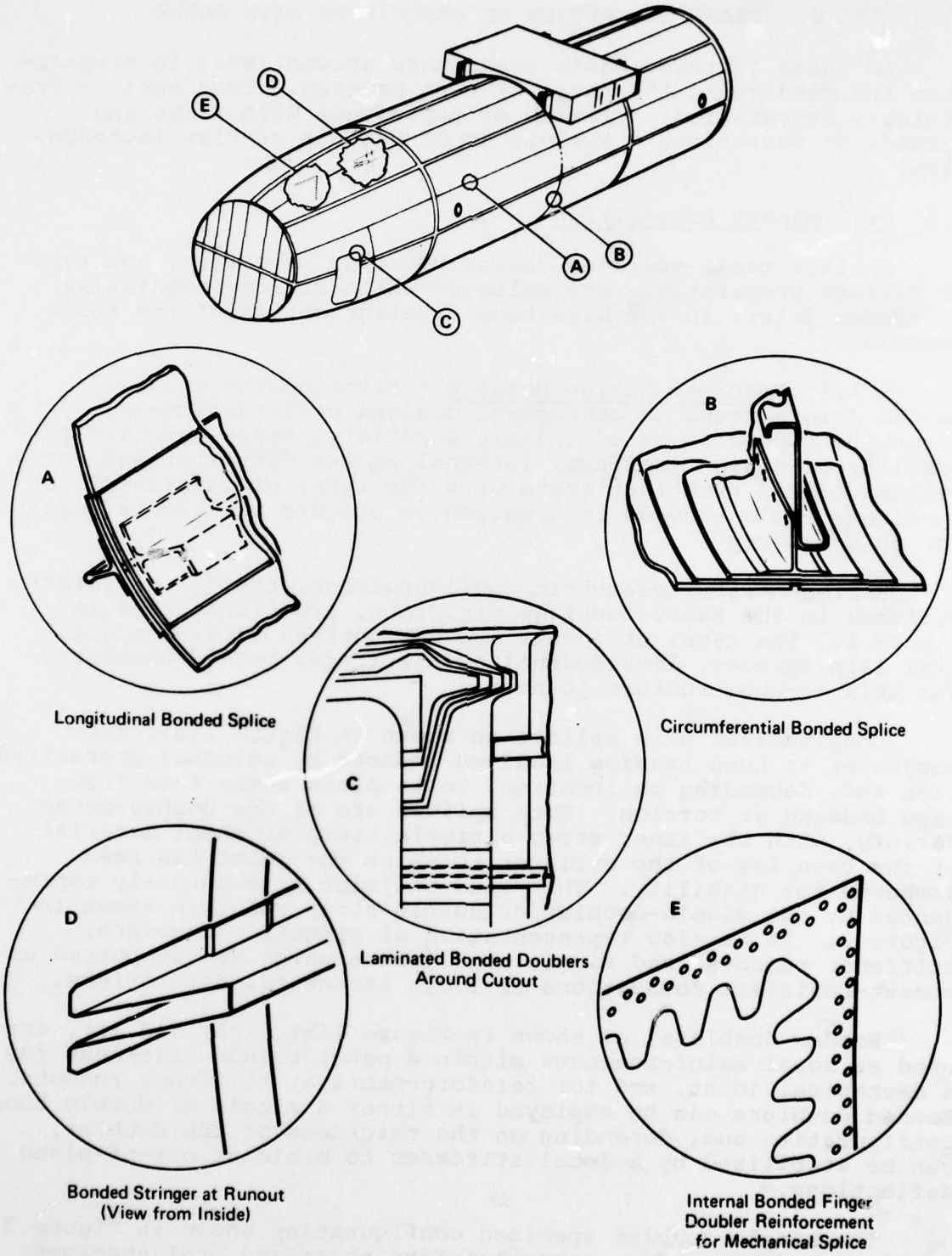

FIGURE 1
TYPICAL ADHESIVE BONDED JOINTS ON WIDE BODY FUSELAGE

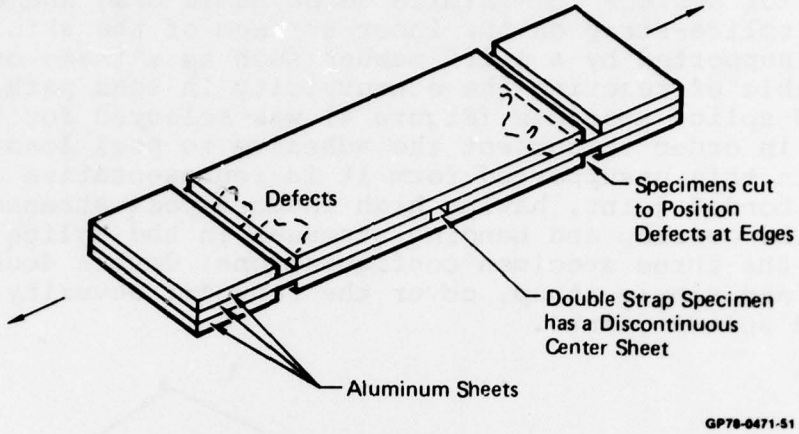

FIGURE 2
DOUBLE-DOUBLER AND DOUBLE STRAP TEST SPECIMENS

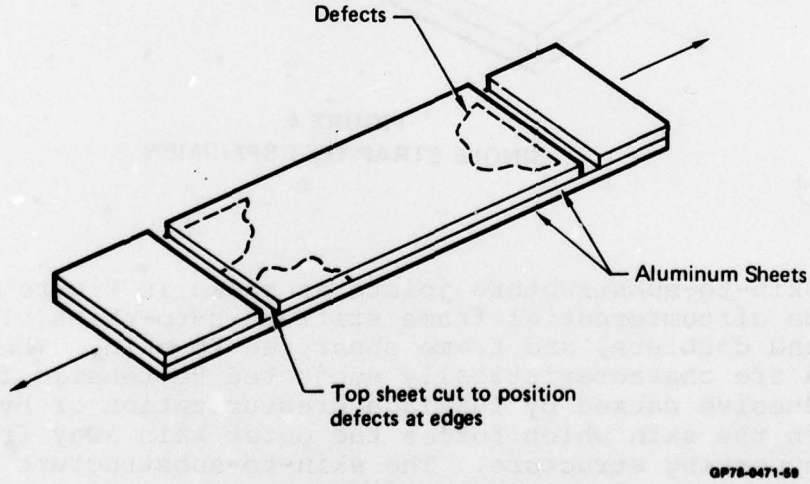

FIGURE 3
SINGLE-DOUBLER TEST SPECIMEN

Circumferential skin splices (Figure 1(b)) are flush with the exterior surface to minimize aerodynamic drag and contain a single splice-strap on the inner surface of the skin. The joint is supported by a stiff member such as a frame or shear clip capable of reacting the eccentricity in load path. An unsupported splice specimen (Figure 4) was selected for testing in Phase II in order to subject the adhesive to peel loading conditions. In this unsupported form it is representative of a poorly designed bonded joint, having high induced peel stresses at the ends of the overlap and bending stresses in the splice. Taken as a set the three specimen configurations, double doubler, single doubler, and single-strap, cover the range of severity of stresses in bonded splice joints.

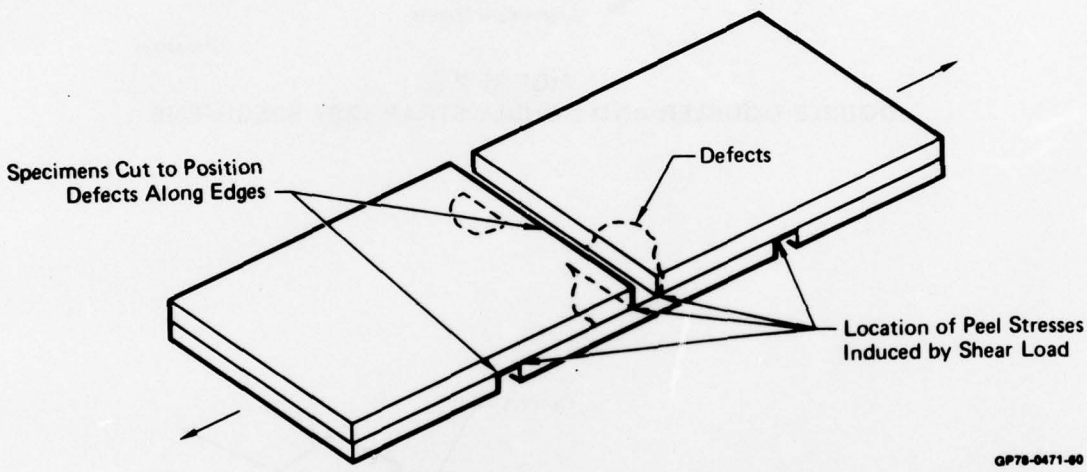

FIGURE 4
SINGLE-STRAP TEST SPECIMEN

Skin-to-substructure joints as shown in Figure 1(a) and (b) include circumferential frame stiffeners-to-skins, longerons-to-skin and doublers, and frame shear tee-to-skin. These types of joints are characteristically subjected to tensile forces in the adhesive caused by fuselage pressurization or by shear buckling in the skin which forces the outer skin away from the internal supporting structure. The skin-to-substructure tee specimen shown in Figure 5 was designed to represent this type of bonded structure. Tension forces are induced in the bondline by loads applied to the upstanding leg of the tee and reacted by shear and tension loads in the skin.

2.1.2 Materials Selection - Many of the materials used in the PABST Program had not been selected at the initiation of this program. The materials proposed for use in the PABST Program, however, were reviewed and selections are as follows:

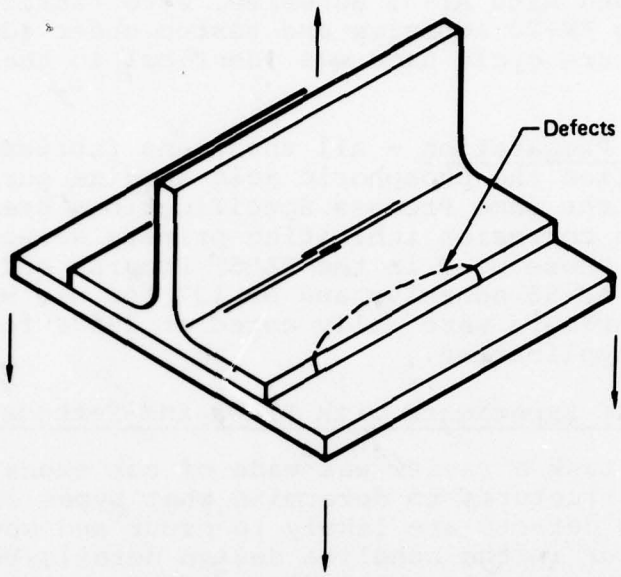

FIGURE 5
SKIN-TO-SUBSTRUCTURE TEE SPECIMEN

Adherends - Unclad 2024-T3 was selected as the skin and doubler material for all specimens. Although unclad, 7075-T6 and 7475 were also candidates at the time, unclad 2024-T3 was more readily available from local suppliers and was equally acceptable. Extruded 7075-T6511 was selected for the substructure tee material.

Adhesive - The AF-55 adhesive (0.045 lb/sq.ft.) with non-woven mat carrier was selected initially because it exhibits good strength and durability properties, and has a high X-ray absorption capability which allows radiography to be used to detect and locate small defects in structural bonds. A non-woven mat type support was selected because it exhibits better durability characteristics than the knit type support and also because the mat support does not trap as much air as the woven mat.

The adhesive cure cycle, as recommended by the adhesive manufacturer, was as follows:

Heat-up Rate:	2-5° per minute
Pressure:	40 ± 5 psi
Cure-Time:	60 minutes at 250 ± 10°F

Later, after FM-73 was chosen for the primary adhesive system in the PABST Program, several specimens of identical configuration to those bonded with AF-55 adhesive, were fabricated in this program using FM-73 adhesive and tested under identical conditions. The cure cycle used was identical to that for the AF-55 adhesive.

Surface Preparation - All specimens fabricated in Phases II and III utilized the phosphoric acid anodize surface treatment according to the same Process Specifications used in the PABST Program. The corrosion inhibiting primers selected were also identical to those used in the PABST Program and were XA 3950 for use with AF-55 adhesive and BR 127 for use with FM-73 adhesive. Both primers were fully cured at 255°F for 60 minutes prior to adhesive application.

2.2 Review of Experience with Flaws and Methods of Detection

In this task a review was made of our experience with adhesive bonded structures to determine what types of detectable manufacturing defects are likely to occur and where they are likely to occur in the bondline design details being considered for primary structural applications. Defects not detectable by state-of-the-art NDE, such as weak bonds resulting from adherend surface contamination, were not included in the survey even though they may occur during the manufacturing process.

As a result of these studies, four basic types of flaws were chosen to be evaluated in the Phase II test program. They were: large voids (either crack-like or circular in geometry), porosity, mechanical damage, and variable adhesive thickness. Typical types of adhesive bondline flaws are listed in Table 1. These were determined from a review and evaluation of MCAIR discrepancy reports for production components. The components were produced at four different subcontractor facilities and in MCAIR facilities. All the flaws were cause for rejection based on MCAIR acceptance/rejection criteria. To determine frequencies of occurrence, discrepancy reports for 187 production assemblies, chosen at random, were reviewed and the total number of each type of flaw recorded. The results of this sampling are summarized in Table 2. The relative frequency of occurrence is indicated by the percentage of each type of flaw with respect to the total number of rejectable flaws detected. Metal-to-metal voids and disbonds were by far the most frequently occurring type of rejectable flaw. Metal-to-metal type voids and disbonds can occur for numerous reasons such as the difference between the height of the closure web of a honeycomb structure and the core height, misfit, slippage of tooling, improper pressure, voids in the uncured adhesive, failure to remove the adhesive protective release film and trapped foreign material.

Adhesive voids in metal-to-metal bonds can be caused by lack of pressure in the tooling or by air trapped in the adhesive prior to curing. It can also be caused by the combination of

TABLE 1
GENERIC FLAW TYPES AND FLAW PRODUCING MECHANISMS

Flaw Producing Mechanism	Generic Flaw Type				
	Metal-to-Metal	Metal-to-Core	Core	Surface	Adhesive
1. Disbonds, Internal	X				
2. Disbonds, Part Edge	X	X			
3. Disbonds, High Core	X				
4. Porosity	X	X	X		X
5. Unremoved Protective Release Film from Adhesive	X	X			
6. Foam Adhesive in Film Adhesive Bond Line	X	X			
7. Cut Adhesive	X	X			X
8. Adhesive Gaps	X	X			
9. Missing Adhesive	X	X	X		
10. Weak Bonds	X	X	X		
11. Extra Layers of Film Adhesive	X	X			
12. Foreign Objects	X	X	X		X
13. Double Drilled or Irregular Holes	X			X	
14. Disbonds, Low Core		X			
15. Void or Gap, Chemical Milled Land		X			
16. Void or Gap, Doublers		X			
17. Missing Fillets		X			
18. Voids, Closure-to-Core		X			
19. High Density Inclusions, (Chips, etc.)	X	X			X
20. Voids, Foam Joint		X	X		
21. Disbond, Shear Ties	X	X			
22. Lack of Sealant at Fasteners		X			
23. Thick Foam Adhesive		X			
24. Broken Fasteners	X	X			
25. Crushed Core			X		
26. Wrinkled Core			X		
27. Condensed Core			X		
28. Distorted Core			X		
29. Blown Core			X		
30. Node Bond Separation			X		
31. Missing Core (Short Core)		X	X		
32. Cut Core		X	X		
33. Water in Core			X		
34. Cracks				X	
35. Scratches				X	
36. Blisters				X	
37. Protrusions				X	
38. Indentations (Dents/Dings)				X	
39. Wrinkles				X	
40. Pits				X	

GP76-0471-30

TABLE 2
FREQUENCY OF REJECTABLE FLAWS IN ADHESIVELY BONDED ASSEMBLIES

Defect	Number of Defects	Percent of Total
Metal-to-Metal Voids and Disbonds	378	74
Skin-to-Core Voids and Disbonds	19	3
Gap in Core-to-Closure Bond	9	2
Lack of Foaming Adhesive or Voids in Foaming Adhesive	22	4
Difference in Core Density	6	2
Lack of Fillets	1	1
Crushed or Missing Core	32	6
Short Core	40	8
Totals	**507**	**100**

GP78-0471-25

imperfect parts and a rigid bonding tool, which prevents pressure sure from forcing the parts together. In a radiograph produced by low kilovoltage X-ray techniques the voids appear as dark, fairly well-defined images with a gray background. If the void results from insufficient pressure, the adhesive will be porous as indicated by dark spots or by a waffle pattern (freckles). The waffle pattern shown in the positive print of a radiograph in Figure 6, can occur with adhesives that have an embossed release film which transfers to the adhesive surface. Porosity can also be caused by small metal particles being left in the bondline following machining operations. Even with proper pressure, large, well-defined metal-to-metal flaws can result from trapped air. Because the air is trapped and pressure is applied along with an increase in temperature, the air bubble can cover a large area resulting in a void plus a thinning of the adhesive. Flaws caused by trapped air in the form of long, narrow (crack-like), circular, or porous areas were found to be the most frequently occurring types of metal-to-metal flaws. Other flaws occurring less frequently are variations in bondline thickness caused by poor fit-up of skin to substructure details, and linear-shaped unbonds resulting from gaps in the adhesive during layup or from failure to remove strips of the plastic or paper protective release film from the adhesive prior to fit-up with the assembly details.

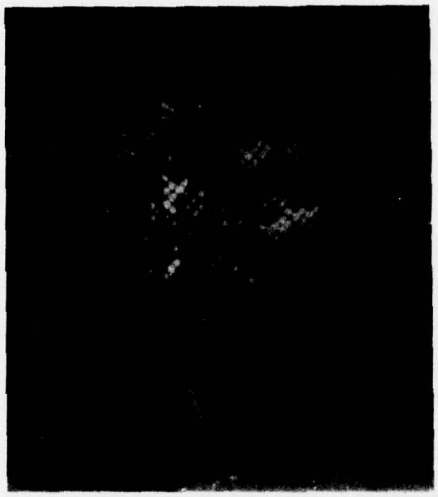

GP78-0471-26

FIGURE 6
FLAWS FROM LACK OF PRESSURE ARE VISIBLE IN RADIOGRAPH

Mechanically induced bondline damage is not created during the adhesive bonding process and was not included in Table 1. When skin-to-stringer subassemblies are handled without the structural stiffness they later gain when assembled into a large completed assembly, large peel stresses may result. Flaws which initiate as a result of handling damage are more like sharp cracks than the flaw formed during curing when the adhesive is semi-liquid and can form a fillet at the flaw boundary. Mechanically induced flaws are most likely to be formed at the edge of a bond, where flexure induced peel forces are highest. Edges of bonds generally experience the highest stresses in service.

2.3 Methods of Flaw Introduction

In this task, various methods of producing natural flaws in adhesive bonds were evaluated. This effort was directed at producing specific flaws in the type of specimens to be tested in Phase II.

As a result of these studies, methods of producing flaws were developed to produce the four naturally occurring flaws discussed in Section 2.2. The methods are: adhesive cut-out, wire insertion and a driven wedge. Although several other methods were evaluated, these particular methods gave the best results for the flaws selected to be reproduced in test specimens.

2.3.1 Adhesive Cut-Out - In order to make crack-like (elongated) voids and circular voids representative of naturally occurring adhesive bondline voids, cutouts were made in the adhesive film prior to curing. Crack-like voids in the adhesive were formed by cutting out long rectangular shapes. As the adhesive cured under temperature, it partially filled the cut-out creating a cracklike void such as shown in Figure 7.

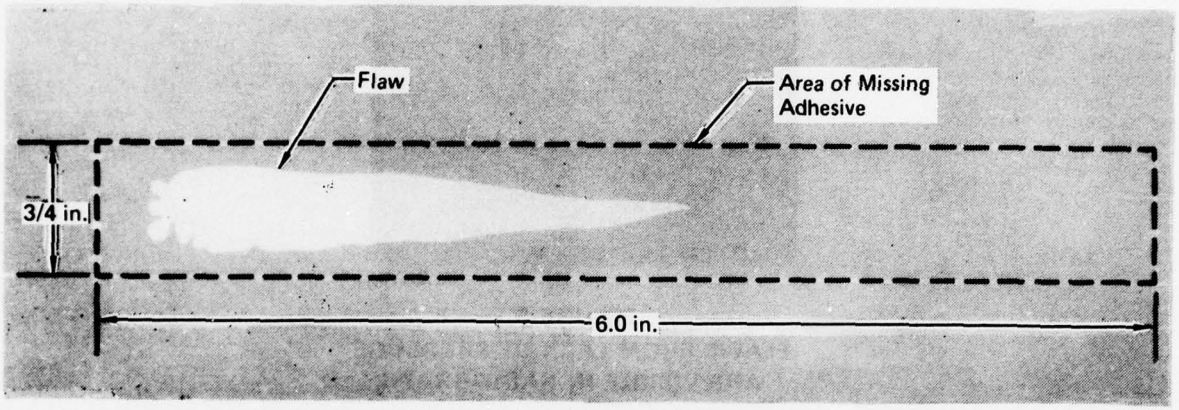

GP78-0471-7

FIGURE 7
FLAW PRODUCING MECHANISM - 3/4 IN. ADHESIVE GAP

2.3.2 Wire Insertion - Porosity can result from mismatched adherends, surface irregularities, and distortion in framing members. This type of flaw was reproduced by placing wires of specific diameters in the bondline prior to the cure cycle. The wires prevent proper bonding pressure between the adherends and cause porosity in the vicinity of the wire as shown in Figure 8. The wires are later removed during the machining process of the test specimens which then contain only the adjacent porosity. The wire insertion method is also used to produce thick-to-thin adhesives. In this case, wires are arranged such that specimens can be cut with the adhesive thickness variations in the desired direction.

2.3.3 Mechanical Damage - Mechanically damaged bondlines were created by driving a wooden or plastic wedge between two adhesively bonded adherends. In most cases, tabs were machined into one of the adherends where it was desired to separate the adherends. The wedge was then driven against the bond edge at the tab location, forcing a cleavage failure in the adhesive.

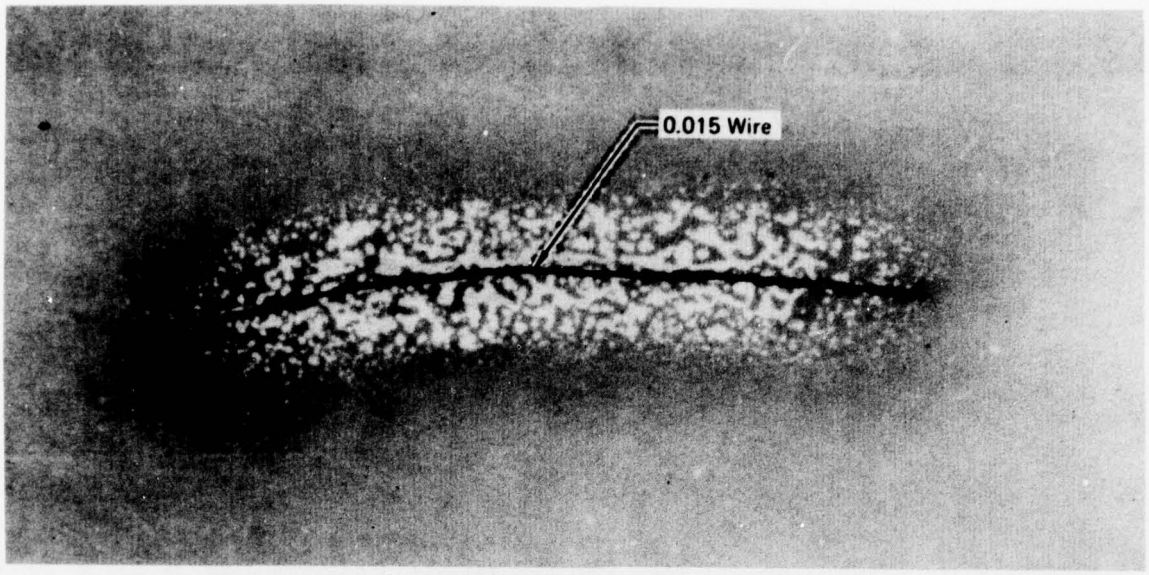

GP78-0471-6

FIGURE 8
FLAW PRODUCING MECHANISM - 0.015 WIRE INSERTION

2.4 Methods of Flaw Detection

Radiographic and ultrasonic non-destructive inspection methods were used to detect bondline flaws in Phase II test specimens.

Low kilovoltage x-ray was very effective in locating adhesive voids and porosity in specimens bonded with AF-55 adhesive because it is radio-opaque. Voids in specimens bonded with FM-73 adhesive, which is essentially a radio-transparent adhesive, were also detectable but required more careful inspection of the radiograph. X-ray parameters ranged from 30 to 35 kilovolts and 23 to 25 milliamperes, depending on the thickness of the bonded aluminum sheets. Exposure time was one minute on Kodak AA Ready Pack film. The focal spot-to-film distance was 60 inches.

The thru-transmission reflector plate ultrasonic technique was used to find initially induced unbonds in the specimens as well as those occurring as a result of fatigue cycling. A detailed description of this NDE method is in Section 4.2. Using this method, a multi-tone printout, as shown in Figure 9, was obtained for each specimen showing flaw locations. Flaws are shown as solid white areas and bonded areas are printed out as multi-tone lines. The multi-tone printout is achieved through an electronic gating device which monitors the strength of the

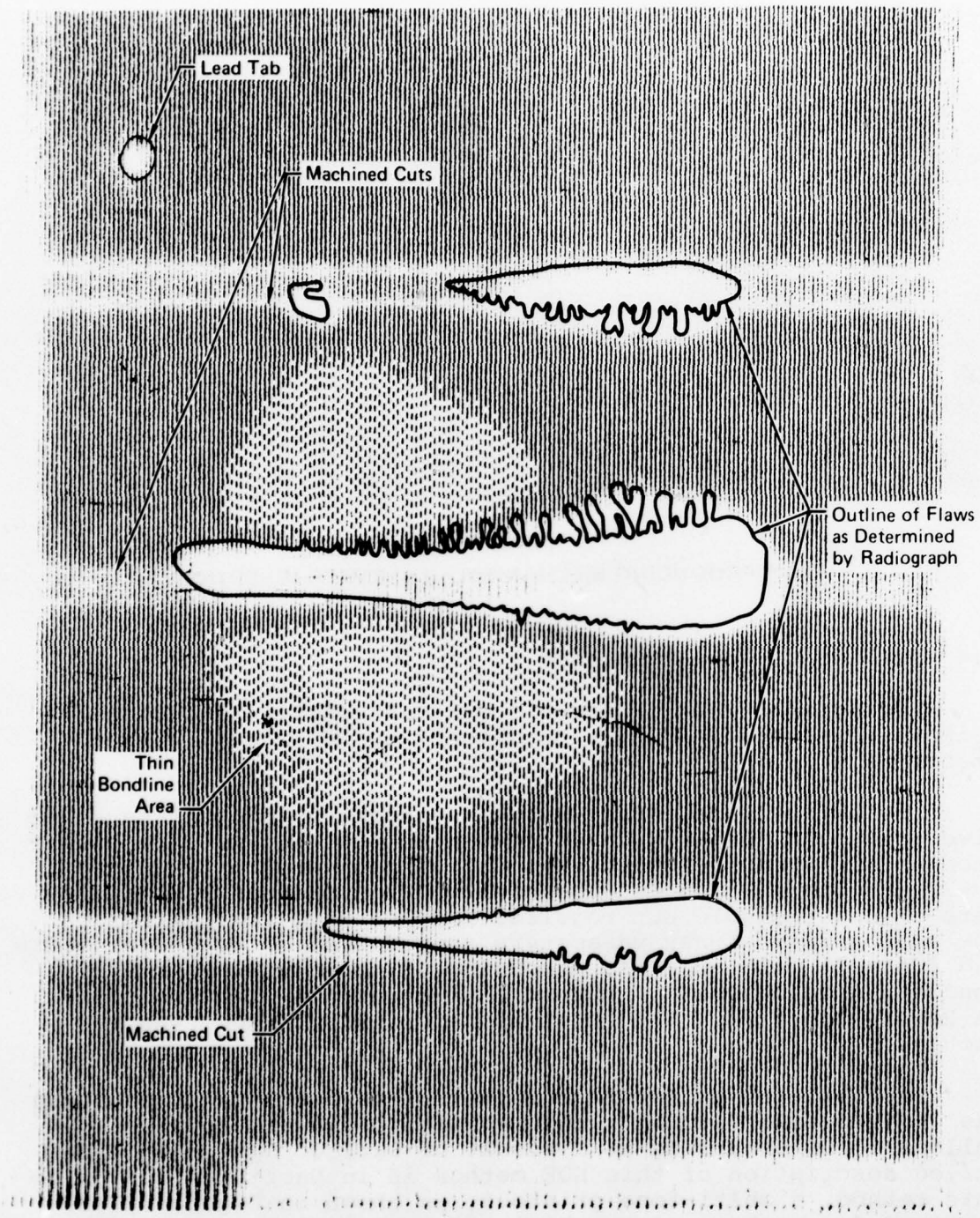

GP78-0471-24

FIGURE 9
MULTI-TONE C-SCAN OF FLAWED SPECIMEN

signal received from the ultrasonic search unit and triggers the printer to produce certain types of lines, depending on preselected signal levels. Light gray lines, progressing to darker lines, correspond to an increasing signal strength. Dashed lines correspond to very high signal strengths, above a preselected level. In the figure, the dashed lines indicate a very thin adhesive. The gray horizontal images are machined slots in the adherends. Lead tabs attached to the specimen are used for calibrating the printout instrument. Outlines of the flaws as determined from radiographs are superimposed on the c-scans to illustrate the accuracy of the method.

3. PHASE II - SIMPLE SPECIMEN EVALUATION

The objective of this task was to determine whether or not flaws grow under cyclic loadings, and, if flaws do grow, what combinations of specimen type, flaw type, and environment are the most critical for flaw growth. A two phase test program was conducted to evaluate growth characteristics of the most commonly occurring flaws. Test specimens were designed to represent selected adhesive bonded joints of the PABST fuselage structure. Test environments were chosen to cover the range of temperatures and humidity conditions anticipated for the PABST fuselage.

In the first part of this test program, specimens with intentionally induced bondline flaws were fatigue tested under several combinations of loading and environment. In this manner, it was possible to determine which combinations of test specimen configuration and test condition were the most critical for flaw growth. Except for a preliminary investigation on the effect of cycle rate, all of this testing was done at the fast cycle rate of 30 Hz.

In the second part of the test program flaw growth for those critical combinations of flaw types, specimen configurations and environments were evaluated by fatigue testing at a slow cycle rate of two load cycles per hour.

3.1 Phase II Test Plan

In a preliminary evaluation of the effect of cycle rate on flaw growth, eight double-doubler specimens were fatigue tested at room temperature. Three specimens were tested at each of two cycle rates, 30 Hz and 8 Hz, and two were tested at the slow cycle rate of two cycles per hour. The objective of these preliminary tests was to verify the findings of other investigators which had shown adhesive bonded joints to have a higher number of cycles to failure when loaded at fast-cycle rates, e.g. 30 Hz, than when cycled at much slower rates. Although these preliminary tests were not conclusive in themselves, the Air Force and other industry investigators had, by this time, done sufficient testing to conclude that the durability of bonded joints was affected by the test cycle rate. In light of this information and in order to provide the most meaningful data, this program was revised by substituting tests at a slow cycle rate for some of the fast cycle tests. As part of the revised program plan, provisions were made for fabricating six self-contained environmental test chambers for testing specimens at the slow cycle rate.

FM-73 adhesive was selected for the PABST Program after AF-55 adhesive had been selected for this program, and the program was revised to include comparative testing of the two adhesive systems. The purpose of these additional tests was to determine the applicability of AF-55 adhesive flaw growth data to the FM-73 system. Tables 3 and 4 summarize the scope of testing at the

TABLE 3
FAST CYCLE (30 Hz) TEST MATRIX

Specimen Configuration			Environment - °F					
			AF-55			FM-73		
Type	Adherend Thickness	Flaw Type	−50	140 (Hum)	140 (Dry)	−50	140 (Hum)	140 (Dry)
Double-Doubler	0.040/0.080/0.040	Crack-Like Voids	2	1				
		Circular Voids	2	4				
		Mechanical Damage	1	2				
Single-Doubler	0.080/0.040	Crack-Like Voids	6	2				
		Circular Voids	2	2	1			
		Porosity	2	2		2		
		Mechanical Damage	3	1	1			
	0.040/0.020	Crack-Like Voids		2				
		Circular Voids		2				
Single-Strap	0.090/0.080	Crack-Like Voids	4	5		2	2	1
		Circular Voids	2	2		2	2	
		Porosity	2	2	1	3	2	
		Mechanical Damage	1	2			2	
		Variable Adhesive Thickness	4	4	1			
Skin-to-Substructure Tee	0.063/0.040	Crack-Like Voids	2	2			2	
		Circular Voids	3	1	1		2	1
		Porosity	5	1			2	
		Mechanical Damage	2	2	1	2		
	0.063/0.080	Crack-Like Voids	2					
		Circular Voids	2					
		Mechanical Damage	2					
Double-Strap	0.040/0.080/0.040	Crack-Like Voids	2	3			2	
			51	42	6	11	16	2
			99			29		

GP78-0471-21

TABLE 4
DAC CYCLE TEST MATRIX

Specimen Configuration			Environment - °F			
			AF-55		FM-73	
Type	Adherend Thickness	Flaw Type	−50	140 (Hum)	−50	140 (Hum)
Double-Strap	0.040/0.080/0.040	Crack-Like Voids		6		6
Single-Doubler	0.080/0.040	Crack-Like Voids	6	6		
		Circular Voids		6		
		Porosity	6	6		
		Mechanical Damage		6		
Single-Strap	0.090/0.080	Crack-Like Voids	6	6		6
		Circular Voids		6		
		Porosity				
		Mechanical Damage		6		
	0.090/0.080	Variable Adhesive Thickness		6		
Skin-to-Substructure Tee	0.063/0.040	Crack-Like Voids	6	6		
		Circular Voids	6	6		
		Porosity	6	6		
		Mechanical Damage	6	6		
	0.063/0.080	Crack-Like Voids				
		Circular Voids		6		
		Mechanical Damage	6		6	
			48	84	6	12
			132		18	

GP76-0471-22

Load vs Time for the DAC Cycle.

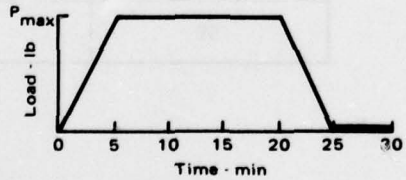

fast and slow cycle rates, respectively. A diagram of load versus time for the slow cycle rate, hereafter referred to as the DAC cycle rate is shown with Table 4. This loading cycle is the same as that used in the PABST Program for slow cycle fatigue testing.

All of the test specimens were sized to be representative of the current range of adherend thicknesses used in the PABST fuselage structure. Flaw types and test conditions were selected to achieve the most information on flaw growth characteristics over the range of anticipated real flight conditions. Crack-like flaws in the adhesive were considered to be the type most likely to grow under cyclic loading and were therefore evaluated in each type of specimen. All flaws were placed in locations of high stress in the specimen bondline. For most specimens, this was near the edge of the bondline where the shear stress is highest. The test environments of -50°F or 140°F combined with a relative humidity of 95-100% were selected because they were the extremes of environments to be experienced by the PABST fuselages. A few specimens were tested at 140°F, but without humidity, for comparison purposes.

3.2 Specimen Analysis

All of the specimens were analyzed with the methods used in the PABST program. These are described in References 4 and 5. In these methods, an elastic-plastic idealization of the actual shear stress-strain curve, as shown in Figure 10, was used. The idealized curve is in the form of a trapezoid which encloses the same area (shear strain energy) as the real shear stress-strain curve. The ultimate values of shear stress (τ_p) and shear strain ($\gamma_e + \gamma_p$) for the idealized curve are set at the maximum values developed on either torsion ring or thick adherend shear specimens. The elastic strain (γ_e) is then set at that value for which the strain energy under the idealized curve is equal to that under the actual curve. The shear modulus is the slope of the elastic portion of the idealized curve. The adhesive properties used for all analysis in this program are summarized in Table 5.

Double-Doubler and Double-Strap Specimen - Longitudinal bonded splices on the PABST fuselage, depicted in Figure 1(a) were simulated by the double-doubler and double-strap type specimen. Configuration details of both type specimens are shown in Figure 11.

This specimen consisted of a sandwich of three sheets of metal. All of the load was introduced into the middle sheet (skin) with some of that load transferred through the bond into

(4) Hart-Smith, L. J., "Adhesive-Bonded Double-Lap Joints", NASA-Langley CR-112235, January 1973.
(5) Hart-Smith, L. J., "Adhesive-Bonded Single-Lap Joints", NASA Langley CR-112236, January 1973.

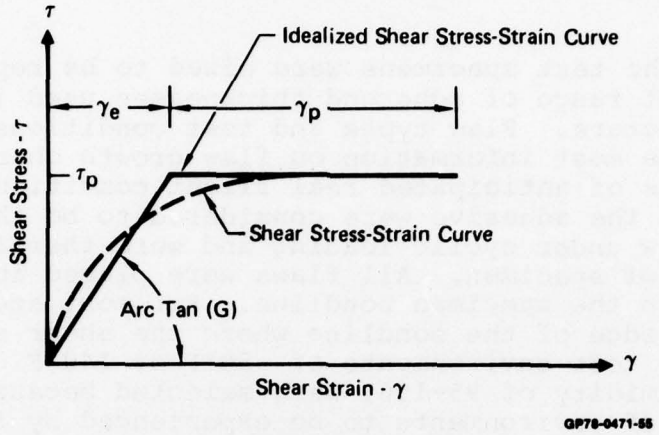

FIGURE 10
IDEALIZATION OF SHEAR STRESS-STRAIN CURVE

TABLE 5
ADHESIVE PROPERTIES USED IN BONDED JOINT ANALYSES

Temperature °F	τ_p (psi)	G (psi)	γ_e (in./in.)	γ_p (in./in.)
R.T. (70°)	5,000	70,000	0.071	1.0
−50°	6,000	80,000	0.075	0.5
140°	2,500	40,000	0.063	1.5

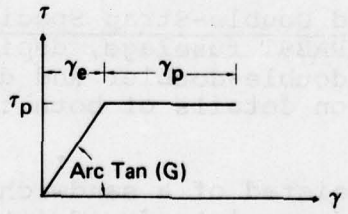

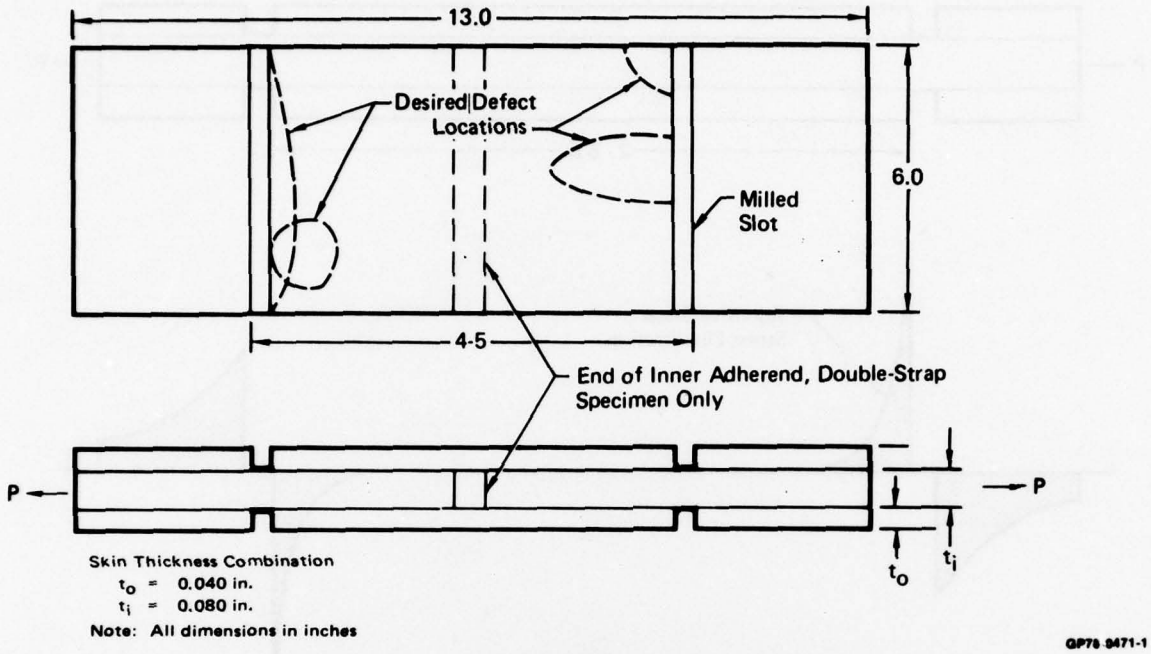

FIGURE 11
DOUBLE-DOUBLER OR DOUBLE STRAP SPECIMEN

the outer sheets (doublers). The machined slots in the doublers were precisely located such that the bondline flaws were in the high shear stress region at the edge of the doublers. The depths of the slots were also precisely machined through the doublers down to the adhesive but not touching the inner adherend.

The double-doubler specimen is also representative of symmetric doublers, stiffener mounts, and single bond joints supported on moment resistant foundations. Although the shear stress distributions at the edge of the doubler were identical for both specimens for a given loading condition, several double-strap specimens were tested under conditions identical to those used for double-doubler specimen tests in order to evaluate residual bondline strength after fatigue cycling. Residual strength of double-doubler specimens could not be determined because the center adherend is continuous throughout the length of the specimen. At the beginning of the program, it was considered improbable that naturally induced flaws could be precisely located in a double-strap joint and therefore the double-doubler specimen was used for initial testing. Later, as more experience was gained, it was possible to precisely locate flaws at the center as well as the ends of the double-strap specimen. Data from both types of specimens are directly comparable because of equivalence in shear stress distributions as illustrated in Figure 12.

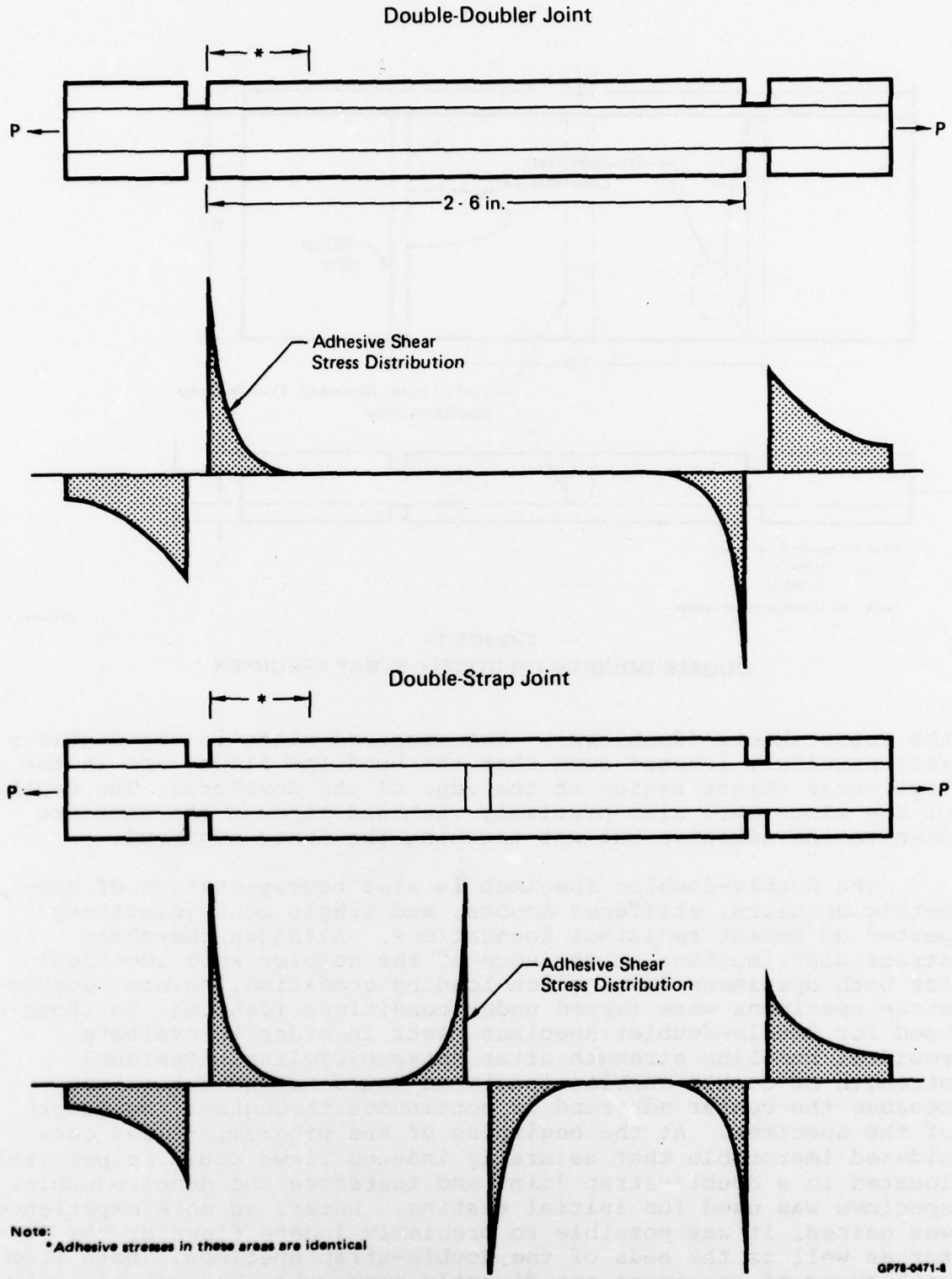

FIGURE 12
EQUIVALENCE OF DOUBLE-DOUBLER AND DOUBLE-STRAP JOINTS

The design running load along the longitudinal skin splice was derived from internal pressurization and the fuselage radius. For the PABST fuselage, this is 770 pounds per inch. By using the methods of analysis presented in References 4 and 5, it can be shown that the maximum adhesive shear stress for a specific double-doubler configuration can be duplicated on different thickness specimens by adjusting the applied load. For example, a maximum shear stress of 1900 psi, produced by the 770 lbs/in loading in the PABST joint thicknesses of 0.025/0.050/0.025, can also be achieved by a loading of 974 lbs in in a double-doubler test specimen with a thickness combination of 0.040/0.080/0.040.

Although geometric parameters such as adherend thickness and splice overlap may vary throughout the fuselage, the shear stress distributions will be very similar over a wide range of loads, geometries and environmental conditions. Adhesive shear stress distributions in a double-doubler specimen for applied loads ranging from 800 to 2400 lbs/inch in three environments, and for overlap lengths ranging from 4 to 6 inches are presented in Figure 13.

The shear stress drops to zero within the first inch of the overlap in each of the three environmental conditions investigated. This is typical of single-doubler and single-strap specimens as well. Therefore, flaws placed in the region along the edge of the specimens will be in the area of high shear stresses.

Single-Doubler Specimen - Configuration details of the single-doubler specimen are shown in Figure 14. This specimen simulates single bonds on the PABST fuselage such as reinforcement doublers (Figure 1(c) and (e)) which do not have the parallel load path of the double-bond joint. Because of this, it experiences slightly higher peel stresses than symmetric joints, a significant distinction when considering flaw growth. The maximum shear stress for a single-doubler specimen is calculated using the same equations as for the double-doubler specimens (see Reference (3)) by assuming the thickness of the skin (inner adherend) and the applied load are doubled. Using the idealized bi-linear shear stress-strain distribution, the maximum adhesive shear stress in this type of specimen is computed to be directly proportional to the applied load until the elastic shear strain of the adhesive is reached. The test loads for the single-doubler specimens, shown in Table 6, were calculated to exactly duplicate maximum shear stresses in the .080 skin/.040 doubler and the .040 skin/.020 doubler combinations used on the PABST fuselage and are the peak shear stresses within the general range of peak shear stresses for the other skin/doubler combinations used on the PABST fuselage.

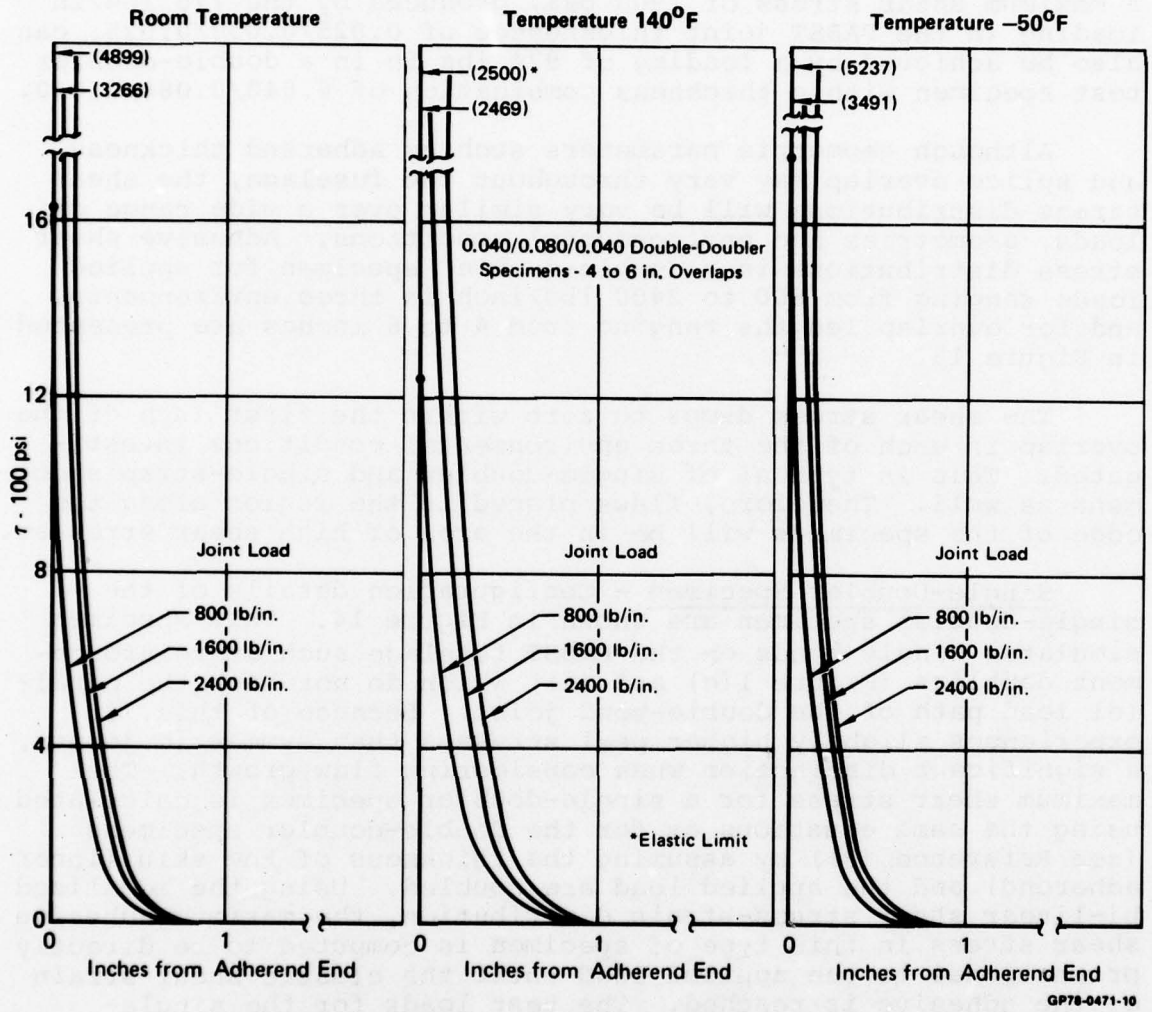

FIGURE 13
SHEAR STRESS DISTRIBUTIONS ARE SIMILAR OVER A WIDE RANGE OF LOADS

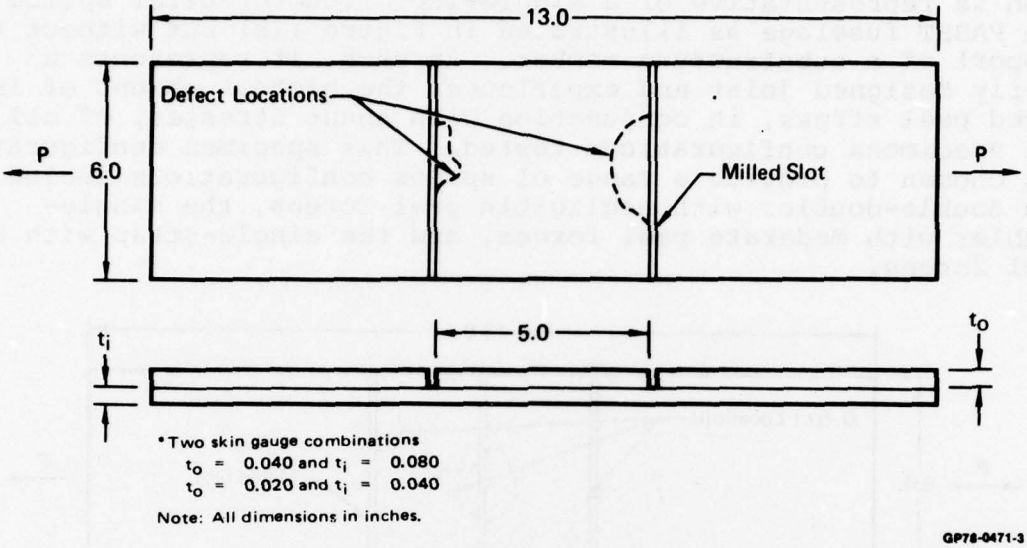

FIGURE 14
SINGLE-DOUBLER SPECIMEN

TABLE 6
COMPARISON APPLIED LOADS TO PABST DESIGN LOADS FOR SINGLE-DOUBLER SPECIMENS

Skin Gauges Skin/Doubler	Applied Load (lb/in.)	Maximum Shear Stress		
		R.T.	140°F	−50°F
PABST Program				
0.050/0.050	1280	4672	2500*	5003
0.050/0.030	1024	5000*	2500*	5775
0.071/0.063	1715	5000*	2500*	6000*
0.080/0.040	1536	5000*	2500*	6000*
Test Specimens				
0.040/0.020	1000	4998	2500*	5350
0.080/0.040	1536	5000*	2500*	6000*

*Exceeded elastic limit

GP78-0471-15

Single-Strap Specimen - Configuration details for the single-strap specimen are shown in Figure 15. This specimen configuration is representative of a single-lap circumferential splice on the PABST fuselage as illustrated in Figure 1(b) but without the support of a substructure member. As such, it represents a poorly designed joint and experiences the highest amount of induced peel stress, in conjunction with shear stresses, of all the specimens configurations tested. This specimen configuration was chosen to provide a range of splice configurations including the double-doubler with negligible peel forces, the single-doubler with moderate peel forces, and the single-strap with high peel forces.

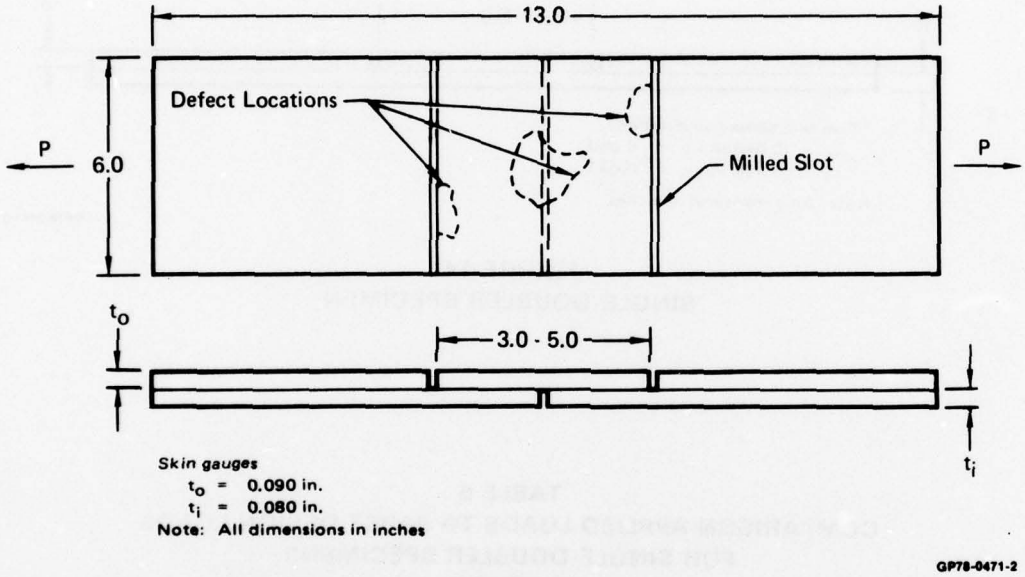

FIGURE 15
SINGLE-STRAP JOINT SPECIMEN

Because of the eccentricity of load path, the unsupported single-strap joint can be critical in the adhesive due to peel forces or in the adherend due to bending. Both of these parameters were evaluated using the analysis methods of Reference 4, in order to design a specimen in which the adhesive stresses were maximized and the adherend stresses minimized. Table 7 contains a summary of the maximum adhesive peel stress, splice adherend stress, and predicted cycles to failure for two specimen thickness combinations, assuming a two inch splice overlap. The test loads are based on axial running loads in the skin caused by fuselage bending and were determined in the PABST program (Reference 1). The 0.080/0.090 thickness combination was used in this program for all single-strap specimen tests. This combination gave the desired high peel stresses in the adhesive and adequate adherend fatigue life. Flaws were located in the areas of peak peel stresses, near the ends of the splice overlap.

TABLE 7

SINGLE STRAP SPECIMEN ANALYSIS SUMMARY

Specimen Configuration 2 In. Overlap	Load (lb)	Maximum RT Peel Stress (psi)	Maximum Strap Stress (psi)	Predicted Strap Life Cycles (RT) 1
0.040 Skin/0.050 Strap	670	4,000	30,000	10^8
0.080 Skin/0.090 Strap	1,000	8,350	34,000	10^7

1 R = 0.10, Constant amplitude cycling based on Military Handbook 5B, Figure 3.2.3.1.8(b).

GP78-0471-17

Skin-to-Substructure Specimen - Configuration details for skin-to-substructure tee specimens are shown in Figure 16. This specimen type simulates circumferential and longitudinal frame stiffeners bonded to the fuselage skin. Loadings for two types of failure modes were considered for this type specimen in order to determine an appropriate load for fatigue cycling tests. One failure mode results from tension forces between the skin and stiffener caused by internal fuselage pressure. In this case, the stiffener may prevent the skin from deflecting enough to carry the loads entirely as hoop tension, thus causing tension forces between the skin and stiffener. A second failure mode occurs at the onset of shear buckling in the skin, also creating tension forces between the skin and stiffener. Loadings for these two failure modes, which were derived in the PABST Program for the full range of expected thicknesses for wide body fuselages, are shown in Figure 17. Test loads were based on this data. The maximum test load for a tee specimen with 0.040 skins was 100 pounds per inch. For tee specimens with 0.080 skins, the maximum test load was increased slightly over that shown in the figure to 80 pounds per inch.

Most flaw types investigated were located along the edge of the tee where maximum shear and peel forces occur. For comparison purposes, several specimens had flaws located in the middle of the tee base.

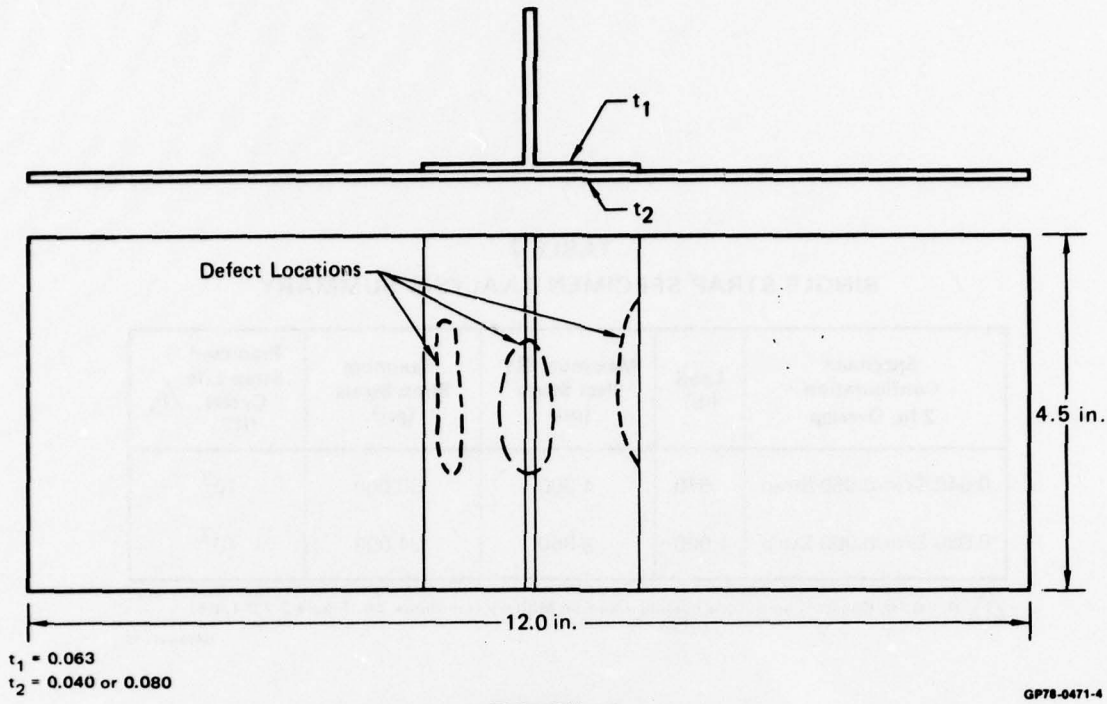

FIGURE 16
SKIN-TO-SUBSTRUCTURE SPECIMEN

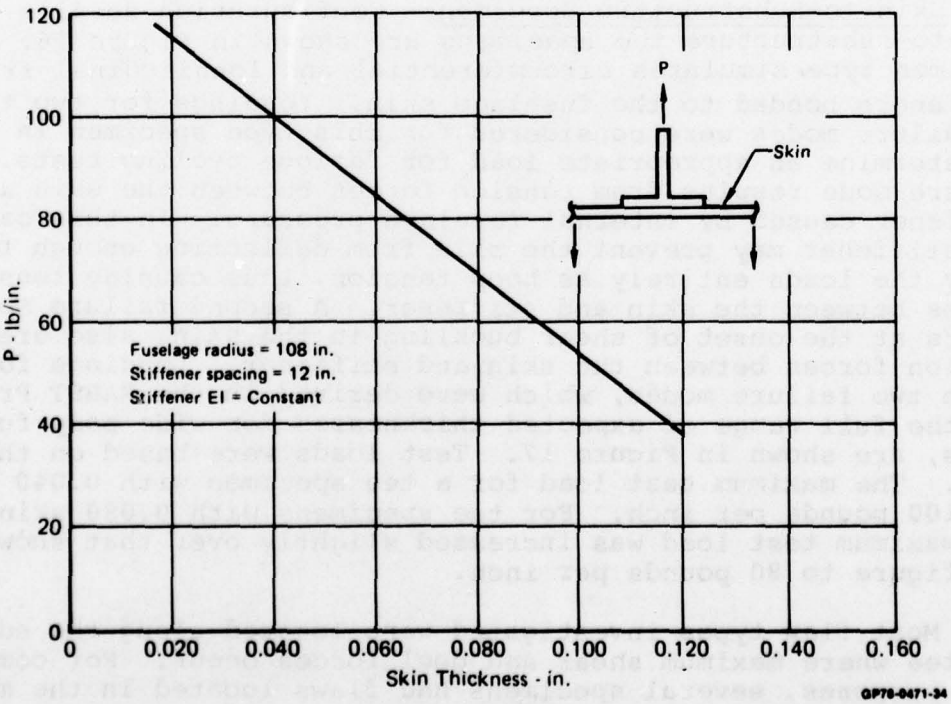

FIGURE 17
TEST LOADS FOR SKIN-TO-SUBSTRUCTURE SPECIMENS

3.3 Test Procedure

All specimens were ultrasonically c-scanned at least twice by the method described in Section 2.0. Prior to testing, they were c-scanned to verify that the flaws were in the intended locations and to provide a baseline print-out record for comparison to scans made later. For fast cycle testing, each specimen was cycled to failure or to one million cycles. Those specimens which endured at least one-half million cycles were removed from the loading fixture and c-scanned to determine if flaw growth had initiated. Following this intermediate c-scan, the specimens were reinstalled in the loading fixture and cycling resumed until 10^6 cycles were accumulated. They were then c-scanned for the third time and flaw growth characteristics noted by comparing to previous c-scans. All single-strap, double-strap, and tee specimens which survived 10^6 cycles were static tested to failure. The failed surfaces of each specimen were closely examined to verify flaw location, size, and growth if it occurred.

The same procedure was followed for specimens cycled at the DAC cycle rate except that no intermediate c-scans were made prior to reaching the goal of 4000 DAC cycles.

Sonntag universal testing machines were used for all fast cycle (30 Hz) fatigue tests. Environmental conditions were controlled by using small insulated chambers around the specimen into which moist pre-heated air or nitrogen gas was pumped. A typical fast-cycle fatigue test setup for the tee specimen and for the all metal lap specimens is shown in Figures 18 and 19, respectively. The eight specimens which were tested in a preliminary evaluation of the effect of cycle rate utilized an MTS machine. A typical test setup for these tests is shown in Figure 20.

Six special loading fixtures were fabricated for cycling specimens at the DAC cycle rate in the specified environments. Two of the fixtures are shown in Figure 21. Each loading fixture consists of a pneumatic piston and housing mounted to a 14 inch diameter by 8-foot long stainless steel cylinder. Load is applied to a string of six specimens by the piston and reacted by a clevis attached to the opposite end of the cylinder. Doors in the sides of the cylinder provide access to the specimens. Sagging of the string of specimens was prevented by intermittent supports. Each fixture is equipped with individual load and temperature controls and serves as an independent environmental chamber. Water placed inside the horizontal fixtures was heated to 140°F by the use of blankets attached to the outer surface of the cylinder. Relative humidity within the chambers ranged from 95 to 100% of saturation. To provide the low temperature (-50°F) environment, boil-off from liquid nitrogen was pumped into the chambers through a solenoid valve actuated by a temperature controller.

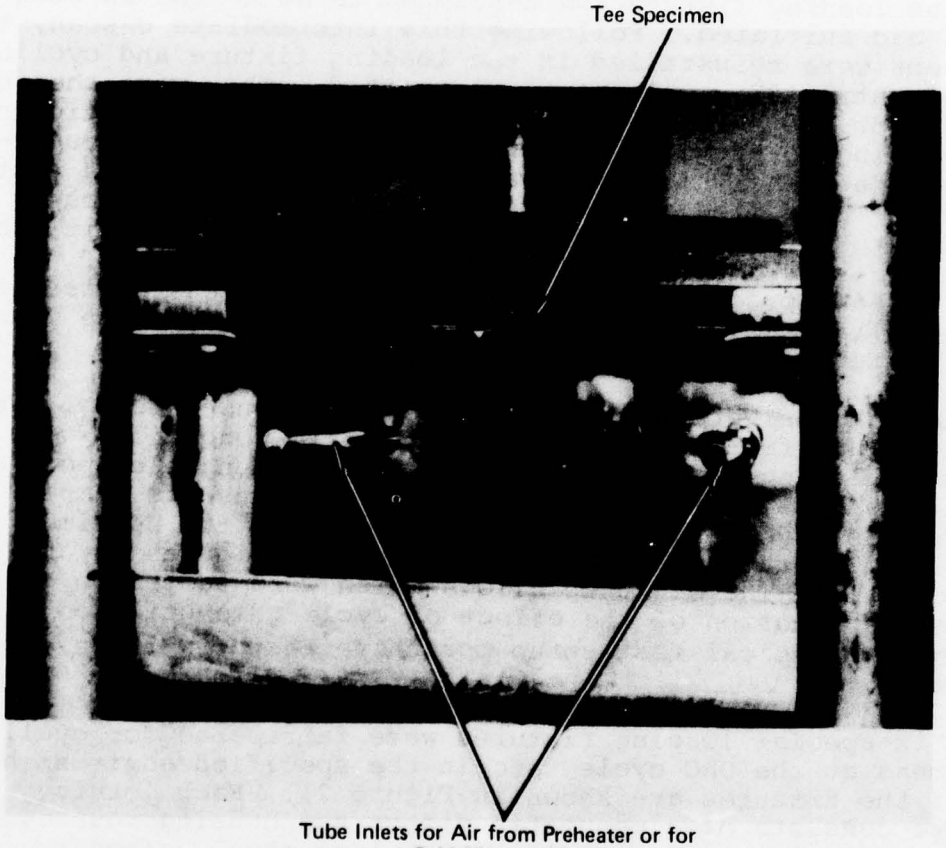

GP78-0471-27

FIGURE 18
FAST CYCLE FATIGUE TEST SETUP FOR TEE SPECIMENS

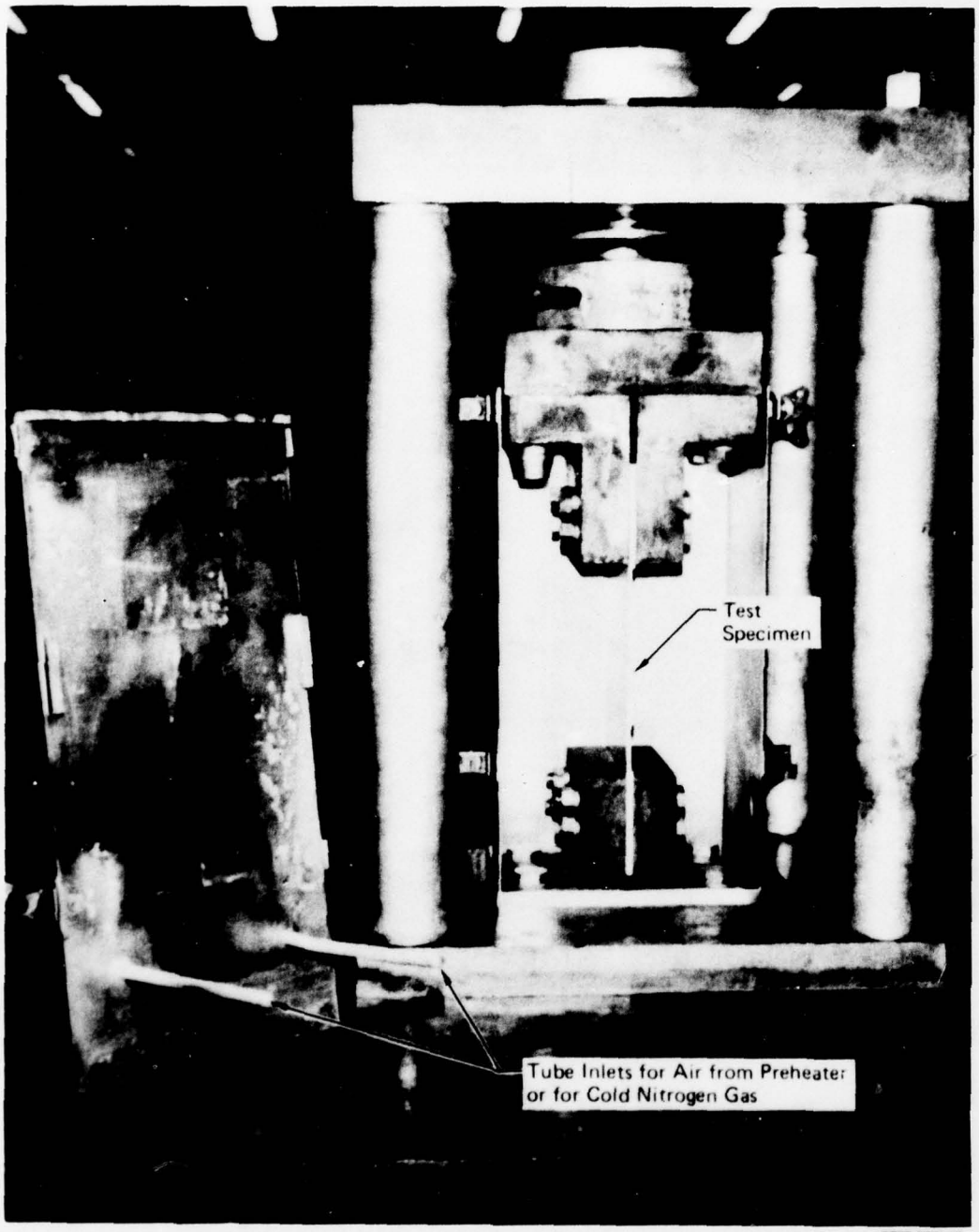

GP76-0471-33

FIGURE 19
FAST CYCLE FATIGUE TEST SETUP FOR METAL LAP SPECIMENS

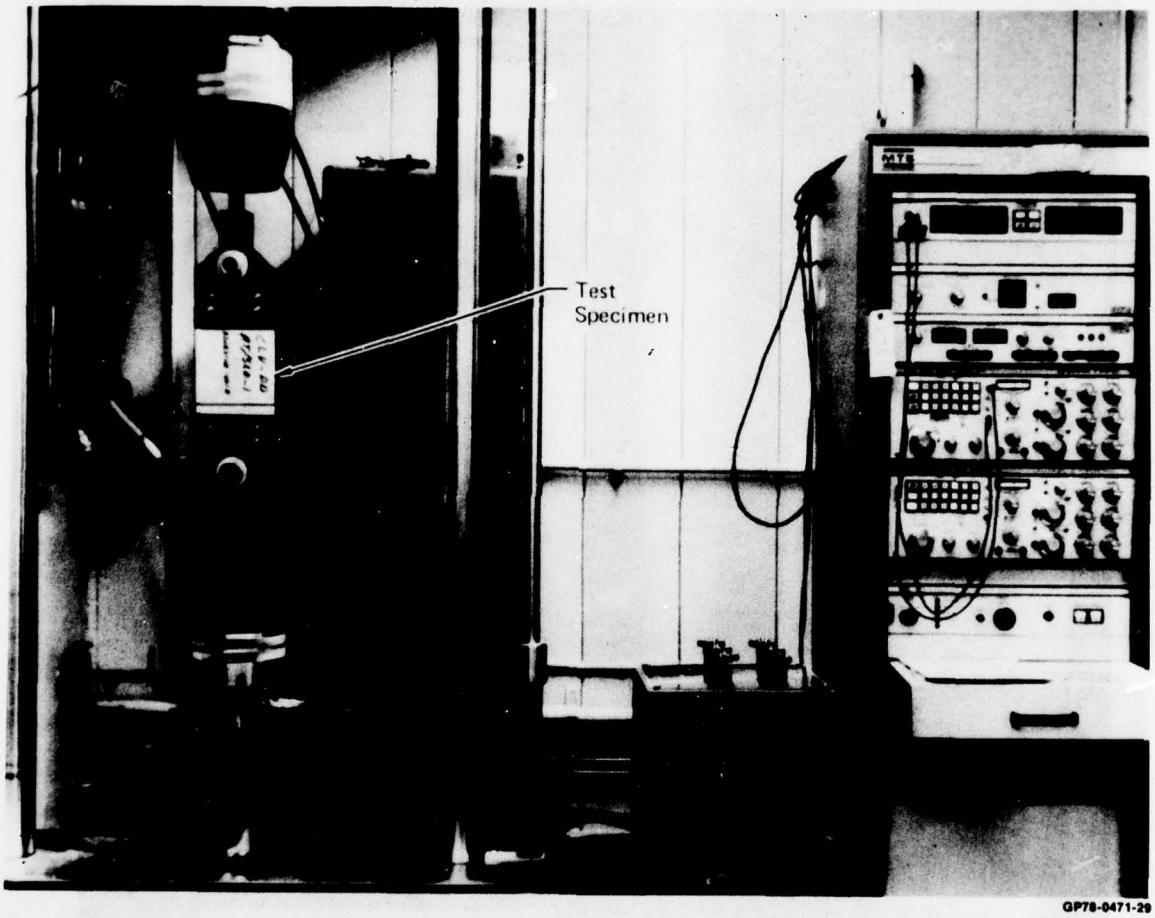

GP78-0471-29

FIGURE 20
TEST SETUP FOR PRELIMINARY TESTS ON EFFECT OF CYCLE RATE

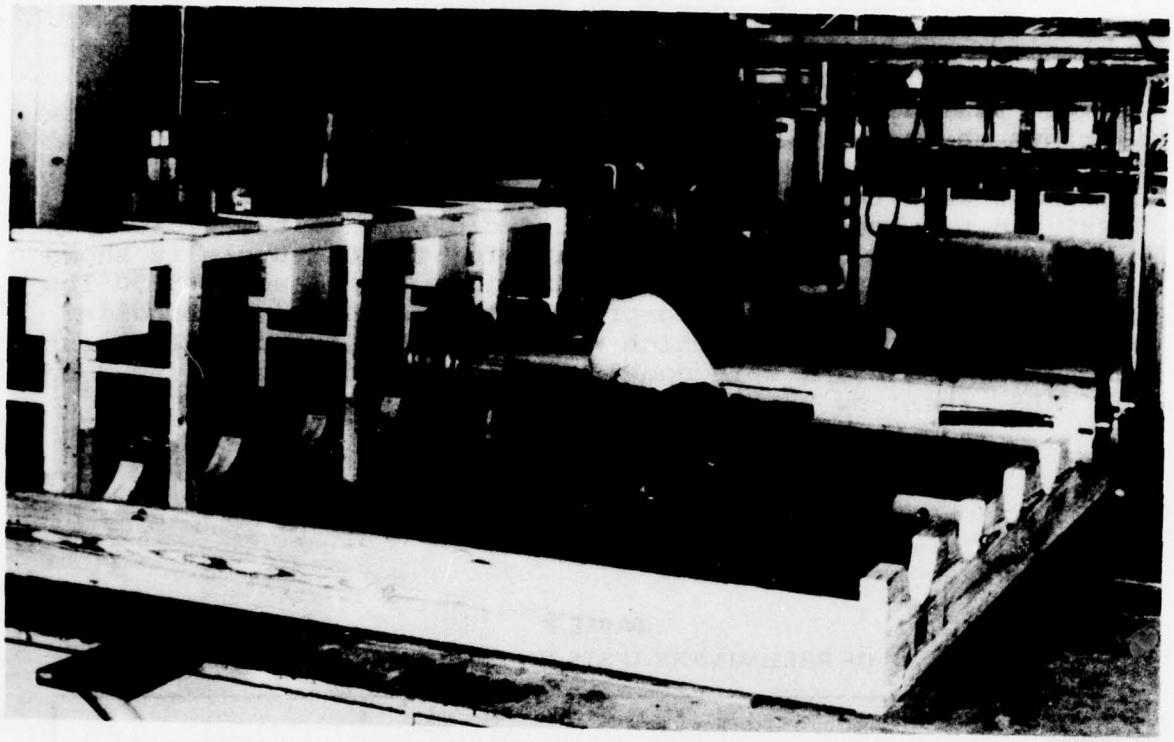

GP76-0471-26

FIGURE 21
SLOW-CYCLE TEST FIXTURES

3.4 Fast Cycle Fatigue Tests

The purpose of this phase of the test program was to determine whether bondline flaws will grow under cyclic loadings. Specimen configurations as described earlier, representative of actual bonded fuselage details, with intentionally induced flaws in the bondline were fatigue tested under extreme hot and cold environmental conditions. The test matrix for fast cycle fatigue is presented in Table 3. It includes specimen configurations, types of bondline flaws, and corresponding environmental test conditions. The basic intent of this series of tests was to obtain information as soon as possible on factors affecting bondline durability. The test cycle rate of 30 Hz was chosen for these investigations in order to evaluate as many combinations of specimen configuration, flaw type, and environment as possible within a reasonable time span. Further characterizations of flaw growth, based on the results of the fast cycle tests, were accomplished by testing similar specimens at the DAC cycle rate of 2 cycles per hour. In addition to the tests described in Table 3, eight specimens were tested in a preliminary investigation of the effect of cycle rate.

3.4.1 Results of Preliminary Testing on Effect of Cycle Rate - The results of the preliminary tests of the effect of cycle rate on durability of specimens with adhesive flaws, are summarized in Table 8. Eight double-doubler specimens were fatigue tested at room temperature. Each consisted of an 0.080 aluminum sheet representing the fuselage skin, with 0.040 aluminum sheets bonded to each side representing doublers. Three specimens were tested at each of two cycle rates: 30 Hz and 8 Hz, and two specimens at the DAC cycle rate of two cycles per hour. A diagram of load versus time for the DAC cycle is shown in the footnotes of Table 8. The maximum test load of 5850 lbs (974 lbs/in) was selected to produce the same maximum bondline shear stress of 1990 psi which would be experienced by the most frequently occurring skin/doubler thickness combination used on the PABST fuselage.

TABLE 8
RESULTS OF PRELIMINARY TESTS ON EFFECT OF CYCLE RATE

Double-Doubler Specimen No.	Specimen Test Parameters				Max Shear Stress (psi)	Results
	Environment	Cycle Rate	Max Load (lb)	Stress Ratio		
1 2 3	RT	30 Hz	5850	R = 0.10	1990	C-Scan of flaws showed no Growth after 10^6 cycles.
4 5 6		8 Hz				C-Scan of flaws indicated no growth after 10^6 cycles.
7 8		DAC* Cycle				C-Scan of flaws indicated no growth after 129 cycles. Test suspended because of program revision.

*The DAC cycle rate is two cycles per hour with a load vs time history as shown below:

GP78-0471-30

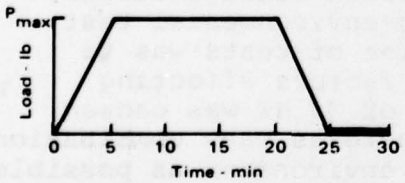

Crack-like voids in the adhesive bondline were located at the edges of the 0.040 doubler similar to that shown in the full-scale radiograph of Specimen No. 1 in Figure 22. Ultrasonic c-scans of the specimens made before, during, and after cycling, were used to determine whether or not flaw growth occurred. The initial and final c-scans of one end of Specimen No. 1 are shown in Figure 23. The flaw, as indicated by the white area located parallel to the edge of the 0.040 doublers, did not change in size or shape during the time of fatigue cycling. This lack of flaw growth was verified by tracing the flaw outline from the original ratiograph and c-scan and over-laying it on the corresponding flaw indication of the c-scan made after the test was completed. Inspection of the c-scans in this manner revealed no evidence of flaw growth after 10^6 cycles for specimens cycled at 30 Hz, 8 Hz, and after 129 cycles for those cycled at the DAC cycle rate. Because no flaw growth occurred in these preliminary "quick look" tests, the original program test plan and test matrix was revised. The revised program plan was to use higher loadings in the fast cycle testing than originally planned as well as larger than anticipated flaws in order to test flawed bondlines under extremely severe conditions. The program plan for slow (DAC) cycle fatigue testing was to use realistic flaw sizes, and actual loading intensities derived from the PABST Program. Testing would be accomplished only under the extreme hot or cold environmental conditions, eliminating tests planned at room temperature.

3.4.2 Results of Fast-Cycle (30 Hz) Fatigue Testing - The test conditions and specimen configurations investigated during this series of testing are summarized in Table 3. The results of these tests influenced the selection of many of the specimen configurations and environmental conditions used in further evaluations of flaw growth characteristics at the DAC cycle rate. Only a relatively small number of double-doubler and double-strap specimens were fatigue tested in this series of tests because of the preliminary tests discussed in Section 3.4.1 which indicated that double-doubler specimens would produce little data on flaw growth. Most testing at the fast cycle rate was conducted with the 0.080 skin/0.090 splice single-strap type specimen because it was believed to be the most critical for flaw growth due to induced peel forces.

At the beginning of this phase of testing, test loads for several specimens were arbitrarily increased above the PABST fuselage design loads in an attempt to load the flawed bondlines as high as possible without failing the adherends. In several specimen configurations, however, the adherends failed in fatigue before the scheduled ultrasonic inspections for flaw growth. To increase fatigue life of the adherends, subsequent test loads were reduced, the minimum test loads being equal to the PABST design loading. Test conditions and results for each of the specimen tests are tabulated and discussed in the following paragraphs.

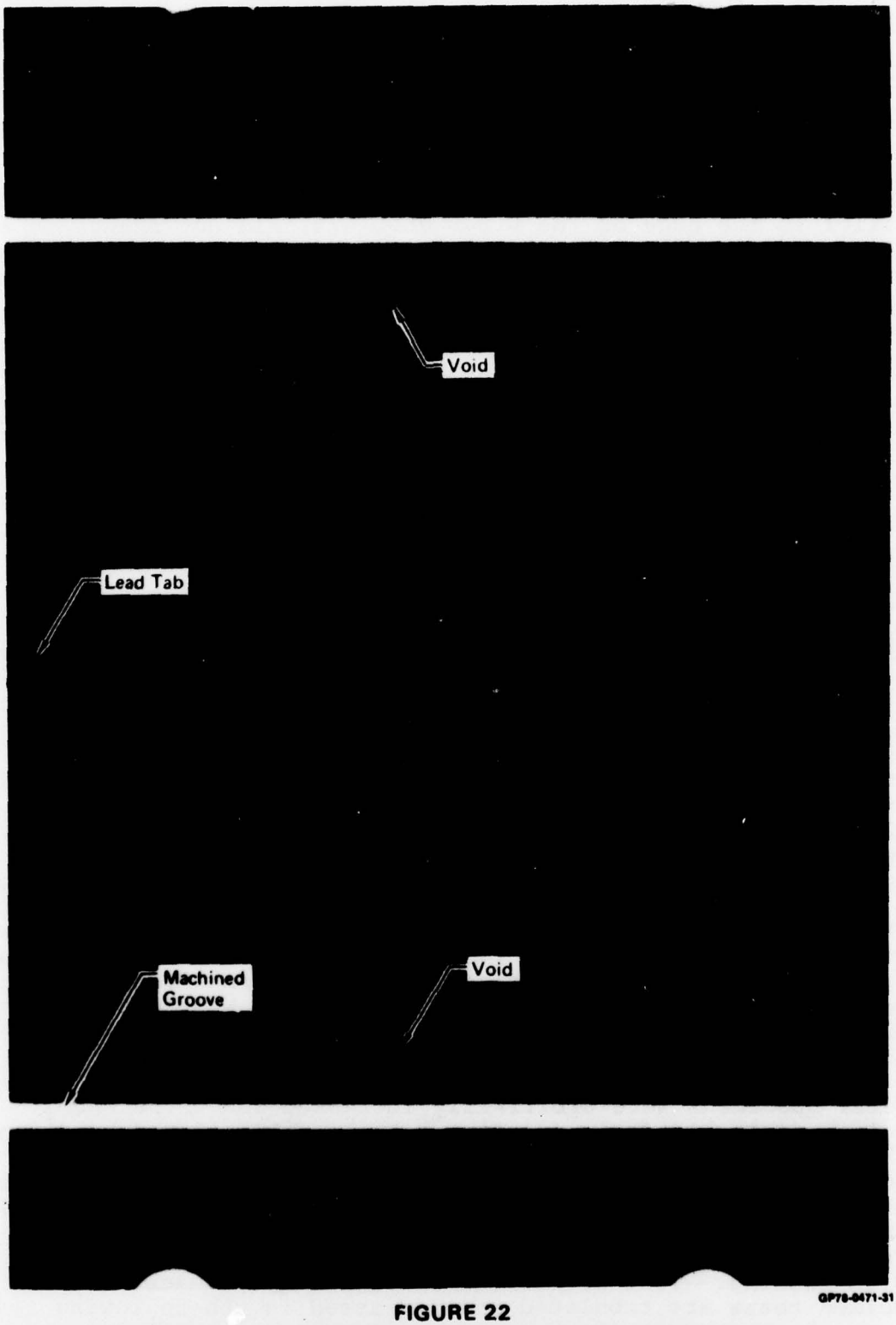

FIGURE 22
FULL-SCALE RADIOGRAPH OF DOUBLE-DOUBLER SPECIMEN NO. 1

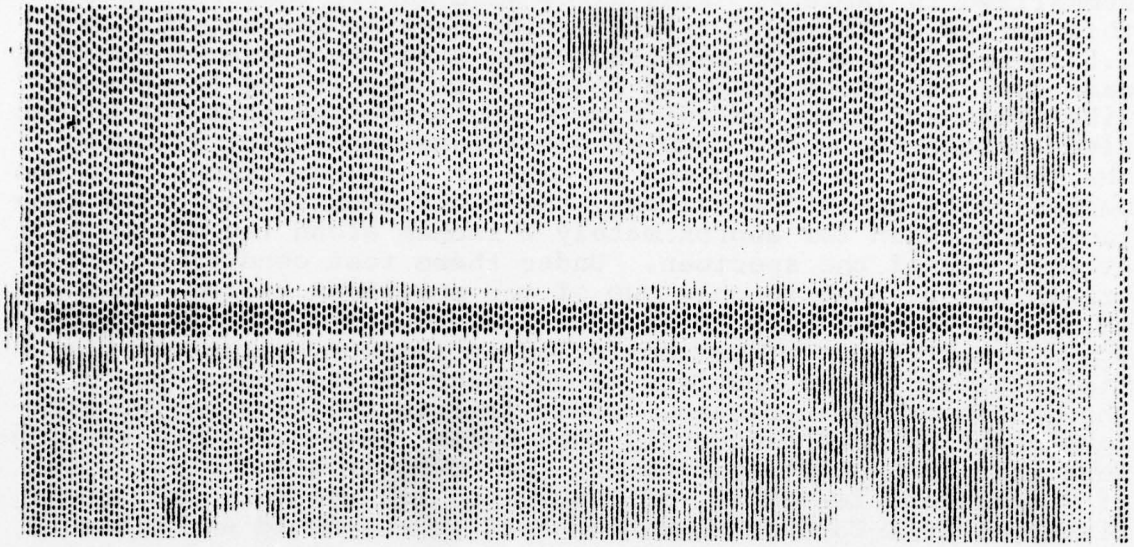

(a) C-Scan Before Cycling

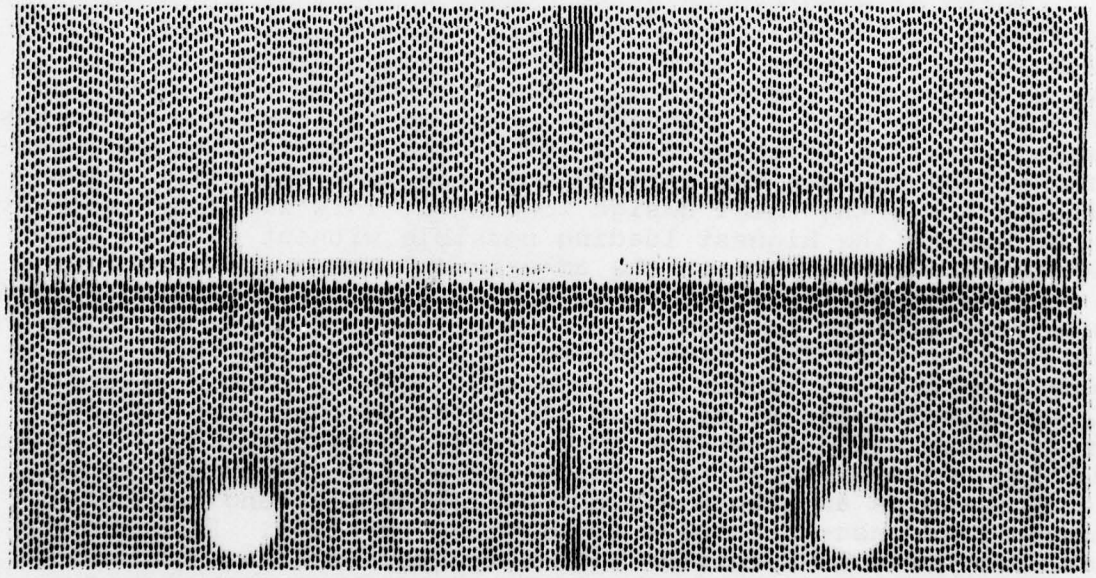

GP78-0471-32

(b) C-Scan After 10^6 Cycles

FIGURE 23
FULL-SCALE C-SCANS OF SPECIMEN NO. 1 BEFORE AND AFTER CYCLING

Tests of Double-Doubler and Double-Strap Specimens - Test results for the double-doubler and double-strap specimen are summarized in Table 9. Flaw sizes were fairly uniform throughout this series of tests. Circular voids were approximately 1.0 - 1.5 inches in diameter and crack-like voids were essentially the same size and shape shown in Figure 22. Several of the crack-like voids and circular voids were positioned so that the milled slot through the 0.040 doubler cut-through the void, allowing the total void to be exposed to ambient test conditions. In the mechanically damaged specimens, the 0.040 doubler was pryed away from 0.080 skin for approximately 2 inches along the milled slot at each end of the specimen. Under these test conditions, flaw growth was evident in only two of the specimens tested, both of which were bonded with FM-73 adhesive. Quite frequently, however, the aluminum adherends failed in fatigue, either at the milled slots in the doublers or adjacent to the center gap in the double-strap specimens. Early fatigue failures in the aluminum occurred more frequently when cycled in a hot-humid environment than in a cold environment. As noted in the Tables, 5 out of 7 specimens tested at -50°F survived 10^6 cycles. The sensitivity of 2024-T3 base aluminum sheet to hot-humid environments was investigated in the PABST program and is discussed in Reference 1. This phenomenon was also observed in several other specimen configurations tested at the fast cycle rate.

Tests of Single-Doubler Specimens - Tests of single-doubler specimens at the fast cycle rate are summarized in Table 10. In this series of tests, flaw growth was evident in six of the twenty-eight specimens tested. Flaw growth was very minor and in some cases hardly detectable. Many of the aluminum adherends failed prior to reaching 0.5×10^6 cycles. Most of these specimens failed because the applied loadings were arbitrarily increased above the PABST design loadings. This was done in order to determine the highest loading possible without causing premature fatigue failure in the adherends. The crack-like flaws were located at the edge of the milled slots in the doublers and were very similar in size, shape, and location to those shown in Figure 22. Circular voids ranged in size from 1.0 inch to approximately 1.5 inches in diameter. Several of the circular flaws were located along the milled slot so that test ambient environment could enter the void area. In spite of this, in the two specimens with circular voids where flaw growth was noted, it appeared as an unbond all across milled slot and was not concentrated near the voids as might be expected. Flaw growth was also noted in specimens with large porous flaws, generally elliptical in shape, and ranging in size from 2 inches to 5 inches. The major axis was oriented perpendicular to the load path. In each of the four cases in which flaw growth was noted, an unbonded area progressed from the side of the porous area to the side of the specimen. It should be noted that the original flaw itself did not grow, but unbonding occurred in the unflawed adhesive immediately adjacent to the flaw.

TABLE 9

RESULTS OF DOUBLE-DOUBLER AND DOUBLE-STRAP SPECIMEN TESTS (FAST CYCLE)

Specimen		Flaw Description		Test Conditions		Fatigue Cycles	Residual Strength (lb)	Average Flaw Growth (in.)	Average Flaw Growth Rate (in./cycle)	Comments
No.	Type	Type	Geometry	Environment	Max Load (lb/in.)					
18	1	Crack-Like Voids	4.0 x 0.25 inch void parallel to milled slot at each end.	−50°F	2000	10^6	–	0	–	–
20			4.0 x 0.4 inch void parallel to milled slot at each end.			10^6	–	0	–	–
19			3.5 x 0.3 inch void parallel to milled slot at one end.	140°F, 95-100% RH		10^6	–	0	–	–
9		Circular Voids	1.0 and 0.5 inch diameter voids at each end near milled slots.	−50°F		10^6	–	0	–	–
17			1.0 and 0.7 inch diameter voids at each milled slot.			10^6	–	0	–	–
10			1.0 and 0.6 inch diameter voids at each milled slot.	140°F, 95-100% RH		0.398×10^6	–	0	–	Failed in grip area at bolt holes.
11			Gross porosity throughout specimen.			0.554×10^6	–	0	–	Failed in 0.080 skin at milled slot.
12			1.0 and 1.3 inch diameter voids tangent to milled slot.			0.829×10^6	–	0	–	Failed in grip area at bolt holes.
16			1.0 and 0.4 diameter voids tangent to milled slots at each end.			0.129×10^6	–	0	–	Failed in 0.080 skin at milled slot.
13		Mechanical Damage	2.2 x 0.5 inch fractured bondline along milled slot at each end.	−50°F		10^6	–	0	–	–
14			2.0 x 0.5 inch fractured bondline along milled slot at each end.			0.37×10^6	–	0	–	Failed in 0.080 skin at milled slot.

GP78-0471-35

TABLE 9 (Continued)
RESULTS OF DOUBLE-DOUBLER AND DOUBLE-STRAP SPECIMEN TESTS (FAST CYCLE)

Specimen		Flaw Description		Test Conditions		Fatigue Cycles	Residual Strength (lb)	Average Flaw Growth (in.)	Average Flaw Growth Rate (in./cycle)	Comments
No.	Type	Type	Geometry	Environment	Max Load (lb/in.)					
15	1	Mechanical Damage	3.5 x 0.75 inch fractured bondline along milled slot at each end.	140°F, 95-100% RH	2000	10^6	–	0	–	–
1	2	Crack-Like Voids	4.0 x 0.5 inch void adjacent to milled slots at each end.	140°F, 95-100% RH	2000	0.237×10^6	–	0	0	Failed in 0.040 doublers at center of specimen.
2			4.5 x 0.5 inch void adjacent to milled slots at each end.			0.188×10^6	–	0	0	
3			4.0 x 0.5 inch void adjacent to milled slots at each end.		974	10^6	31,200	0	0	
4			3.5 x 0.5 inch void adjacent to milled slots at each end.	−50°F	2000	0.173×10^6	–	0	0	Failed in 0.040 doublers at center of specimen.
5			3.0 x 0.5 inch void along each milled slot, and 1.5 x 0.2 inch void on each side of center gap.			10^6	34,600	0	0	
6	3	Crack-Like Voids	3.5 x 0.5 inch void adjacent to milled slot at each end.	140°F, 95-100% RH	2000	0.445×10^6	–	0.7	1.6×10^{-6}	Failed in 0.080 skin at milled slot.
7			3.5 x 0.25 inch void along milled slots at each end.			0.193×10^6	–	2.0	10.4×10^{-6}	Failed in 0.080 doublers at center of specimen and in one bondline.

Notes:
1. All specimens were loaded at a cycle rate of 30 Hz and a stress ratio of R = 0.10.
2. Specimen Types:
   1. Double-doubler with 0.040 doublers, 0.080 skin, and AF-55 adhesive.
   2. Double-strap with 0.040 doublers, 0.080 skin and AF-55 adhesive.
   3. Double-strap with 0.040 doublers, 0.080 skin and FM-73 adhesive.

TABLE 10
RESULTS OF SINGLE-DOUBLER SPECIMEN TESTS (FAST CYCLE)

Specimen		Flaw Description		Test Conditions		Fatigue Cycles	Average Flaw Growth (in.)	Average Flaw Growth Rate (in./cycle)	Comments
No.	Type	Type	Geometry	Environment	Max Load (lb/in.)				
1	1	Crack-Like Voids	4.0 x 0.25 inches each, located along milled slot.	$-50^{o}F$	2400	0.208×10^6	0	–	Failed in 0.080 skin along edge of doubler.
2			3.5 x 0.25 inches each, located along milled slot.		2000	0.388×10^6	0	–	Failed in grip area at bolt holes.
3			3.0 x 0.25 and 2.0 x 0.25 inches, located along milled slots.		1800	0.219×10^6	0	–	Failed in grip area at bolt holes.
4			3.0 x 0.25 inches each, located along milled slots.		2000	0.133×10^6	0	–	Failed in grip area at bolt holes.
5			3.0 x 0.3 and 1.5 x 0.2 inches, located along milled slots.		1800	0.206×10^6	0	–	Failed in 0.080 skin at milled slot.
6			1.5 x 0.25 inches each, located along milled slots.		1500	10^6	0	–	No failure.
7			2.0 x 0.25 inches each, located along milled slots.	$140^{o}F$, 95-100% RH	1500	0.604×10^6	0	–	Failed in grip area at bolt holes.
8			3.0 x 0.125 inches each, located along milled slots.			0.774×10^6	0	–	Failed in 0.080 skin at milled slot.
19	2		4.0 x 0.25 inches each, located along milled slot.		1000	0.385×10^6	0	–	Failed in 0.040 skin at milled slot.
20			4.5 x 0.25 and 2.0 x 0.125 inches, located along milled slot.			0.375×10^6	0	–	Failed in 0.040 skin at milled slot.

GP78-0471-36

TABLE 10 (Continued)
RESULTS OF SINGLE DOUBLER SPECIMEN TESTS (FAST CYCLE)

Specimen		Flaw Description		Test Conditions		Fatigue Cycles	Average Flaw Growth (in.)	Average Flaw Growth Rate (in./cycle)	Comments
No.	Type	Type	Geometry	Environment	Max Load (lb/in.)				
23	1	Circular Voids	Two circular voids at each end, 2.0 and 1.0 inches diameter, tangent to milled slots.	$-50^{o}F$	1500	10^6	0	–	No failure
24			Two circular voids at each end, 1.8 and 0.8 inches diameter, tangent to milled slots.			10^6	0	–	No failure
21			Two circular voids at each end, 1.8 and 1.0 inches diameter, tangent to milled slots.	$140^{o}F$, 95-100% RH	1500	0.415×10^6	0	–	Failed in 0.080 skin at milled slot.
22			Two circular voids at each end, 1.0 and 1.7 inches diameter, tangent to milled slots.			0.803×10^6	0.15	0.2×10^{-6}	Failed in 0.080 skin at milled slot. Flaw growth all along milled slot.
25			Two circular voids at each end, 2.0 and 1.0 inches diameter, tangent to milled slots.	$140^{o}F$ (Dry)		10^6	0	–	No failure
17	2		Two circular voids, at each end 1.5 and 0.5 inches diameter, tangent to milled slots.	$140^{o}F$, 95-100% RH	1000	1.107×10^6	0	–	Failed in 0.040 skin at milled slot.
18			Two circular voids at each end, 0.8 and 0.5 inches diameter, tangent to milled slots.			0.154×10^6	0	–	Failed in 0.040 skin at milled slot.
15	1	Porosity	Semi-circular porous voids, each 2.5 inches diameter, located along milled slot.	$-50^{o}F$	1500	10^6	0.1	0.1×10^{-6}	Unbond initiated along sides of voids.
16			Semi-circular porous voids 2.5 and 1.5 inches diameter, located along milled slots.			10^6	0.1	0.1×10^{-6}	Unbond initiated along side of voids.

TABLE 10 (Concluded)
RESULTS OF SINGLE DOUBLER SPECIMEN TESTS (FAST CYCLE)

Specimen		Flaw Description		Test Conditions		Fatigue Cycles	Average Flaw Growth (in.)	Average Flaw Growth Rate (in./cycle)	Comments
No.	Type	Type	Geometry	Environment	Max Load (lb/in.)				
13	1	Porosity	Semicircular porous voids 2.5 inches diameter, located along milled slots.	140°F, 95-100% RH	1500	0.55×10^6	0	–	Failed in 0.080 skin at milled slot.
14			Semicircular porous voids 2.5 and 1.5 inches diameter, located along milled slots.			0.489×10^6	0	–	Failed in 0.080 skin at milled slot.
27	3		Semicircular porous voids, each 4.5 inches diameter, located along milled slots.	–50°F	1500	10^6	0.1	0.10×10^{-6}	Unbond initiated along sides of voids.
28			Semicircular porous voids, each 4.0 inches diameter, located along milled slots.			10^6	0.1	0.10×10^{-6}	Unbond initiated along sides of voids.
10	1	Mechanical Damage	Fractured bondline at each milled slot, 4.0 inches wide.	–50°F	1500	10^6	0	–	No failure
11			Fractured bondline at each milled slot, 4.5 inches wide.			10^6	0	–	No failure
26			Fractured bondline at each milled slot, 3.6 inches wide.			10^6	0	–	No failure
12			Fractured bondline at each milled slot, 4.0 inches wide.	140°F, 95-100% RH	1500	0.228×10^6	0	–	Failed in 0.080 skin at milled slot.
9			Fractured bondline at each milled slot, 4.5 inches wide.	140°F (dry)		0.639×10^6	0	–	Failed in 0.08 skin under grips.

Notes:
1. All specimens were loaded at a cycle rate of 30 Hz and a stress ratio of R = 0.10.
2. Specimen Types:
   1. 0.080 skin/0.040 doubler, AF-55 adhesive.
   2. 0.040 skin/0.020 doubler, AF-55 adhesive.
   3. 0.080 skin/0.040 doubler, FM-73 adhesive.

Tests of Single-Strap Specimens - Results of single-strap specimens tested at the fast cycle rate are summarized in Table 11. Flaw growth occurred more frequently in this type of specimen than any of the others tested in the program. This is primarily because of the induced peel forces in the bondline. Of the 45 single-strap specimens tested at the fast cycle rate, 30 showed definite signs of flaw initiation and growth either adjacent to the induced flaws or along the milled slots which created the splice joint configuration.

Flaw growth in the adhesive was easily detectable using the optimized c-scan method described in Section 2.4. A typical example of flaw growth is illustrated in Figure 24. Outlines of the crack-like adhesive voids, as indicated by a radiograph of the specimen have been superimposed on the c-scans to show their exact size and location prior to testing. After one-half million cycles, flaw growth had occurred all across the width of the specimens at one end of the splice and part way across the width at the opposite end and in the middle of the splice. After one million cycles, the unbonded area completely engulfed the original flaws in one splice over-lap, leaving only a thin strip of area still bonded. In most cases, flaw growth was more rapid along the sides of the initial flaws creating a filleted area of unbond as shown in Figure 25. Also, in this figure, the boundaries of the original adhesive cut-outs as well as the resulting voids are clearly visible in the figure because the mode of bondline failure in this area changed from cohesive to adhesive. Cohesive failure occurred over the other portions of the splice.

Flaw growth summarized in Table 11 was measured from the c-scans of the specimens and verified by visual inspection of the bondline surface appearance after residual strength testing. Since the amount of flaw growth varied across the specimen width and splice over-lap length, the values shown are average values.

The eccentricity of load path in these specimens causes splice adherend bending stresses which combine with axial tensile stresses and reach a maximum at the center of the 0.090 splice strap. For this reason, many specimens contained fatigue cracks in this area and some even failed in fatigue. Large flaws in the bondline can reduce fatigue life of a joint by causing stress concentrations in the adherend due to a redistribution of the loads through the bondline. Specimen No. 10, which failed prematurely in fatigue of the splice, had a very large flaw in the middle of the splice. In this specimen, applied loads to the skin adherend were forced to be transferred through the bondline along the sides of the specimen to the splice adherend because of the flaw. Failure of the specimen initiated in the 0.090 splice along the center mill cut at the side of the specimen rather than uniformly across the specimen width. The redistri-

TABLE 11
RESULTS OF SINGLE-STRAP SPECIMEN TESTS (FAST CYCLE)

Specimen		Flaw Description		Test Conditions		Fatigue Cycles	Residual Strength (lb)	Average Flaw Growth (in.)	Average Flaw Growth Rate (in./cycle)	Comments
No.	Type	Type	Geometry	Environment	Max Load (lb/in.)					
1	1	Crack-Like Voids	1.7 x 0.25 flaw on one side of center milled slot.	−50°F	1000	0.688×10^6	–	0	–	Fatigue failure of 0.090 splice.
2			1.5 x 0.25 flaw on one side of center milled slot.			10^6	–	0	–	Crack in 0.090 splice.
5			Flaw along each milled slot, average dimensions of 3.5 x 0.5 in.			10^6	20,400	0.8	08×10^{-6}	Flaw growth noted at 0.5×10^6 cycles.
6			Flaw along each milled slot, average size 2.0 x 0.2 in.			10^6	27,500	0.5	0.5×10^{-6}	Flaw growth noted at 0.5×10^6 cycles
3			Flaw along each milled slot, average size of 3.0 x 0.5 in.	140°F, 95-100% RH		10^6	Not Tested	0	–	–
4						0.244×10^6	–	0	–	Adherend failure due to inadvertent overload.
7			Flaw along each milled slot, average size of 3.5 x 0.2 in.			0.348×10^6	–	0.2	0.6×10^{-6}	Failed in 0.080 skin.
13			Flaw along each milled slot, average size 2.5 x 0.25 in.			0.725×10^6	–	0.3	0.4×10^{-6}	Failed in 0.080 skin.
8			Flaw along each milled slot, average size 3.0 x 0.25 in.			0.311×10^6	–	0.2	0.6×10^{-6}	Failed in 0.080 skin.
29	2	Crack-Like Voids	4.5 x 0.25 voids along each of the three milled slots	−50°F	1000	10^6	30,800	0.1	0.1×10^{-6}	Unbond grew (filleted) at side of each flaw.
30			4.5 x 0.25 in. voids along each of the three milled slots.			10^6	30,600	0.2	0.2×10^{-6}	Same as No. 29
35			4.8 x 0.3 in. voids along each of the three milled slots.	140°F, 95-100% RH		0.54×10^6	–	0.3	0.5×10^{-6}	Failure occurred in bond-line.
36			4.5 x 0.3 in. voids along each of the three milled slots.			0.378×10^6	–	1.2	3.1×10^{-6}	Failure occurred in bond-line.
45			4.5 x 0.2 in. void along center milled slot 2.0 x 0.1 in. voids at end slots.	140°F (Dry)		0.912×10^6	–	1.0	1.1×10^{-6}	Failure occurred in bond-line.

GP78-0471-37

TABLE 11 (Continued)

RESULTS OF SINGLE-STRAP SPECIMEN TESTS (FAST CYCLE)

Specimen		Flaw Description		Test Conditions		Fatigue Cycles	Residual Strength (lb)	Average Flaw Growth (in.)	Average Flaw Growth Rate (in./cycle)	Comments
No.	Type	Type	Geometry	Environment	Max Load (lb/in.)					
16	1	Circular Voids	Two 0.8 in. diameter voids tangent to milled slots at each end.	−50°F	1000	10^6	14,500	0.4	0.4×10^{-6}	Bondline unbonded across width of specimen along all three milled slots. Flaw growth filleted next to circular voids
17			Two pairs of circular voids tangent to each end milled slot, 0.8 and 0.5 in. diameter.			10^6	30,000	0.5	0.5×10^{-6}	Same as No. 16
14			Same as No. 17.	140°F, 95-100% RH		0.75×10^6	–	0.25	0.3×10^{-6}	Failed in 0.080 skin. Flaw growth filleted next to circular voids.
15			Two 0.8 in. diameter voids tangent to milled slots at each end.			0.149×10^6	–	0.1	0.7×10^{-6}	Failed in 0.090 splice
31	2	Circular Voids	Two pair of 1.25 in. diameter voids, one pair tangent to center slot and one tangent to end slot	−50°F	1000	10^6	29,800	0.1	1.0×10^{-6}	Flaw growth filleted along intersection of original void and milled slot.
32			Two 1.4 diameter void over center slot and two 0.7 in. diameter voids tangent to end slot.			10^6	11,550	0.2	0.2×10^{-6}	–
37			One pair of 1.0 in. diameter voids at center slot and one pair of 0.6 in. diameter voids at one end slot.	140°F, 95-100% RH		0.198×10^6	–	0.4	0.8×10^{-6}	Failure occurred in 0.080 skin
38			Two pair of 1.0 in. diameter voids. One pair tangent to end milled slot and one pair over center slot.			0.338×10^6	–	0.3	0.9×10^{-6}	Failure occurred in 0.090 splice
9	1	Porous Voids	Porous area over entire splice length. 2.0 in. wide at center slot and 1.0 in. wide at end slots.	−50°F	1000	10^6	29,500	0.1	0.1×10^{-6}	Flaw growth filleted along intersection of porous area and milled slots

TABLE 11 (Continued)
RESULTS OF SINGLE-STRAP SPECIMEN TESTS (FAST CYCLE)

Specimen		Flaw Description		Test Conditions		Fatigue Cycles	Residual Strength (lb)	Average Flaw Growth (in.)	Average Flaw Growth Rate (in./cycle)	Comments
No.	Type	Type	Geometry	Environment	Max Load (lb/in.)					
10	1	Porous Voids	3.5 in. diameter porous void centered over center milled slot.	−50°F	1000	0.547×10^6	–	0.2	0.4×10^{-6}	Failure occurred in 0.080 skin and bondline. Bondline flaw believed to have caused local adherend overload leading to fatigue failure.
11			Same as No. 10.	140°F, 95-100% RH		0.107×10^6	–	0.2	0.4×10^{-6}	Bondline and adherend failure Flaw area exceeded 50% of bondline.
12			2.0 in. wide porous area extending across both splice overlaps.			0.210×10^6	–	0.1	2.0×10^{-6}	Failure occurred in 0.090 splice.
44			Same as No. 38.	140°F (Dry)		0.563×10^6	–	0.2	0.5×10^{-6}	Failure occurred in 0.090 splice. Flaw growth more prominent at center slot.
33	2	Porosity	Porous area extends across both splice overlaps 2.5 in. wide in middle and 1.5 on ends.	−50°F	1000	0.018×10^6	–	0.2	0.4×10^{-6}	Failure occurred in bondline. Failure was adhesive type over 75% of splice.
34			Same as No. 33			0.977×10^6	–	0.6	1.0×10^{-6}	Failure occurred in bondline. Flaw growth filleted at intersection of void and milled slots.
46			Porous area extends across both splice overlaps 2.5 in. wide in middle and 1.0 and 0.5 wide on ends.			10^6	22,300	0.4	0.6×10^{-6}	Cohesive failure over 80% of bondline.
39			1.5 to 2.0 in. wide porous area across both splice overlaps.	140°F, 95-100% RH		0.103×10^6	–	0.2	0.4×10^{-6}	Failure occured in bondline.
40			2.0 to 2.5 in. wide porous area across both overlaps.			0.111×10^6	–	0.2	2.0×10^{-6}	Combined failure in 0.090 splice and bondline.
24	1	Mechanical Damage	Same as No. 18	−50°F	1000	10^6	19,150	No	–	Aluminum failed in residual strength test.

TABLE 11 (Concluded)
RESULTS OF SINGLE-STRAP SPECIMEN TESTS (FAST CYCLE)

Specimen		Flaw Description		Test Conditions		Fatigue Cycles	Residual Strength (lb)	Average Flaw Growth (in.)	Average Flaw Growth Rate (in./cycle)	Comments
No.	Type	Type	Geometry	Environment	Max Load (lb/in.)					
18	1	Mechanical Damage	4.0 x 0.7 in. wide fractured bandline at each end milled slot.	140°F, 95-100% RH	1000	0.156×10^6	–	0.2	2.0×10^{-6}	Bondline failure, crack in 0.090 splice.
19			Same as No. 18.			0.125×10^6	–	0.2	–	Bondline failure. Flaw growth evident after 0.10×10^6 cycles.
41	2	Mechanical Damage	4.0 in. wide by 1.0 in. deep along each end milled slot.	140°F, 95-100% RH	1000	0.153×10^6	–	0.2	1.3×10^{-6}	Failure in 0.049 splice.
42			Same as No. 41			0.125×10^6	–	0.2	1.6×10^{-6}	Failure in 0.090 splice.
20	1	Variable Adhesive Thickness	Thickness across width of specimen varied from 0.001 to 0.004.	–50°F	1000	10^6	34,000	0	–	Cohesive bond failure.
21			1.5 in. diameter porous area and thick (0.010) adhesive across center slot.			10^6	34,200	0	–	Cohesive bond failure.
22			Thickness varied across width from 0.007 to 0.009.			10^6	34,350	0	–	Cohesive bond failure.
43			Adhesive thickness varied across width from 0.007 in middle to 0.012 along sides.			10^6	31,450	0	–	Failed in 0.080 skin at mill cut.
26			A 2.5 in. diameter void over each end milled slot. Adhesive 0.015 thick in this area.	140°F, 95-100% RH		0.474×10^6	–	0	–	Failure in 0.080 skin.
27			2.0 in. diameter void and thick (0.015) adhesive at center milled slot.			0.175×10^6	–	0	–	Failure in 0.080 skin.
25			Same as No. 23.			10^6	31,250	0	–	Cohesive failure in bondline.
28			Same as No. 23.			0.402×10^6	–	0	–	Failure in 0.090 splice.
23			Thickness varied across width from 0.015 in. in middle to 0.007 in. at the sides.	140°F (Dry)		0.531×10^6	–	0	–	Failure in 0.080 splice.

Notes:

1. All specimens were loaded at a cycle rate of 30 Hz and a stress ratio of R = 0.10.
2. Specimen Types:
   1. 0.080 skin, 0.090 splice, AF-55 adhesive
   2. 0.080 skin, 0.090 splice, FM-73 adhesive

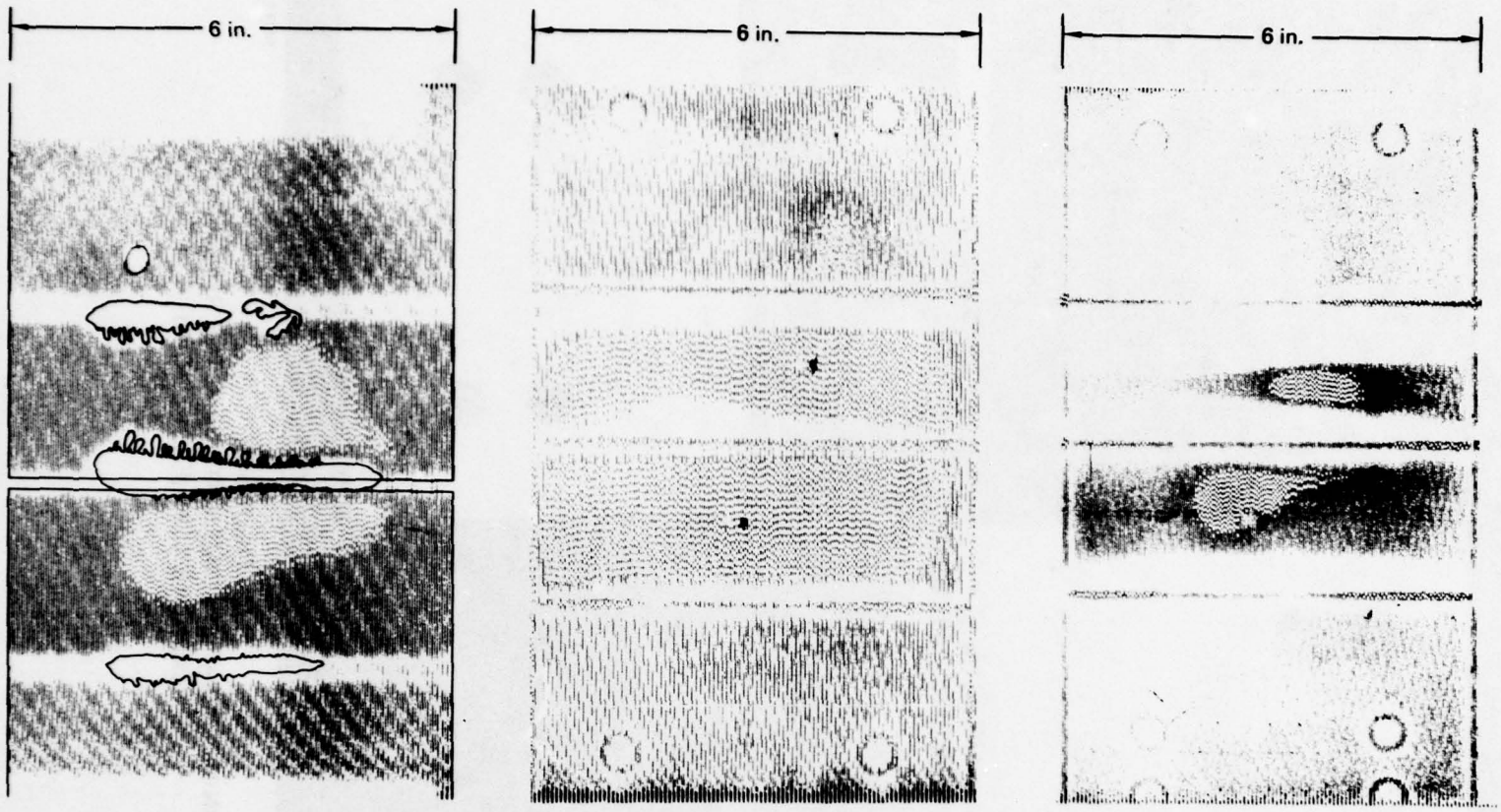

a) Before Cycling

b) After 500,000 Cycles

c) After 10^6 Cycles

GP78-0471-61

FIGURE 24
C-SCANS OF SINGLE-STRAP SPECIMEN NO. 5

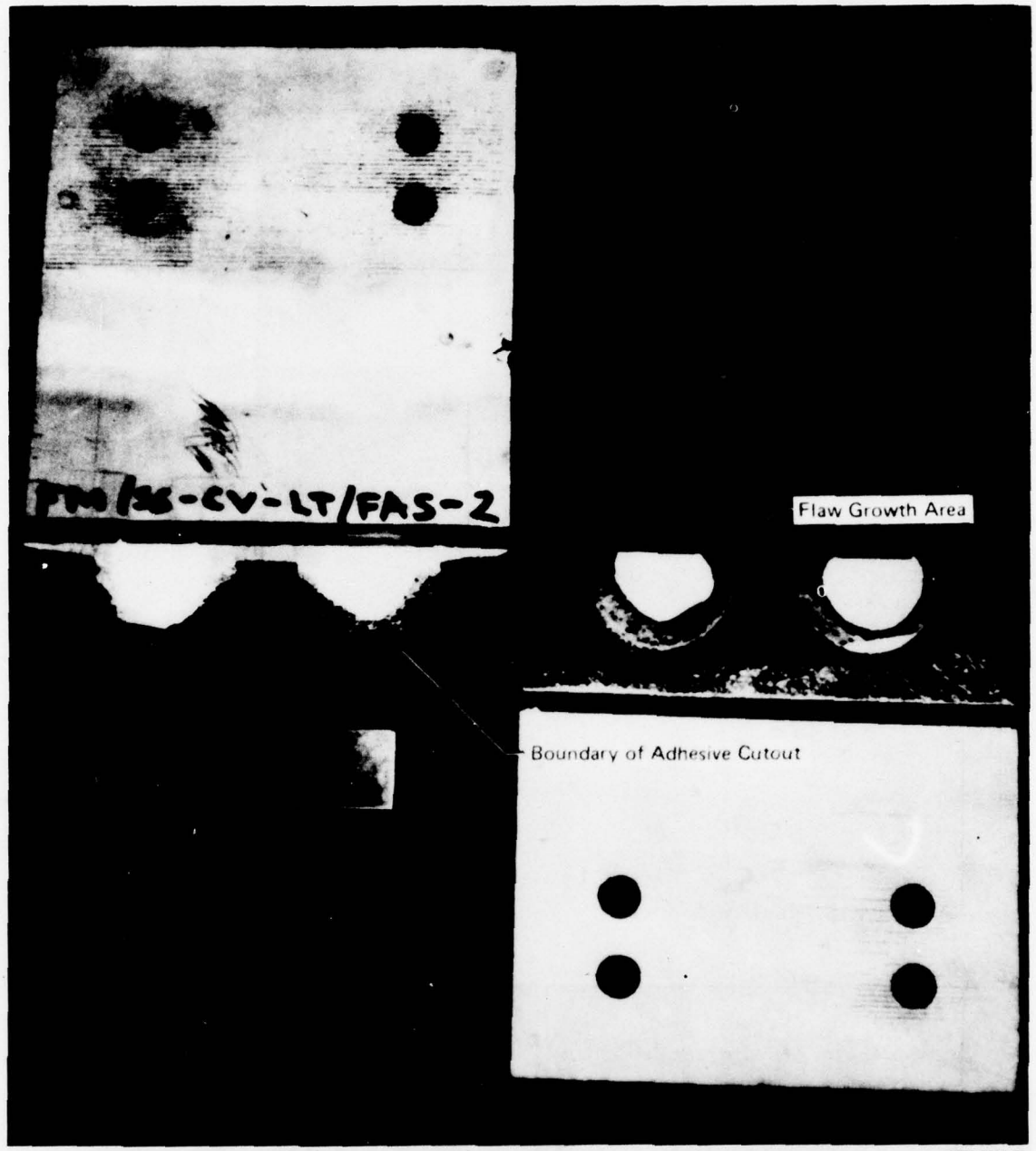

GP78-0471-66

FIGURE 25
SINGLE-STRAP SPECIMEN NO. 32 AFTER RESIDUAL *STRENGTH TEST (FAST CYCLE)*

bution of loads around the flaw, apparently caused increased stresses along the sides of the specimens. The sensitivity of the 2024-T3 bare aluminum plate to hot and wet environments was further demonstrated in the single-strap specimens in that only 3 of the 22 specimens tested in a hot-humid environment survived 10^6 cycles whereas 16 out of 19 specimens tested at -50°F survived 10^6 cycles. Four specimens were tested in a hot-dry environment in order to determine the relative effect of moisture on the life of the adherend. In three of the four specimens, total accumulated cycles before failure were almost double those of corresponding specimens tested in a hot-humid environment indictating that moisture has a definite effect. In the fourth specimen, cycles accumulated in the hot-dry environment were slightly less than corresponding specimens tested in a hot-humid environment.

Visual inspection of specimens after residual strength tests, using a 10-30X variable power viewer, revealed that flaw growth always initiated on the surface of the terminating adherend at the edges of the machined grooves as shown in Figure 26. It then propagated to and along the adhesive-primer interface of the continuing adherend. This failed surface is described as a combined adhesive-cohesive failure because small pieces of adhesive (visible only with the viewer) remained bonded to the primer. Static overloads after cycling caused the remaining adhesive to fail cohesively, i.e., totally within the adhesive.

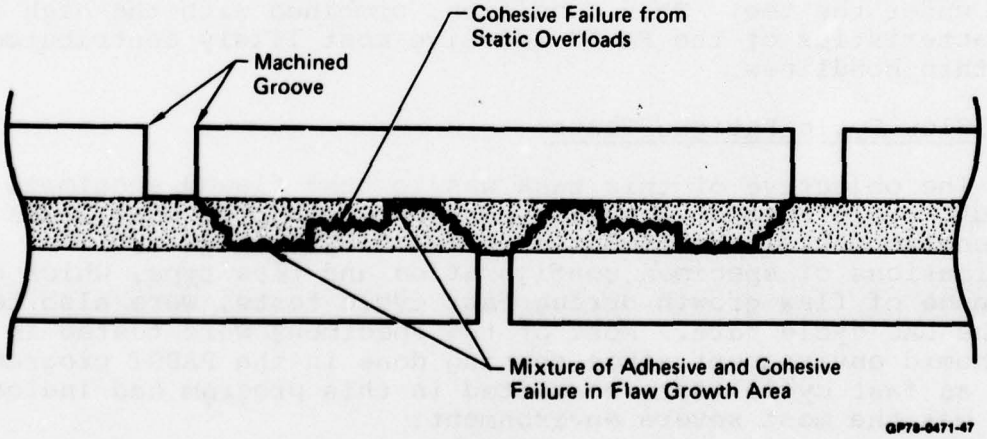

FIGURE 26
FLAW GROWTH CHARACTERISTICS OF SINGLE-STRAP SPECIMENS

Skin to Substructure (Tee) Specimens - Tests of tee specimens at the fast cycle rate are summarized in Table 12. Each specimen with an 0.040 skin was cycled for 0.2×10^6 cycles instead of 10^6 cycles with an intermediate c-scan at 0.1×10^6 cycles to check for flaw growth. Specimens with an 0.080 skin were cycled to 10^6 cycles with an intermediate c-scan at 0.5×10^6 cycles. Flaw growth was evident in 18 of the 35 specimens tested. Most of the flaw growth occurred while being exposed to a hot-humid environment. The only specimens which exhibited flaw growth in the -50°F environment were configured with 0.080 skins and a mechanically damaged bondline. Under these conditions, flaw growth occurred in both AF-55 and FM-73 adhesive.

The most critical type of flaw appears to be the crack-like void along the edge of the tee. Although flaw growth rate was much smaller for the mechanically damaged bondline, it was the only type flaw which produced flaw growth in both hot-wet and cold environments. The area along the edge of the tee experiences high adhesive shear and peel forces.

In general, results of specimens tested with FM-73 adhesive were not consistent with the results obtained on similar specimens bonded with AF-55 adhesive. Specimens bonded with AF-55 adhesive failed most often in the 0.040 aluminum skins whereas specimens of the same configuration bonded with FM-73 adhesive failed most frequently in the adhesive. Post-test inspection of the failed surfaces revealed that the bondlines were very thin (0.001-0.003 inch). In several local areas, the adhesive was less than 0.001 inches thick. In specimens with AF-55 adhesive, the bondline thickness was normal (0.002-0.004 inch) with no isolated thin areas. In the fabrication of tee specimens, no special precautions were taken to restrict the flow of adhesive from under the tee. This condition, combined with the high flow characteristics of the FM-73 adhesive most likely contributed to the thin bondlines.

3.5 Slow Cycle Fatigue Tests

The objective of this task was to test flawed specimens at the DAC cycle rate of 2 cycles per hour using the same loads and environmental conditions of the PABST fuselage article. Combinations of specimen configuration and flaw type, which gave evidence of flaw growth during fast cycle tests, were also tested at the DAC cycle rate. Most of the specimens were tested in the hot/humid environment since testing done in the PABST program as well as fast cycle tests completed in this program had indicated this was the most severe environment.

Each specimen was ultrasonically c-scanned before testing and again after exposure to 4000 cycles in the test environment. The number of cycles (4000) was chosen so that the most number of specimen configurations could be tested within the time span of the program. Each series of 4000 cycles required approximately 3 months to complete. The test set-up and loading fixtures are discussed in Section 3.3.

TABLE 12
RESULTS OF SKIN-TO-SUBSTRUCTURE (TEE) SPECIMENS (FAST CYCLE)

Specimen		Flaw Description		Test Conditions		Fatigue Cycles	Residual Strength (lb)	Average Flaw Growth (in.)	Average Flaw Growth Rate (in./cycle)	Comments
No.	Type	Type	Geometry	Environment	Max Load (lb/in.)					
7	1	Crack-Like Voids	2.5 x 0.2 inch void along one edge of base.	−50°F	100	0.107×10^6	–	0	–	Failed in 0.040 skin when specimen inadvertently overloaded.
8			1.7 x 0.4 inch void in middle of base.			0.196×10^6	–	0	–	Failed in 0.040 skin adjacent to support.
19			Same as No. 20	140°F, 95-100% RH		0.10×10^6	–	0.10	1×10^{-6}	Test stopped because of large crack in 0.040 skin.
20			2.0 x 0.5 inch void in middle and 2.0 x 0.5 inch void along edge.			0.047×10^6	–	0.75	16×10^{-6}	Total bondline failure.
21	2		2.0 x 0.25 inch void along edge and 0.8 inch dia void in middle.	−50°F	80	10^6	2035	0	–	Cohesive failure after fatigue.
22			2.0 x 0.2 inch void along edge and 0.9 x 0.5 inch void in middle.			10^6	2135	0	–	Cohesive failure after fatigue.
27	3		3.0 x 0.5 cutout at each edge filled in with very thin adhesive.	140°F, 95-100% RH	100	0.052×10^6	–	0.6	11.5×10^{-6}	Bondline failure. Adhesive flowed to fill up voids resulting in a very thin bondline.
28			Same as No. 28			0.067×10^6	–	0.75	11×10^{-6}	One side of tee unbonded after 50,000 cycles. Extremely thin bondline.
4	1	Circular Voids	1.3 x 0.4 inch void in middle of base.	−50°F		0.326×10^6	–	0	–	Failed in 0.040 skin near support.
5			1.2 x 0.4 inch void on each edge of base.			0.244×10^6	–	0	–	Failed in 0.040 skin adjacent to tee.
6			0.6 x 0.5 inch void on each edge of base.			0.300×10^6	–	0	–	Failed in 0.040 skin adjacent to tee.

GP78-0471-38

TABLE 12 (Continued)
RESULTS OF SKIN-TO-SUBSTRUCTURE (TEE) SPECIMENS (FAST CYCLE)

Specimen		Flaw Description		Test Conditions		Fatigue Cycles	Residual Strength (lb)	Average Flaw Growth (in.)	Average Flaw Growth Rate (in./cycle)	Comments
No.	Type	Type	Geometry	Environment	Max Load (lb/in.)					
12	1	Circular Voids	0.5 x 0.4 inch void in middle.	140°F (Dry)	100	0.124×10^6	–	0.06	0.5×10^{-6}	Failed in 0.040 skin near support. Unbonded along edge of tee.
13			0.3 inch diameter void in middle.	140°F, 95-100% RH		0.079×10^6	–	0.06	0.7×10^{-6}	Failed in 0.040 skin near support.
23	2		0.7 inch diameter void in middle.	–50°F	80	10^6	2850	0	–	Cohesive failure after fatigue.
24			0.5 inch diameter void in middle.			10^6	2760	0	–	Cohesive failure after fatigue.
29	3		0.4 x 0.2 inch void in middle.	140°F, 95-100% RH	100	0.078×10^6	–	0.3	3.8×10^{-6}	Bondline failure over one side of tee. Unbond propagated from edge of tee.
30			Same as No. 29			0.106×10^6	–	0.3	2.8×10^{-6}	Failed in 0.040 skin and bondline.
31			Extremely thin adhesive along edges of base.	140°F (Dry)		0.080×10^6	–	0.4	5.0×10^{-6}	Bondline failure. Very thin bondline.
1	1	Porosity	1.5 x 0.3 inch porous area along each edge.	–50°F	125	1.28×10^5	–	0	–	Failed in 0.040 skin adjacent to tee.
2			0.75 x 0.5 inch porous area along each edge.		100	1.37×10^5	--	0	–	Failed in 0.040 skin adjacent to tee.
3			Small porous areas throughout bondline.			2.40×10^5	–	0	–	Failed in 0.040 skin at support.
10			2.0 x 0.5 inch porous areas along each edge.			0.193×10^6	–	0	–	Failed in 0.040 skin at support.
11			2.5 x 0.5 inch porous areas along each edge.			0.072×10^6	–	0	–	Failed in 0.040 skin at support
9			1.5 x 0.4 inch porous area along each edge of base.	140°F, 95-100% RH	100	0.10×10^6	–	0.1	1.0×10^{-6}	Failed in 0.040 skin at support.

TABLE 12 (Concluded)
RESULTS OF SKIN-TO-SUBSTRUCTURE (TEE) SPECIMENS (FAST CYCLE)

Specimen		Flaw Description		Test Conditions		Fatigue Cycles	Residual Strength (lb)	Average Flaw Growth (in.)	Average Flaw Growth Rate (in./cycle)	Comments
No.	Type	Type	Geometry	Environment	Max Load (lb/in.)					
32	1	Porosity	1.0 x 0.5 inch porous void along each edge.	140°F, 95-100% RH	100	0.261×10^6	–	0.5	1.9×10^{-6}	Failed in 0.040 skin at support. Tee width increased to 2.45 in. from 1.5 in.
33			0.7 x 0.5 inch porous void along each edge.			0.245×10^6	–	0.6	2.5×10^{-6}	
14	1	Mechanical Damage	2.0 x 0.5 inch bondline fracture along each edge.	–50°F	100	0.176×10^6	–	0	–	Failed in 0.040 skin at support.
15			2.5 x 0.5 inch bondline fracture along each edge.			0.091×10^6	–	0	–	Failed in 0.040 skin at support.
17			2.5 inch long bondline fracture on each edge.	140°F, 95-100% RH	80	0.183×10^6	–	0.1	0.5×10^{-6}	Failed in 0.040 skin at support
26			3.0 x 0.5 inch bondline fracture on each edge.		100	0.20×10^6	–	0.2	1.0×10^{-6}	No failure.
18			2.2 x 0.4 inch bondline fracture on each edge.	140°F (Dry)		0.096×10^6	–	0	–	Failed in 0.040 skin at support
34	4		2.4 x 0.7 inch bondline fracture along each edge.	–50°F	80	10^6	935	0.8	0.8×10^{-6}	No failure. Unbond occurred on one side at one end only.
35			2.5 x 0.6 inch bondline fracture along each edge.			10^6	1405	0.4	0.4×10^{-6}	No failure. Unbond occurred on one side at one end only.
25	2		2.7 x 0.7 inch bondline fracture on each edge.	–50°F	80	10^6	1595	0.8	0.8×10^{-6}	Only one end on one side unbonded. No growth after 0.5×10^6 cycles.
16			Same as No. 25		60	1.044×10^6	1860	0.4	0.4×10^{-6}	

Notes: 1. All specimens were loaded at a cycle rate of 30 Hz and a stress ratio of R = 0.10
2. Specimen Types:
   1. 0.040 skin/0.060 stiffener, AF-55 adhesive
   2. 0.080 skin/0.063 stiffener, AF-55 adhesive
   3. 0.040 skin/0.063 stiffener, FM-73 adhesive
   4. 0.080 skin/0.063 stiffener, FM-73 adhesive

Specimens and flaw combinations that experienced flaw growth during fast cycle testing also experienced flaw growth in the DAC cycle. Flaw growth rate, however, was much higher in the DAC cycle tests. With both fast and slow cycling, the tee and single-strap specimens had the highest growth rates whereas those with lesser amounts of peel had lower flaw growth rates.

Tests of Double-Strap Specimens - Results of double-strap specimens tested at the DAC cycle rate are summarized in Table 13.

This series of tests provided a comparison between the flaw growth characteristics of AF-55 and FM-73 adhesive. At the end of 4000 cycles, the specimens bonded with FM-73 adhesive had exhibited unbonding in the splice region, particularly along the sides of the specimen whereas the AF-55 specimens showed no change in bondline. The FM-73 specimens have been returned to the test environment and are continuing to cycle at the same DAC cycle rate. An example of the type of unbonding occurring in the FM-73 specimens is shown in c-scans of specimen No. 7 before and after cycling (Figure 27). For comparison, c-scans before and after cycling of specimen No. 2, an AF-55 specimen, are shown in Figure 28. Similar results were obtained in the fast cycle tests for both adhesives. In the fast cycle tests, specimens bonded with FM-73 and tested in the hot/humid environment exhibited a small amount of flaw growth before failure occurred in the aluminum, whereas specimens bonded with AF-55 adhesive, and tested under identical conditions, did not exhibit flaw growth. Results of the FM-73 specimens currently being cycled at the DAC cycle rate will be reported to the Air Force at the conclusion of testing.

Tests of Single-Doubler Specimens - Tests of single-doubler specimen tests are summarized in Table 14. The only single-doubler specimens which exhibited flaw growth were the specimens with mechanically damaged or porous bondlines. In both cases, flaw growth occurred in the hot/humid environment. No flaw growth of any kind was observed on specimens cycled in the -50°F condition. Flaw growth which occurred in specimens with porosity was generally of the same magnitude as occurred after 10^6 cycles at 30 Hz. Also, in both cases, flaw growth initiated along the side of the flaw.

Tests of Single-Strap Specimens - Tests of single-strap specimens are summarized in Table 15. Almost all of the specimens tested in the hot/humid environment showed some amount of flaw growth whereas none of the specimens tested at -50°F showed any signs of flaw growth. Of the flaw types evaluated, the mechanically damaged bondline appears to produce the greatest amount of flaw growth. The magnitude of flaw growth for all specimens (0.1 - 0.3 inches) was roughly equal to the magnitude observed on corresponding specimens after 10^6 cycles at 30 Hz.

TABLE 13
RESULTS OF DOUBLE-STRAP SPECIMEN TESTS
DAC Cycle

Specimen		Flaw Description		Test Conditions		Fatigue Cycles	Residual Strength (lb)	Average Flaw Growth (in.)	Average Flaw Growth Rate (in./cycle)	Comments
No.	Type	Type	Geometry	Environment	Max Load (lb/in.)					
1	1	Crack-like Voids	3.5 x 0.4 inch void along specimen width at each end mill cut. 2.5 x 0.2 inch void on each side of center.	140°F, 95-100% RH	1,536	4,032	34,450	0	0	Failed in 0.040 aluminum splice straps.
2			3.0 x 0.4 inch void along specimen width at each end milled slot.				33,850	0	0	
3			Same as No. 1				34,900	0	0	
4			Same as No. 1				35,000	0	0	
5			Same as No. 2				34,600	0	0	
6										Dummy specimen
7	2	Crack-like Voids	3.5 x 0.3 inch void along specimen width at each end mill cut.	140°F, 95-100% RH	1,536	4,032	(3)	0.1	25×10^{-6}	Unbonding across width at milled slots and on sides at center gap.
8			4.0 x 0.4 inch void along specimen width at each end mill cut.					0.2	50×10^{-6}	Unbonding only at edges of specimen at milled slots and center gap.
9			3.5 x 0.3 inch void along specimen width at one end mill cut. Slight (1.5 x 0.1) void at opposite end.					0.3	75×10^{-6}	Unbonding along specimen sides over full splice length.
10			Same as No. 7					0.2	25×10^{-6}	Unbonding only at edges of specimen at center gap.
11			Same as No. 7					0.2	25×10^{-6}	Unbonding only at sides of specimen at along full splice length.
12			Void along one side of specimen, across each splice, 0.5 x 2.0.					0.2	25×10^{-6}	Unbonding at sides of specimen along full splice length.

Notes:
1. All specimens cycled at the DAC cycle rate of 2 cycles per hour.
2. Specimen types:
   1. 0.080 skin, 0.040 splice straps, AF-55 adhesive.
   2. 0.080 skin, 0.040 splice straps, FM-73 adhesive.

(3) Air Force requested these specimens continue cycling to 19,000 cycles or failure, whichever occurs first.

GP78-0471-42

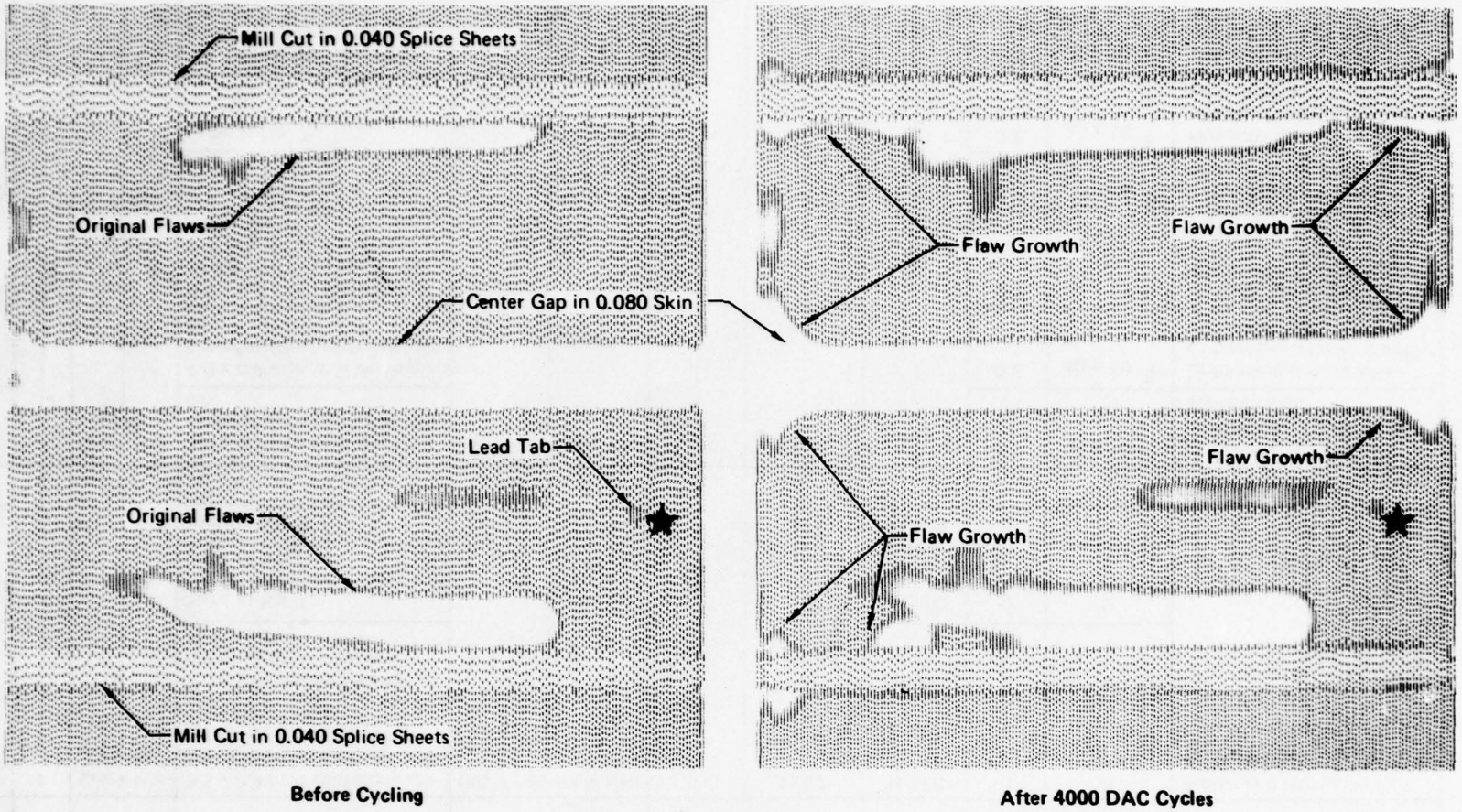

FIGURE 27

C-SCANS OF DOUBLE-STRAP SPECIMEN NO. 7 BEFORE AND AFTER CYCLING

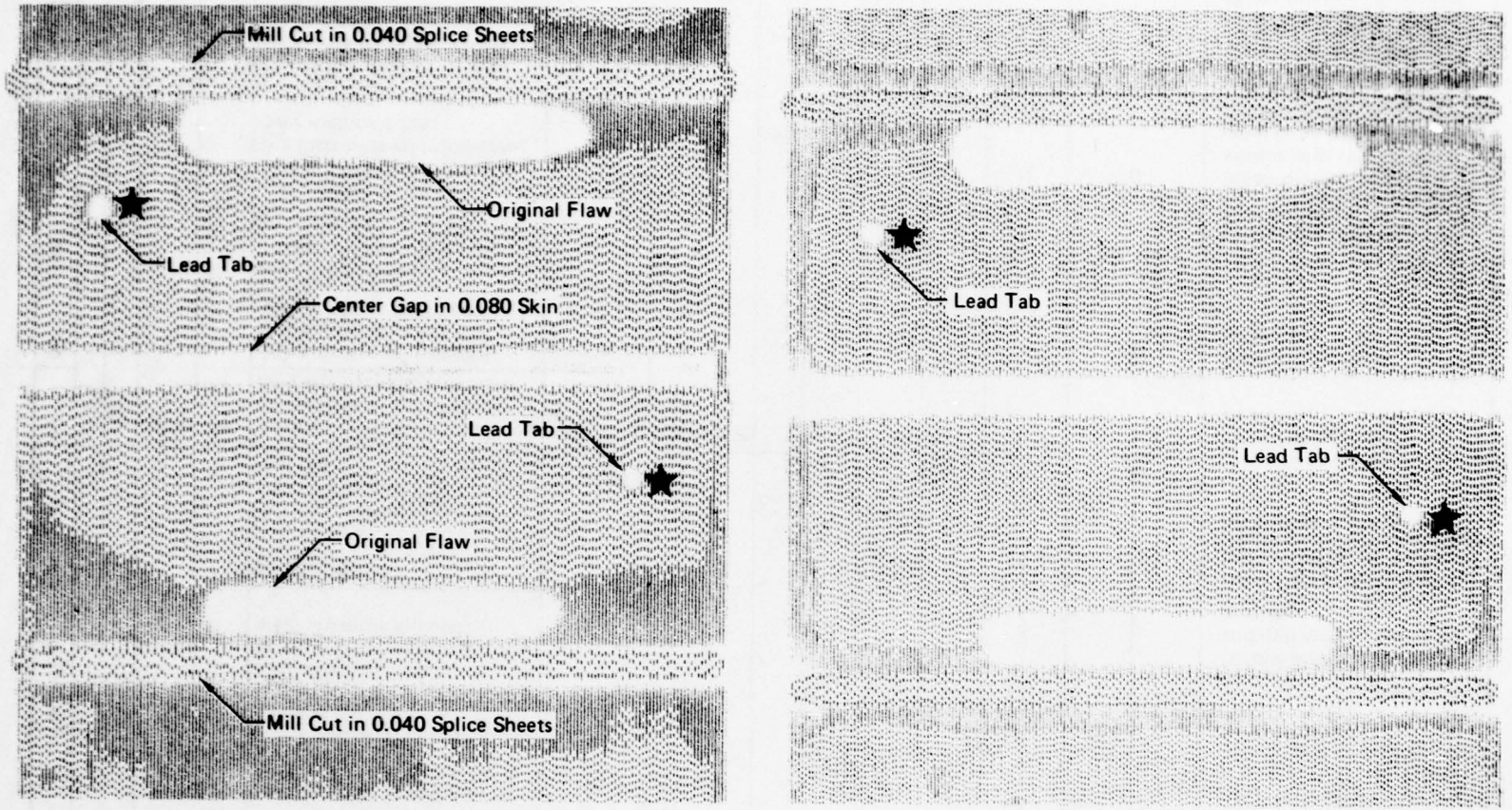

Before Cycling

After 4000 DAC Cycles

GP78-0471-49

FIGURE 28

C-SCANS OF DOUBLE-STRAP SPECIMEN NO. 2 BEFORE AND AFTER CYCLING

TABLE 14
RESULTS OF SINGLE-DOUBLER SPECIMEN TESTS
DAC Cycle

Specimen		Flaw Description		Test Conditions		Fatigue Cycles	Average Flaw Growth (in.)	Average Flaw Growth Rate (in./cycle)	Comments
No.	Type	Type	Geometry	Environment	Max Load (lb/in.)				
1	1	Porosity	4.0 inch wide elliptical porous area centered in width of specimen and over each mill cut	−50°F	1536	4028	0	0	No change in bondline.
2			Same as No. 1						
3			Same as No. 1						
4			Same as No. 1 except porous areas are more circular.						Porous areas extend from end mill cuts to center of specimen.
5			Same as No. 4						Porous areas cover almost one-half of bonded area.
6			4.0 inch wide porous void centered in width over each mill cut.						No change in bondline.
7	1	Porosity	1.5 inch diameter porous area centered in width of specimen and over each mill cut.	140°F, 95-100% RH	1536	4004	0	0	Flaw area open to ambient.
8			4.0 inch diameter porous area centered in width of specimen and over each mill cut.				0	0	Flaw area open to ambient.
9			3.0 inch wide elliptical porous area over each mill cut.				0.1	25×10^{-6}	Slight filleting of unbond along edge of porous area near mill cut.
10			One 4.5 inch wide and one 3.5 inch wide elliptical area over each mill cut.				0	0	Small bonded areas within large porous area grew but overall area did not grow.
11			One 3.5 inch and one 2.5 inch wide elliptical porous area over each mill cut.				0.1	25×10^{-6}	Slight filleting of unbond along edge of porous area near mill cut.
12			Same as No. 8.						Slight filleting of unbond along edge of porous area near mill cut.

GP78-0471-41

TABLE 14 (Continued)
RESULTS OF SINGLE-DOUBLER SPECIMEN TESTS
DAC Cycle

Specimen		Flaw Description		Test Conditions		Fatigue Cycles	Average Flaw Growth (in.)	Average Flaw Growth Rate (in./cycle)	Comments
No.	Type	Type	Geometry	Environment	Max Load (lb/in.)				
13	1	Crack-Like Voids	2.5 x 0.1 inch long void across width of specimen at each mill cut	140°F, 95-100% RH	1536	4004	0	0	No change in bondline.
14			1.5 x 0.1 inch long void across width of specimen at each mill cut.						Voids were open to ambient.
15			3.5 x 0.1 inch long void across width of specimen at each mill cut.						
16			2.5 x 0.3 inch long void across width of specimen at each mill cut.						
17			4.5 x 0.2 inch long void across width of specimen at each mill cut.						One void open to ambient.
18			Same as No. 13						No change in bondline.
19	1	Mechanical Damage	3.5 inch wide fractured bondline (0.20 inch deep)	140°F, 95-100% RH	1536	4032	0.1	25×10^{-6}	Unbond grew in the 0.2 dimension only.
20			Same as No. 19				0.1	25×10^{-6}	Unbond grew in the 0.2 dimension only.
21			Same as No. 19				0.2	50×10^{-6}	Unbond grew like Nos 19 and 20 but slight filleting along side of flaw as well.
22			Same as No. 19				0.05	12×10^{-6}	Very slight flaw growth.
23			Same as No. 19				0.05	12×10^{-6}	Slight filleting along edges of flaw.
24			4.0 inch wide fractured bondline (0.3 inch deep)				0.1	25×10^{-6}	Unbond grew in the 0.3 dimension.

TABLE 14 (Concluded)
RESULTS OF SINGLE-DOUBLER SPECIMEN TESTS
DAC Cycle

Specimen		Flaw Description		Test Conditions		Fatigue Cycles	Average Flaw Growth (in.)	Average Flaw Growth Rate (in./cycle)	Comments
No.	Type	Type	Geometry	Environment	Max Load (lb/in.)				
25	1	Circular Voids	A pair of 1.5 and 1.0 inch diameter voids tangent to each mill cut.	140°F, 95-100% RH	1536	4032	0	0	All four voids open to ambient.
26			A pair of 1.5 and 0.7 inch diameter voids tangent to each mill cut.						Three of four voids were open to ambient.
27			Same as No. 26.						Three of four voids were open to ambient.
28			A pair of 1.6 x 0.8 inch diameter voids tangent to each mill cut.						All four voids open to ambient.
29			Same as No. 28						All four voids open to ambient.
30			A pair of 1.5 and 1.0 inch diameter voids tangent to each mill cut.						All four voids open to ambient.
31	1	Crack-Like Voids	1.7 x 0.2 inch long void across width of specimen at each mill cut.	−50°F	1536	4056	0	0	Flaws were within 0.1 inch of mill cut.
32			3.5 x 1 inch long void across width of specimen at each mill cut.						One flaw was open to ambient.
33			3.5 x 0.25 inch long void across width of specimen at each mill cut.						Both flaws open to ambient.
34			3.0 x 0.3 inch long void across width of specimen at each mill cut.						One flaw open to ambient.
35			4.0 x 0.3 inch long void across width of specimen at each mill cut.						Flaws were within 0.1 inch of mill cut.
36			Same as No. 35.						One flaw open to ambient.

Notes:
1. All specimens cycled at the DAC cycle rate of 2 cycles per hour.
2. All specimens were single-doubler, Type 1, 0.080 skin, 0.040 doubler, and AF-55 adhesive.

TABLE 15
RESULTS OF SINGLE-STRAP SPECIMEN TESTS
DAC Cycle

Specimen		Flaw Description		Test Conditions		Fatigue Cycles	Residual Strength (lb)	Average Flaw Growth (in.)	Average Flaw Growth Rate (in./cycle)	Comments
No.	Type	Type	Geometry	Environment	Max Load (lb/in.)					
1	1	Crack-Like Voids	4.5 x 0.5 inch voids along width of specimen at each mill cut.	140°F, 95-100% RH	1000	3818	28,050	0.1	25×10^{-6}	All three flaws showed slight growth in the 0.5 inch dimension.
2			4.5 x 0.3 inch voids along width of specimen at each mill cut.				29,400	0.1	25×10^{-6}	Slight filleting of unbonds along side of voids. Cohesive failure.
3			Same as No. 2.				31,650	0.1	25×10^{-6}	Same as No. 2. Cohesive failure.
4			Same as No. 2.				–	1.0	250×10^{-6}	One side of splice failed at 3818 cycles.
5			5.0 x 0.3 inch voids along width of specimen at each mill cut.				29,000	0.1	25×10^{-6}	Slight filleting of unbonds along side of voids. Cohesive failure.
6			4.5 x 0.4 inch voids along width of specimen at each mill cut.				29,550	0.1	25×10^{-6}	Slight filleting of unbonds along side of voids. Cohesive failure.
7	1	Variable Bondline Thickness	Thickness varied across width from thick in middle to thin along sides.	140°F, 95-100% RH	1000	4016	33,250	0.1	25×10^{-6}	Unbonding along all three milled slots. Cohesive bond failure.
8			Same as No. 7.				32,650	0.1	25×10^{-6}	
9			Thickness varied across width from thick in middle to thin along sides.				29,300	0.2	50×10^{-6}	
10			2.0 inch wide porous area across both splices. Adhesive thins out towards specimen edges.				31,650	0.1	25×10^{-6}	Slight unbonding along each milled cut. Cohesive bond failure.

GP78-0471-40

TABLE 15 (Continued)

RESULTS OF SINGLE-STRAP SPECIMEN TESTS

DAC Cycle

Specimen		Flaw Description		Test Conditions		Fatigue Cycles	Residual Strength (lb)	Average Flaw Growth (in.)	Average Flaw Growth Rate (in./cycle)	Comments
No.	Type	Type	Geometry	Environment	Max Load (lb/in.)					
11	1	Variable Bondline Thickness	1.0 inch diameter porous area across center cut. Adhesive thins out towards outer edges.	140°F, 95-100% RH	1000	4016	33,100	0.05	12×10^{-6}	Slight unbonding along each milled cut. Cohesive bond failure.
12			Same as No. 10				21,750	0.1	25×10^{-6}	Slight unbonding along each milled cut. Cohesive bond failure.
13	1	Crack-Like Voids	4.5 x 0.2 inch void along width of specimen at each mill cut.	−50°F	1000	4080	33,400	0	0	Cohesive bondline failure.
14			4.5 x 0.3 inch void of center mill cut, 4.0 x 0.2 inch void at one end mill cut.				33,850	0	0	
15			5.0 x 0.3 inch void at center mill cut and 5.0 x 0.1 inch void at each end mill cut.				33,150	0	0	
16			Same as No. 15				33,450	0	0	
17			4.5 x 0.2 inch void at center mill cut and 4.0 x 0.1 inch void at each end mill cut.				34,150	0	0	
18			4.5 x 0.2 inch void at center mill cut and 4.0 x 0.1 in void at each end mill cut.				16,300	0	0	Aluminum (0.090) failed at mill cut.
19	1	Circular Voids	A pair of 1.2 inch diameter voids in each splice overlap	140°F, 95-100% RH	1000	4080	17,350	0.1	25×10^{-6}	Flaw growth at center mill cut only. Cohesive failure.
20			Same as No. 19				27,000	0.1	25×10^{-6}	Short flaw growth along center and end milled slots. Cohesive failure.

TABLE 15 (Continued)
RESULTS OF SINGLE-STRAP SPECIMEN TESTS
DAC Cycle

Specimen		Flaw Description		Test Conditions		Fatigue Cycles	Residual Strength (lb)	Average Flaw Growth (in.)	Average Flaw Growth Rate (in./cycle)	Comments
No.	Type	Type	Geometry	Environment	Max Load (lb/in.)					
21	1	Circular Voids	A 1.2 inch diameter void tangent to center milled cut and two 0.5 inch diameter voids tangent to end mill cut.	140°F, 95-100% RH	1000	4080	31,700	0	0	Cohesive failure.
22			Same as No. 19				–	1.7	420×10^{-6}	Bondline failed while being removed from fixture.
23			Pair of 1.2 inch dia voids tangent to center milled cut and pair of 0.5 inch diameter voids at end cuts.				24,250	0.1	25×10^{-6}	Cohesive failure.
24			Same as No. 21				31,250	0	0	Possible slight filleting at edges of circular voids.
25	1	Mechanical Damage	4.5 inch wide x 1.0 inch deep fractured bondline.	140°F, 95-100% RH	1000	4128	25,150	0.2	50×10^{-6}	Unbonding fairly uniform along fracture line.
26			4.5 inch wide x 1.2 inch deep fractured bondline.				18,450	0.3	75×10^{-6}	Unbonding along fracture line and along center milled cut.
27			4.0 inch wide x 1.0 inch deep fractured bondline.				23,400	0.1	25×10^{-6}	
28			Same as No. 26				24,300	0.2	50×10^{-6}	
29			Same as No. 27				27,450	0.1	25×10^{-6}	Slight filleting of unbond along side of fracture line and unbonding along center mill cut.
30			Same as No. 27				27,750	0.1	25×10^{-6}	Unbonding along fracture line.

TABLE 15 (Concluded)
RESULTS OF SINGLE-STRAP SPECIMEN TESTS
DAC Cycle

Specimen		Flaw Description		Test Conditions		Fatigue Cycles	Residual Strength (lb)	Average Flaw Growth (in.)	Average Flaw Growth Rate (in./cycle)	Comments
No.	Type	Type	Geometry	Environment	Max Load (lb/in.)					
31	2	Crack-Like Voids	4.0 x 0.25 inch long void at center mill cut and 1.5 x 0.2 inch long voids at each end mill cut.	140°F, 95-100% RH	1000	4080	(3)	0	0	No change in bondline.
32			4.5 x 0.2 inch long void at center mill cut and 4.0 x 0.1 inch long void at each end mill cut.					0	0	No change in bondline.
33			Same as No. 1					0.1	25×10^{-6}	Slight filleting of unbond at side of void.
34			Same as No. 1					0.1	25×10^{-6}	
35			4.5 x 0.2 inch long void across specimen width at each mill cut.					0.1	25×10^{-6}	
36			Same as No. 35					0.05	12×10^{-6}	Very slight filleting at unbonds at sides of voids.

Notes:
1. All specimens cycled at the DAC cycle rate of 2 cycles per hour.
2. Specimen types:
   1. 0.080 skin and 0.090 splice strap with AF-55 adhesive.
   2. 0.080 skin and 0.090 splice strap with FM-73 adhesive.

(3) Air Force requested these specimens continue cycling to 19,000 cycles or failure whichever occurs first.

Unlike the double-strap specimens bonded with FM-73 where considerable flaw growth was observed, the single-strap specimens bonded with FM-73 exhibited only a small amount of flaw growth and about equal to the amount observed on similar specimens bonded with AF-55 adhesive. The specimens bonded with FM-73 adhesive are continuing to cycle at the DAC cycle rate and the test results will be reported to the Air Force at their conclusion. Only two of the 36 specimens tested ruptured in the bond line during testing. Specimen No. 4 failed after 3818 cycles and specimen No. 22 failed as it was being removed from the test chamber after completing 4080 cycles.

Tests of Skin-to-Substructure Specimens - Tests of skin-to-substructure tee specimens tested at the DAC cycle rate are summarized in Table 16. C-scans of these specimens after 4000 cycles indicated that flaw growth had occurred in both hot/humid and cold environments. Specimens with mechanically damaged and porous bondlines and 0.040 skins were the only specimen configurations which showed evidence of flaw growth in both environments. Much like the other specimens, the magnitude of flaw growth after 4000 DAC cycles was roughly equal to the amount observed on similar specimens, tested at the fast cycle rate, after approximately 1,000,000 cycles, confirming the results of other investigators which indicated adhesive durability to be dependent on cycle rate.

3.6 Summary of Residual Strength Tests

Double-strap, single-strap, and tee specimens which survived fatigue testing were statically tested to failure. Failure loads are recorded in the tables where the results of fatigue tests for each specimen are summarized.

Residual strength tests were conducted on sixteen single-strap specimens which survived the fast cycle fatigue tests and on twenty-seven specimens which survived the DAC cycle fatigue tests. Two specimens which had not been exposed to either type of fatigue cycle were static tested to failure for comparison purposes. Eleven of the sixteen specimens surviving the fast cycle tests had residual net shear strengths below that of the uncycled specimens. Net shear strength was based on the actual bonded area after fatigue testing. Residual net shear strength of twenty-six of the twenty-seven specimens surviving the DAC cycle tests were below that of the uncycled specimens. A bar chart depicting these results as well as the scatter in data is presented in Figure 29. The lowest average residual net shear strength, for specimens cycled at either cycle rate, was recorded for specimens with variable adhesive thickness or mechanical damage. Specimens with crack-like voids exhibited the highest residual net shear strength of specimens cycled at either cycle rate. Residual net shear strengths of fast cycle specimens with crack-like and circular voids, and bonded with AF-55 adhesive were higher than similarly flawed specimens bonded with FM-73 adhesive. One specimen with porous bondline flaws and bonded with AF-55 had a slightly lower residual net shear strength than a similarly flawed FM-73 specimen.

TABLE 16
RESULTS OF SKIN-TO-SUBSTRUCTURE (TEE) SPECIMEN TESTS
DAC Cycle

Specimen		Flaw Description		Test Conditions		Fatigue Cycles	Residual Strength (lb)	Average Flaw Growth (in.)	Average Flaw Growth Rate (in./cycle)	Comments
No.	Type	Type	Geometry	Environment	Max Load (lb/in.)					
1	1	Porosity	Porous area along edge of tee base on both sides, 1.5 x 0.3 inches.	−50°F	100	3908	2970	0	0	C-Scans show no change in bondline.
2			Same as No. 1				3220	0	0	C-Scans show no change in bondline.
3			Light porosity along edge of tee base on both sides of specimen.				3065	0.05	12×10^{-6}	Very small unbond area along edges of tee base.
4			2.0 x 0.3 inch porous area along edge of tee base, both sides.				3260	0.05	12×10^{-6}	
5			Same as No. 4				3075	0.05	12×10^{-6}	
6			Same as No. 4				–	0.5	120×10^{-6}	Bondline failure after 3908 cycles.
7	1	Porosity	Light porosity area 2.0 x 0.4 inches along edge of tee base, both sides.	140°F, 95-100% RH	100	4016	2965	0.15	40×10^{-6}	Most unbonding was next to porous area along edge of tee base.
8			Light porosity area 1.5 x 0.4 inches along edge of tee base, both sides.				2890	0.2	50×10^{-6}	Most unbonding was next to porous area along edge of tee base.
9			Light porosity area 1.5 x 0.4 inches along edge of tee base, both sides.				3115	0.15	40×10^{-6}	Most unbonding occurred next to porous areas along edge of tee base.
10			Same as No. 9				2475	0.2	50×10^{-6}	Same as No. 9
11			Light porosity area 2.0 x 0.5 inches along edge of tee base, both sides.				1850	0.4	100×10^{-6}	One side almost completely unbonded.
12			Same as No. 11				2550	0.3	75×10^{-6}	Unbonding progressed from sides of porous areas toward center of specimen.

GP78-0471-39

TABLE 16 (Continued)

RESULTS OF SKIN-TO-SUBSTRUCTURE (TEE) SPECIMEN TESTS

DAC Cycle

Specimen		Flaw Description		Test Conditions		Fatigue Cycles	Residual Strength (lb)	Average Flaw Growth (in.)	Average Flaw Growth Rate (in./cycle)	Comments
No.	Type	Type	Geometry	Environment	Max Load (lb/in.)					
13	1	Crack-Like Voids	Three 1.0 x 0.10 inch voids along one side of tee base.	−50°F	100	4032	2345	0	0	No change in bondline. Cohesive failure.
14			Same as No. 13				2070	0	0	
15			A 1.0 x 0.10 inch void at each corner of specimen along edge.				2065	0	0	
16			1.2 x 0.3 inch void along one edge of one side of tee.				1760	0	0	
17			1.5 x 0.5 inch void along one edge of tee base.				1795	0	0	
18			1.5 x 0.2 inch void along each side of tee base.				1955	0	0	
19	1	Mechanical Damage	2.0 x 0.5 inch fractured bondline on each side of tee base.	−50°	100	4008	1460	0.1	25×10^{-6}	Unbond area progressed from side of bondline fracture.
20			Same as No. 19				1885	0.15	40×10^{-6}	Most unbonding at sides of fractured area along edge of tee base.
21			2.3 x 0.6 inch fractured bondline on each side of tee base.				1760	0.10	25×10^{-6}	
22			Same as No. 21				1860	0.10	25×10^{-6}	
23			2.5 x 0.5 inch fractured bondline on each side of tee base.				1655	0.15	40×10^{-6}	
24			Same as No. 23				2360	0.1	25×10^{-6}	

TABLE 16 (Continued)

RESULTS OF SKIN-TO-SUBSTRUCTURE (TEE) SPECIMEN TESTS

DAC Cycle

Specimen		Flaw Description		Test Conditions		Fatigue Cycles	Residual Strength (lb)	Average Flaw Growth (in.)	Average Flaw Growth Rate (in./cycle)	Comments
No.	Type	Type	Geometry	Environment	Max Load (lb/in.)					
25	1	Mechanical Damage	2.0 x 0.5 inch fractured bondline along both sides of tee base.	140°F, 95-100% RH	100	4032	1315	0.1	25×10^{-6}	Unbonding progressed from edges of tee base toward center of speciman.
26			Same as No. 25				1925	0.1	25×10^{-6}	
27			2.3 x 0.5 inch fractured bondline along both sides of tee base.				1470	0.15	40×10^{-6}	
28			2.5 x 0.6 inch fractured bonding along both sides of tee base.				1210	0.15	40×10^{-6}	Unbonded along edges of tee base and along edge of fracture toward center of specimen.
29			Same as No. 27				1465	0.15	40×10^{-6}	
30			Same as No. 27				1585	0.15	40×10^{-6}	
31	2	Crack-Like Voids	1.7 x 0.2 inch void along edge of tee base on one side.	140°F, 95-100% RH	80	4032	1590	0.1	25×10^{-6}	Unbonded all along edges of tee base. Cohesive failure.
32			2.0 x 0.25 inch void along edge of tee on one side.				1575	0.1	25×10^{-6}	
33			Same as No. 32				1710	0.1	25×10^{-6}	
34			1.5 x 0.2 inch void along edge of tee on one side.				1705	0.1	25×10^{-6}	
35			1.7 x 0.25 inch void along each edge of tee base.				1710	0.15	40×10^{-6}	
36			None				2155	0.1	25×10^{-6}	

TABLE 16 (Continued)
RESULTS OF SKIN-TO-SUBSTRUCTURE (TEE) SPECIMEN TESTS
DAC Cycle

Specimen		Flaw Description		Test Conditions		Fatigue Cycles	Residual Strength (lb)	Average Flaw Growth (in.)	Average Flaw Growth Rate (in./cycle)	Comments
No.	Type	Type	Geometry	Environment	Max Load (lb/in.)					
37	1	Circular Voids	1.5 x 0.8 inch void in center of specimen under upstanding leg.	140°F, 95-100% RH	100	4032	1570	0.1	25×10^{-6}	Unbonded along edges of tee base.
38			Same as No. 37				2025	0.1	25×10^{-6}	
39			1.6 x 0.7 inch void in center of specimen under upstanding leg.				2165	0.1	25×10^{-6}	
40			Same as No. 39				1750	0.1	25×10^{-6}	Unbonded area along edges of tee progressed almost to original void.
41			Same as No. 39				2230	0.1	25×10^{-6}	Same as No. 37
42			1.2 x 0.7 inch void in center of specimen under upstanding leg.				2240	0.1	25×10^{-6}	Same as No. 40
43	2	Mechanical Damage	2.5 x 0.5 inch fractured bondline along edge of both sides of tee base.	−50°F	80	4128	2060	0	0	C-Scans show no noticeable change in bondline. Cohesive failure after fatigue cycling.
44			Same as No. 43.				1490	0	0	
45			3.0 x 0.7 inch fractured bondline along edge of both sides of tee base.				2070	0	0	
46			2.5 x 0.6 inch fractured bondline along edge of both sides of tee base.				1700	0	0	
47			2.7 x 0.65 inch fractured bondline along edge of both sides of tee base.				1725	0	0	
48			2.8 x 0.7 inch fractured bondline along edge of both sides of tee base.				1800	0	0	

TABLE 16 (Continued)
RESULTS OF SKIN-TO-SUBSTRUCTURE (TEE) SPECIMEN TESTS
DAC Cycle

Specimen		Flaw Description		Test Conditions		Fatigue Cycles	Residual Strength (lb)	Average Flaw Growth (in.)	Average Flaw Growth Rate (in./cycle)	Comments
No.	Type	Type	Geometry	Environment	Max Load (lb/in.)					
49	3	Mechanical Damage	3.0 x 0.7 inch fractured bondline on each side of tee base.	−50°F	80	4128 △1	–	0	0	△1
50			Same as No. 49				–	0	0	
51			Same as No. 49				–	0	0	
52			2.5 x 0.6 inch fractured bondline on each side of tee base.				–	0	0	
53			Same as No. 52				–	0	0	
54			3.0 x 0.7 fractured bondline on each side of tee base.				–	0	0	
55	1	Crack-Like Voids	No flaws	140°F, 95-100% RH	100	4176	–	0.1	25×10^{-6}	This was a replacement specimen for one that failed after a few cycles.
56			1.0 x 0.2 void along one edge of tee base.				2060	0.1	25×10^{-6}	Unbonded along edge of tee base on both sides.
57			1.7 x 0.4 void along one edge and 1.7 x 0.2 inch void along other side.				2210	0.1	25×10^{-6}	Unbonded along both edges of tee base.
58			2.0 x 0.2 void along one side. Opposite side almost completely void.				2425	0.15	40×10^{-6}	Only center half of bondline area remained bonded.
59			1.8 x 0.3 void along one side of tee base.				2565	0.1	25×10^{-6}	Unbonded along edges of tee base.
60			1.2 x 0.2 void along one side of tee base.				2220	0.15	40×10^{-6}	Unbonded along edges of tee base.

TABLE 16 (Concluded)
RESULTS OF SKIN-TO-SUBSTRUCTURE (TEE) SPECIMEN TESTS
DAC Cycle

Specimen		Flaw Description		Test Conditions		Fatigue Cycles	Residual Strength (lb)	Average Flaw Growth (in.)	Average Flaw Growth Rate (in./cycle)	Comments
No.	Type	Type	Geometry	Environment	Max Load (lb/in.)					
61	1	Circular void	1.2 x 0.7 inch void in center of tee	−50°F	100	4000	2505	0	–	Cohesive type failures
62			1.5 x 0.5 inch void in center of tee				2660	0	–	
63			1.5 x 0.8 inch void in center of tee				2220	0	–	
64			1.3 x 0.7 inch void in center of tee				2475	0	–	
65			0.7 inch diameter void in center of tee				2760	0	–	
66			1.5 x 0.6 inch void in center of tee.					0	–	

Notes:
1. Air Force has requested that these specimens be allowed to continue cycling until 19,000 cycles are accumulated or failure.
2. All specimens were cycled at the DAC cycle rate of 2 cycles per hour.
3. Specimen types:
   1. 0.040 skin, 0.063 tee, AF-55 adhesive
   2. 0.080 skin, 0.063 tee, AF-55 adhesive
   3. 0.080 skin, 0.063 tee, FM-73 adhesive

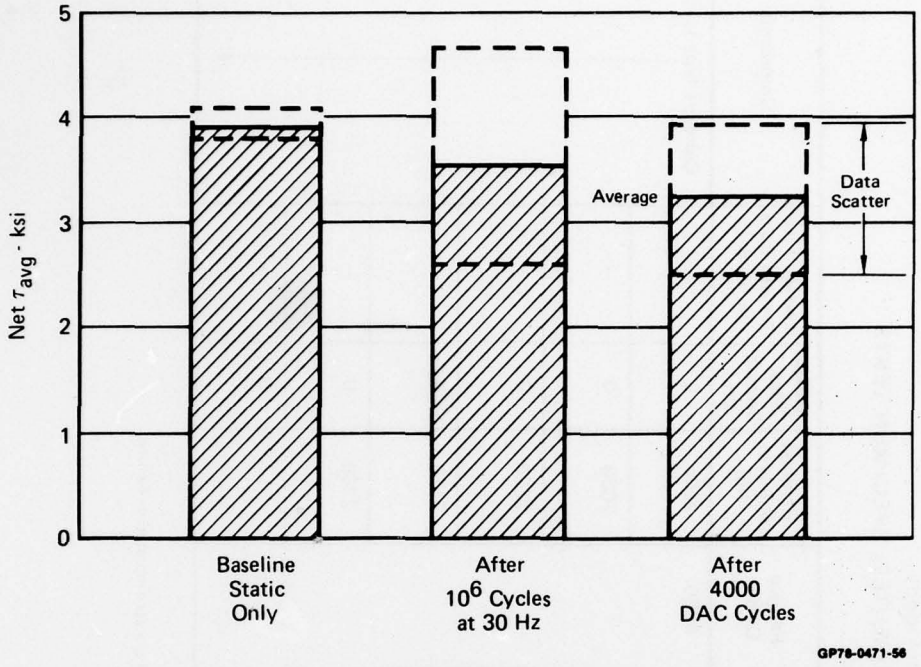

FIGURE 29
RESIDUAL STRENGTH TESTS OF SINGLE-STRAP SPECIMENS

Eight tee specimens with 0.080 skins and tested in the -50°F environment were the only specimens that survived fatigue cycling at the fast cycle rate and for which residual tension strength tests were conducted. Two of these specimens were bonded with FM-73 adhesive and the remainder with AF-55. Four of the eight specimens had mechanically damaged bondlines, two bonded with FM-73 adhesive and two with AF-55. The average residual net tension strength of the two AF-55 specimens was approximately twice that of specimens bonded with FM-73. Net tension strength was based on the actual bonded area after fatigue testing. Residual net tension strength of AF-55 specimens with either crack-like voids or circular voids were also higher than the FM-73 specimens but lower than the mechanically damaged AF-55 specimens.

Residual net tension strength was also determined for fifty-eight tee specimens which survived fatigue cycling at the DAC cycle rate. All of the specimens tested were bonded with AF-55 adhesive. Twelve of these specimens were configured with 0.080 skins, six being cycled in a hot/wet environment and six at -50°F. The remaining forty-six specimens had 0.040 skins. The six specimens with 0.080 skin and tested in the -50°F environment had an average residual net tension strength of 437 psi compared to 544 psi for similarly configured specimens cycled

at the fast cycle rate. The forty-six specimens with 0.040 skin were used to evaluate four types of bondline flaws; porosity, crack-like voids, circular voids, and mechanical damage. One half of the specimens for each type flaw were cycled in a hot/wet environment and one half at -50°F. Residual net tension strength of these specimens were essentially equal with the exception of specimens with crack-like voids. In this case, the specimens cycled at -50°F had a much lower residual net tension strength than those cycled in a hot/wet environment.

All of the double-strap specimens failed in the 0.040 aluminum straps at the center of the specimen.

4. PHASE III - NDE ASSESSMENT (COMPLEX SPECIMENS)

In this task, specimens that represented actual design detail configurations used on the PABST fuselage article were fabricated with bondline defects. These specimens are for use in assessing the capabilities of state-of-the-art NDE techniques in detecting and discriminating between the various defects being considered. Design details were fabricated using hardware from the PABST program. Defects and defect locations were, as much as possible, also representations of what might be expected to occur in production.

Two sets of three configurations each were fabricated. The first set was used to confirm the methods of introducing the defects and verifying their existence by destructive testing. The second set was non-destructively inspected and provided to the Air Force for use in future efforts to assess the capabilities of new NDE equipment.

4.1 Design and Fabrication of Complex Specimens

The three specimens fabricated were representative of three types of structural configurations used on the PABST wide body fuselage demonstration article. They represent the external longeron region, the internal longeron region and a side shear panel region.

Flaws were intentionally induced in the bondlines by cutting out portions of the film adhesive or by inserting wires in the bondline prior to bonding. No attempt was made to prevent naturally occurring flaws such as might result from misfits, joggles, or drilling operations through bonded parts.

The adhesive used was AF-55 rather than FM-73 the adhesive used on the PABST fuselage. The AF-55 adhesive was selected to take advantage of its radio-opacity locating flaws by x-ray prior to submitting them to evaluations by other NDE techniques.

In general, the flaws produced were smaller in size than had been produced in flawed simple specimens. Although there were no special precautions taken to insure good fit-up, flaws other than those intentionally induced were also found under bonded joggle areas. All flaw sizes and corresponding methods of production were documented before commencing fabrication of the second set of complex specimens.

An envelope bagging system was used in bonding the specimen details. Longerons and tee-frame members were held in a picture frame aluminum tool while skins and doublers were held in place with pressure sensitive tape. Precautions were taken prior to curing to insure that the mylar envelope bag would not tear due to improper fit in the corners of the detail parts. The bonding cycle was identical to the cycle used in fabricating the PABST fuselage demonstration article. All detail parts to be bonded

were cleaned, phosphoric acid anodized, and primed per Douglas Process Specifications. A faying surface seal, MIL-S-81733, Type IV-12, was applied between all mechanically fastened skin joints.

The internal longeron specimen, shown in Figure 30, is representative of the upper portion of the fuselage where longerons are located on the inner moldline of the fuselage cover skins. This specimen includes a frame longeron intersection, a longeron splice, a circumferential splice, and a bonded crack stopper under the longeron.

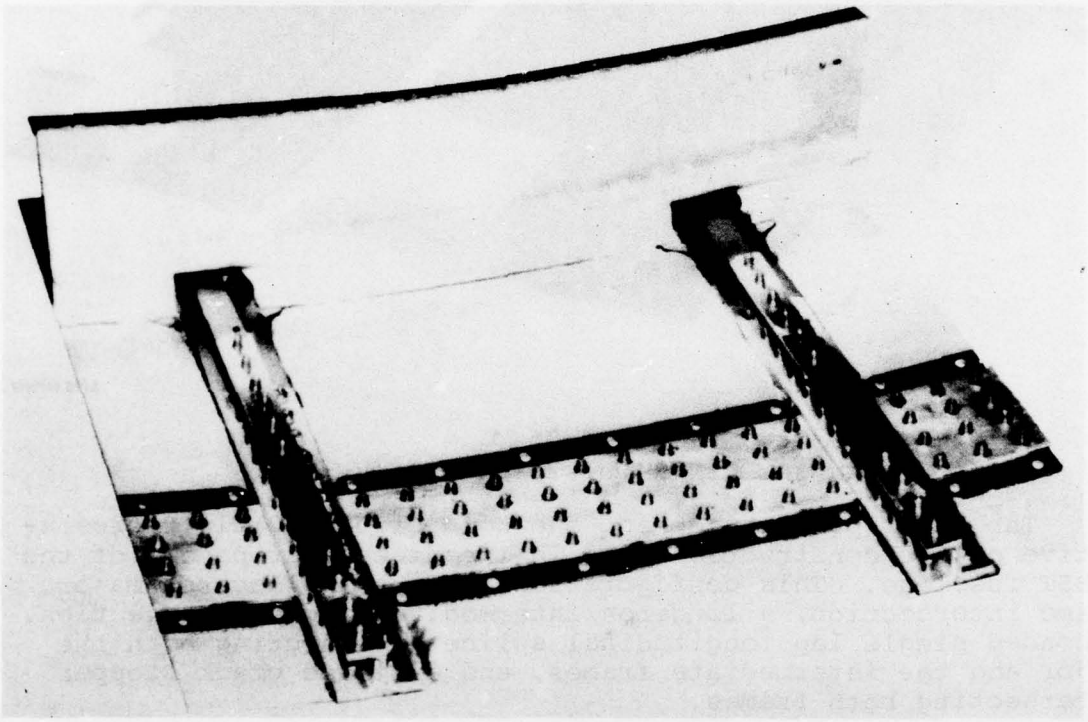

GP78-0471-43

FIGURE 30
COMPLEX SPECIMEN - INTERNAL LONGERON

The external longeron specimen, shown in Figure 31, is representative of the lower portion of the PABST fuselage where longerons are located on the outer moldline of the fuselage cover skins. This specimen includes a frame/longeron intersection, a longeron splice, and a bonded double-lap longitudinal splice intersecting a mechanically fastened circumferential splice, and a bonded double-lap longitudinal splice intersecting a mechanically fastened circumferential splice as well as a bonded circumferential splice.

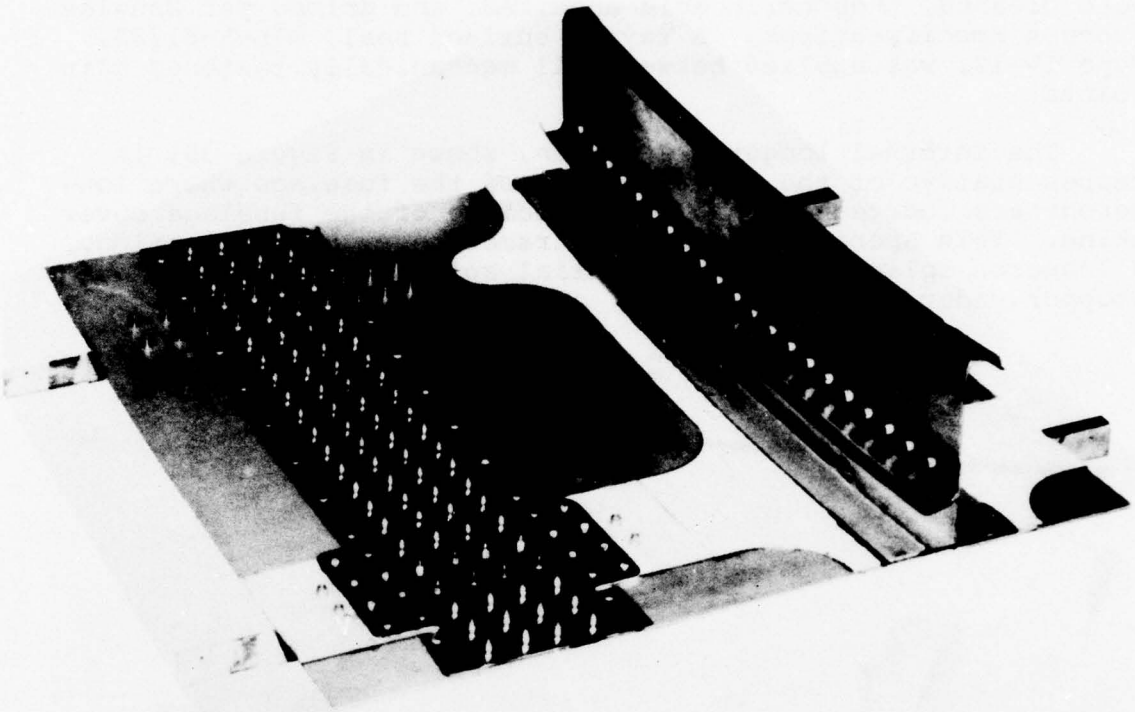

GP78-0471-44

FIGURE 31
COMPLEX SPECIMEN - EXTERNAL LONGERON

The shear panel specimen, shown in Figure 32, is representative of the construction used in the side shear panels of the PABST fuselage. This configuration includes a longeron/major frame intersection, a longeron/intermediate frame intersection, a bonded single lap longitudinal splice intersecting both the major and the intermediate frames, and a bonded crack stopper intersecting both frames.

4.2 Assessment of NDE Methods

Each of the three complex specimens were inspected using low kilovoltage radiography, ultrasonic through-transmission reflector plate and Fokker Bondtester techniques. The shear panel specimen was additionally inspected by the squirter-coupled ultrasonic through-transmission and Shuretronic Harmonic Bondtester (eddy-sonics) techniques. Good correlation was obtained between flaws found by each of the NDE methods, especially between the full thickness measuring techniques of radiography and through-transmission ultrasonics. Flaw indications in some configurations, using the Fokker Bondtester, differed from the through-the-part techniques because it essentially locates flaws only in the nearest bondline. Tetrabromo-ethane was used on several single-strap specimens to assess its ability to detect flaws and flaw growth.

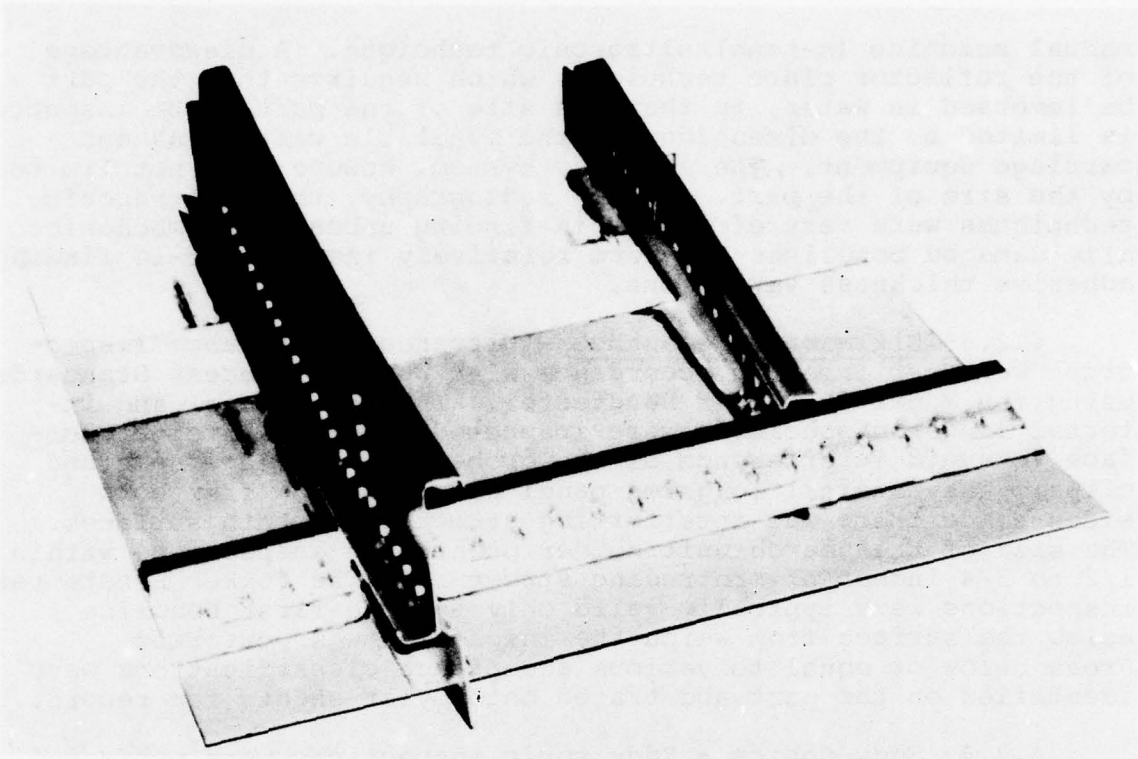

GP78-0471-45

FIGURE 32
COMPLEX SPECIMEN - SHEAR PANEL

4.2.1 Radiography - The low kilovoltage radiography technique used to inspect the complex specimens was exceptionally effective in finding adhesive voids, porosity and metal particles left in the bondline. The use of AF-55 adhesive, which has a relatively high radio-opacity, makes this technique particularly attractive. Interference from structural members adjacent to the bondlines can be avoided by using angle-beam exposures.

Radiography was not effective in finding unbonds and mechanically damaged bondlines because in both of these conditions the appearance of the radiograph is unaffected. Abrupt changes in bondline thickness are often visible in the radiograph as a halo or dark shadow and could be easily overlooked by the inspector.

4.2.2 Through-Transmission Ultrasonics - The reflector plate and squirter-coupled through-transmission ultrasonic techniques yielded c-scan presentations showing a plan view of the structure and excellent definitions of the bondline flaws. Attached structural members such as tee stiffeners and frames interferred with the search units of both methods and prevented the inspection of certain areas. These areas were inspected by

manual scanning (A-scan) ultrasonic technique. A disadvantage of the reflector plate technique, which requires that the part be immersed in water, is that the size of the part to be inspected is limited by the dimensions of the available water tank and carriage equipment. The squirter system, however, is not limited by the size of the part. Unlike radiography, these ultrasonic techniques were very effective in finding unbonds and mechanically damaged bondlines but were relatively ineffective in finding adhesive thickness variations.

4.2.3 Ultrasonic Resonance - Ultrasonic resonance inspections were performed in accordance with Douglas Process Standards using the Model 70 Fokker Bondtester. The shear panel and internal longeron specimens were inspected from the external surface to avoid interference of the probe by attached frames and clips. The external longeron panel was inspected from both sides since there was interferring structure on both surfaces. The size of the search unit holder prohibited inspections within 1/2 to 3/4 inches of protruding structure. The Fokker Bondtester inspections were typically valid only for the first bondline below the surface from which the inspection was performed. Areas below or equal to various acceptance classifications were identified on the part and traced onto mylar sheets for record.

4.2.4 Eddy Sonics - Eddy sonic inspections were performed using the Shuretronic Harmonic Bondtester. Inspections were limited to the first bondline below the surface. Access to the bondline being inspected was limited to within 1/2 to 3/4 inches of protruding structural members because of the size of the search unit. Flawed areas found by this method were traced from marks made on the specimen to mylar sheets. This technique was found to be the least effective method for locating adhesive bondline flaws. This technique was also the most time consuming.

4.2.5 Tetrobromo-ethane - Tetrobromo-ethane (TBE), a radio-opaque penetrant, was applied to the bondline of three single-strap specimens in an experiment to determine whether or not flaw growth, as indicated by ultrasonic c-scans, could be verified by x-ray.

One part of Magnaflux ZL2A Penetrant was mixed with ten parts TBE to aid in penetrating flawed areas. Penetration was aided by placing the specimens in a bell jar and applying a partial vacuum. Indications of the initially induced flaws, which were open to the atmosphere, were intensified by the TBE and showed up extremely well, whereas flaws closed to the atmosphere remained unchanged. Comparisons of flaw growth indications on both the x-ray and c-scan show good correlation. However, indications of flaw growth were more definitive on the c-scans than on the x-rays. The probable reason for the poorer indication in the x-rays is that there is only a small opening between the aluminum adherends into which the TBE can penetrate. This opening also tends to become very thin close to the leading edge of the flaw and therefore contains considerably less TBE.

4.3 Documentation of NDE Procedures

The NDE procedures used to inspect the complex specimens were documented for future reference.

Radiography - The X-ray machine used for all radiographs is a constant potential type with a 3mm focal spot and a beryllium window. Small lead tabs and letters were used for location markers and identification. All bondlines were x-rayed over their entire area. Intersecting bondlines of skin stiffeners and skin doublers were often x-rayed more than once in order to fully define the defects. Each negative produced was visually inspected on a light table. Flaws were outlined on the negative with a grease pencil. This identification mark was then transferred to a mylar sheet for permanent record.

Through-Transmission Reflector Plate - This technique requires the specimen to be completely immersed in water. This method uses a standard Branson 600 Ultrasonic Instrument in conjunction with an Automation Industries recorder and an immersion tank. Slight modifications were made to the Branson 600 in order to print out the multi-tone lines which are characteristic of this method. A 2-1/4 MHz, 3/4 inch diameter SIJ search unit was focused at 4 inches in water. Sensitivity was adjusted so that 1/8 x 1/8 inch by 3-ply lead tabs (0.005 inch per ply) printed to size as white areas. Using this technique, the bonded areas are printed out as multi-tone lines. This is accomplished through an electronic gating device which monitors the strength of the signal received from the search unit.

Squirter-Coupled Ultrasonics - In this technique, the transducers are coupled to the part with water streams from 1/4 inch diameter water squirters. The system is operated in a through-transmission mode using a MCAIR built pulser-receiver and associated electronic equipment. The ultrasonic information is stored in a mini-computer and can be recalled and processed for output either during or at the conclusion of scanning. The system provides a gray tone C-scan with the gray shades representing an attenuation range chosen by the operator at the time of the print out. Two 2-1/4 MHz, 3/4 inch diameter SIJ search units with a 4 inch focal length in water were used in the system for these inspections. The part was scanned at a 0.040 inch scan index. The printout was made in a 32 dB attenuation gray tone range with 1/8 x 5/8 x 2-ply lead tape tabs set to print a medium gray and 1/8 x 1/8 x 2-ply lead tape tabs set to print a light gray. With this set up, flaws printed a dark gray to black.

Eddy Sonics (Shurtronics Harmonic Bondtester) - The eddy sonics technique does not require the use of a couplant. Vibrations are introduced into the test piece through alternating eddy currents and the resulting resonance tones are monitored acoustically. The instrument output level and sensitivity are adjusted to give a full scale meter deflection on a loose top

sheet and below midrange deflection over bonded area. The alarm level is set at 70% meter deflection. The part is scanned and indications of unbonds marked on the part. The set-up must be readjusted over each change in structure. When the part is completely scanned, flaw indications are transferred to a mylar to retain the inspection results.

Fokker Bondtester - For Fokker Bondtester inspections, the instrument is set up and used in accordance with Douglas Process Specifications for acceptance limits and probe selection. The probe is placed, with ultrasonic couplant, on a loose top sheet. The A-scale (frequency shift) is set to zero and the B-scale (impedance) is set to 90 $\pm$ 10%. The appropriate acceptance limits are then set and the part is carefully scanned. Any flaw indication is marked on the panel. Once again, any change in structure being scanned requires a new instrument set up. At the conclusion of scanning, any flaw indications are transferred to a mylar to retain the inspection results.

5. CONCLUSIONS

The major conclusions reached as a result of the tests conducted in this program relative to the definition and non-destructive detection of adhesive bondline flaws are summarized in this section.

a. Bondline flaws in regions of high adhesive shear stresses produce stress concentrations adjacent to the flaws much like hole stress concentrations in metal.

b. Flaw growth initiates at bondline stress concentrations and propagates incrementally with cyclic loadings.

c. Flaw growth is most likely to occur where peel or tension forces are present in the adhesive.

d. Bondline flaws and their growth can be detected with state-of-the-art NDE.

e. Flaw growth rate per cycle is higher with the slower cycle rate.

f. The hot/humid environment is more conducive to flaw growth than room temperature or cold environments.

g. Extremely thin bondlines are types of flaws that may be undetected and be sites of bondline crack initiation and growth.

h. Massive bondline flaws can cause a redistribution of load in the metal, resulting in premature metal fatigue.

6. REFERENCES

1. AFFDL-TR-76-141, "Primary Adhesively Bonded Structure Technology (PABST); Phase Ib: Preliminary Design", dated December 1976.

2. AFFDL-TR-77-135, "Primary Adhesively Bonded Structure Technology (PABST); Phase II: Detail Design", dated August 1977.

3. AFML-TR-77-163, "Fracture Mechanics for Structural Adhesive Bonds", dated August 1977.

4. Hart-Smith, L.J., "Adhesive-Bonded Double-Lap Joints", NASA-Langley CR-112235, January 1973.

5. Hart-Smith, L.J., "Adhesive-Bonded Single-Lap Joints", NASA-Langley CR-112236, January 1973.

☆U.S.Government Printing Office: 1978 — 657-002/308